Sensory computation and decision making in *C. elegans*

a computational approach

Tom Sanders

Submitted in accordance with the requirements for the degree of

Doctor of Philosophy

The University of Leeds

School of Computing

March 2016

The candidate confirms that the work submitted is his own, except where work which has formed part of jointly authored publications has been included. The contribution of the candidate and the other authors to this work has been explicitly indicated below. The candidate confirms that appropriate credit has been given within the thesis where reference has been made to the work of others.

Cohen, N, and Sanders, T, 2014, Nematode locomotion: dissecting the neuronal-environmental loop, in *Current Opinion in Neurobiology*, 25:99-106.
My contributions: This is a review paper with NC being first author. TS contributed substantially to all parts of the paper, but especially to the navigation section, that relates directly to his PhD research.
Chapters based on this work: Chapter 1.

Acknowledgements

I would like to start by thanking my supervisor Netta Cohen, for giving me the opportunity to do this PhD, for her great feedback, guidance, numerous suggestions and help!

Many thanks to the Biosystems group: Chris, Claudia, the three Daves, Elaine, Elpi, Iakovos, Ian, Jordan, Keeran, Malcolm, Marc, Mattia, Nik, Patricija, the two Robs, Sam, Tom, Vilius and Yi for all the good times and great feedback!

I thank my girlfriend, Renske, for her tips and for always supporting me! You are the best!

Finally, I thank the EPSRC for funding my PhD as part of grant EP/J004057/1 and the School of Computing for hosting me.

Abstract

In *Caenorhabditis elegans* (*C. elegans*) and in neuroscience generally, a hierarchical view of nervous systems prevails. Roughly speaking, sensory neurons encode the external environment, interneurons encode internal state and decisions, and motor neurons encode muscle activation. Here, using an integrated approach to model sensory computation and decision making in *C. elegans*, I show a striking phenomenon. Via the simplest modulation possible, sensitization and desensitization, sensory neurons in *C. elegans* can also encode the animal's internal state.

In this thesis, I present a modeling framework, and use it to implement two detailed models of sensory adaptation and decision making. In the first model I consider a decision making task, in which worms need to cross a lethal barrier in order to reach an attractant on the other side. My model captures the experimental results, and predicts a minimal set of requirements. This model's mechanism is reminiscent of similar top-down attention modulation motifs in mammalian cortex.

In the second model, I consider a form of plasticity in which animals alternate their perception of a signal from attractive to repulsive. I show how the model encodes high and low-level behavioral states, balancing attraction and aversion, exploration and exploitation, pushing the 'decision making' into the sensory layer. Furthermore, this model predicts that specific sensory neurons may have the capacity to selectively control distinct motor programs.

To accomplish these results, the modeling framework was designed to simulate a full sensory motor pathway and an *in silico* simulation arena, allowing it to reproduce experimental findings from multiple assays. Hopefully, this allows the model to be used by the *C. elegans* community and to be extended, bringing us closer to the larger aim of understanding distributed computation and the integrated neural control of behavior in a whole animal.

Contents

List of figures

List of tables

Part I

The beginning

Chapter 1

Introduction

"There's a difference between knowing the path and walking the path"

– Morpheus

Long before I learned about (computational) neuroscience, the brain was studied by generations of scientists and (natural) philosophers. Already in ancient Egypt, 5000 years ago, a physician correlated brain damage with impaired movement of the limbs [36]. In ancient Greece, around 400 BCE, the Hippocratic doctors first proposed that the brain is the source of every thought, emotion and action [43]. However, it was not until the Renaissance that the brain became generally accepted as the source of cognition, and it took until the nineteenth century for Santiago Ramón y Cajal to convince the scientific community that the brain consists of a large number of brain cells called neurons which communicate through specialized branches forming a distributed network. Finally, in 1952 Hodgkin and Huxley showed how a neuron 'holds' (encodes) information by altering the potential across its membrane using the flow of ions in and out of the cell [48]. Using their experimental results, they created the Hodgkin-Huxley model of a neuron, which is so good at describing a neuron's basic functioning, that it is still used in many computational models today.

Of all cognitive faculties the one perhaps most amenable to research is plasticity, or the ability to learn. Indeed, 'will', consciousness, and even reasoning are very difficult to capture experimentally or even to define. Thus, not surprisingly, the start of modern neuroscience begins with the quest for the *engram*: the physical trace of a memory in the brain.

In the 1960s Eric Kandel set out to find the *engram*. He figured that by combining the black box approach of psychology with mechanistic understanding from biology he could make an animal learn while simultaneously watching its brain for any changes. To make this task somewhat simpler, Kandel decided to use a sea snail, *Aplysia*, which has $\approx$ 20 000 large neurons[1]. The size of the neurons allowed Kandel to physically stick an electrode into a single neuron and measure its electrical activity. Contrary to the commonly held view at the time that simple organisms were incapable of complex learning, Kandel found that the the snail's gill withdrawal reflex (where it closes its gill if you poke it) was amenable to habituation (weakening over time), sensitization (strengthening over time) and associative conditioning (coupling with another unrelated stimulus). Using these learning paradigms in several clever experiments, Kandel successfully located the individual neurons involved in the reflex and found the *engram*: the genetic and molecular changes leading to a weakening or strengthening of the connection between two neurons, effectively holding the memory for the strength of the gill withdrawal reflex. In 2000 he won the Nobel Prize in Physiology or Medicine for this discovery.

Neuroscience has continued to bridge psychology and biology while adding physics, chemistry and computer science into the mix. Since the fifties we have learned a tremendous amount and created a very powerful set of tools to probe the mysteries of the mind. It is thus that the next big question of neuroscience can be explored: how do

[1]The cell body size of *Aplysia* abdominal ganglion neurons is between 0.05-0.1 mm in diameter with the largest neurons around 1 mm [39], humans have approximately a trillion neurons, the largest of which are around 0.1 mm.

brains make decisions? Arguably, behind every behavior lies a decision. In the simplest case whether to perform an action or not, and in other cases a choice between many possible alternatives. Indeed, if they are to maximize their fitness, animals should weigh their options carefully, making sure they find sufficient food, mates and shelter, all while avoiding predators and hazardous environments.

To understand how a nervous system produces complex behavior, I believe one should find the simplest organism that shows a behavior of interest, taking care to choose an animal that has an easy to study nervous system. While there are many model organisms in neuroscience, Kandel's sea snails, fruit flies, zebrafishes and mice, to name some, only a single species has had its complete nervous system, complete genome and complete cell lineage mapped: the roundworm, *Ceanorhabditis elegans* (*C. elegans*). Thousands of researchers over the course of more than fifty years have massively expanded our knowledge of this otherwise unremarkable animal. While this was not clear to the early pioneers, many of the molecular, cellular and macroscopic pathways are conserved between worms and humans. Thus, the more we learn about *C. elegans*, the better we understand genetics, development, cognition and their interaction across the animal kingdom and in ourselves.

1.1 The worm

Roundworms are one of the most successful species on earth. This group of animals, also known as the phylum *Nematoda*, is so ubiquitous, that if everything except nematodes suddenly disappeared the shape of our planet would remain visible consisting of billions of worms.

One of these wonderful nematodes is the roundworm *C. elegans*. While not well known outside of science, or even beyond biology and neuroscience, *C. elegans* might well be the best studied multicellular organism on earth. It was the first multicellular species to

have its full genome sequenced [34], the first species to have its complete cell lineage reconstructed [96] and the first and only species to have its nervous system including every connection mapped [109].

Behavioral studies have shown conclusively that *C. elegans* is capable of richly responding to its environment – it can find food, avoid predators, and seek habitable environmental conditions – integrating external cues with internal state to produce the most adaptive behavior.

1.2 Aims and methodology

The main objective of my PhD was to develop a generic computational model of *C. elegans* decision making. Such a model could increase our understanding of circuit mechanisms underlying sensory integration. In our daily lives, we continuously have to process endless streams of information from all of our senses. We combine our sight, smell, hearing and body posture into a single continuous representation of ourselves and the surrounding world. While we do this seemingly without effort, the immense complexity underlying this feat has become painfully apparent from the world of artificial intelligence. Even in relatively well constrained domains, such as driving a car on the highway, the problem of knowing your surroundings and more importantly predicting the effects of your actions, is incredibly hard.

This PhD was done in the School of Computing, so unsurprisingly, this thesis revolves around computational modeling. One of the things I like best about the field of computing is the breath of topics it can be applied to. However, one could argue neuroscience stands out in its blending with informatics. Not only have highly reliable models of neurons stood the test of time but cognition itself is a form of computation. While our own brains are (still) far too complex to study the neuronal computation beyond several tens

of thousands of neurons simultaneously[2] [74], *C. elegans* is simple enough to look at how its nervous system is calculating what decision to make.

Computational models of *C. elegans* have varied considerably in approaches and research questions. Some models have focused on the neuronal level [62] while other, high level models, have set out to account for specific behaviors; the latter class of models typically lack or include very simplistic representations of the nervous systems [79, 94]. Here, I am concerned with intermediate level models that include some neuronal and neural circuit details and aim to offer explanatory and predictive power on the neural specification of behavior.

To remain grounded in physiological and behavioral evidence, such models tend to focus on a limited subset of the nervous system. This class of models therefore distinguishes itself from models of the entire head nervous system [114], or even the entire nervous system of the animal [98] that focus instead on patterns of connectivity and circuit-level insights. Of the above, Xu et al. [114] is particularly noteworthy as it models both uni-sensory and multi-sensory navigation behaviors and offers interesting predictions on possible pathways for speed regulation. The inclusion of a fully realistic circuit avoids the assumption of a single or very limited neural pathway. However, it is important to note that for many of the neurons included in such models, no experimental evidence of behavioral function exists. Thus, the potential power of circuit-wide models to gain circuit wide insight, or to implicate new neurons or neural pathways in a computation is also the source of their limitation.

Most intermediate-level models (focusing on specific subcircuits) have also focused on a single assay or type of assay. Prominent examples include chemotaxis on a salt gradient assay [3, 37, 56, 57] or forward locomotion [13, 16, 79, 108]. Such models vary in their level of detail. For example, Boyle et al. [13] and later Izquierdo and Beer [56] include a

[2] though the Human Brain Project is trying to create a model of a complete human brain over the coming decade

more realistic worm body to support forward locomotion, the latter within the context of a salt chemotaxis task. Models of chemotaxis behaviors have mostly focused on a single sensory-motor pathway, and a single motor behavior – either steering [55–57, 112, 113] or a biased random walk [32, 33, 37]. The first chemotaxis model to consider both motor programs in detail is Appleby's model of salt chemotaxis [3], followed by Xu et al. [114]. However, with the exception of Xu and Deng [113], none of these models were tested with multiple experimental assays.

It is a premise of my approach, that in modeling a complex system such as *C. elegans*, the focus on a single assay places a significant limitation on a model's predictive power. In other words, it is likely that a model tuned to account for one assay will fail when tested on another. In embarking on this research, I was motivated by the desire to push the envelope of *C. elegans* modeling to account for multiple behaviors under multiple conditions with a single model. This motivation is driven both by fundamental questions as to the ability of a single model to account for multiple behaviors, and by the desire to provide a useful tool to the research community, a model framework that can in time be extended to include more neurons, more neuronal and circuit mechanisms and more assays.

Here, I set out to build a generalizable model of *C. elegans* capable of reproducing a wide variety of experiments, and capable of rapid inclusion of novel experimental findings. One of the important unifying factors for researchers working on *C. elegans* is the desire to do it all in *C. elegans*, the whole genome, the whole cell lineage, the whole neural circuit and the whole transcriptome. This is because ultimately, the hope is that *C. elegans* can be understood holistically. The same applies for the desire to model the neural basis of behavior: ultimately, the aim is to model the entire animal, its complex recurrent neural circuitry and its ability to support complex behaviors. But we have to take small steps. Hence, to date, most of the modeling work has focused on specific sensory responses, specific forms of learning, and specific motor outputs. With increasing knowledge and improving experimental technologies, over the last decade, we

now have access to crucial data on much more complete sensory-motor pathways, sensory integration, and more complex behaviors. It is beginning to be possible to dream about unifying models into a more coherent unified framework, and to take the first concrete steps in this direction. However, the risk in modeling is that the models produced are under constrained, contain too many parameters and fail to be predictive. Principled approaches for model construction are therefore essential. To constrain my model the following approach was followed:

- creating a modular modeling framework that consists of full sensory-motor pathways and in-silico replication of experimental assays
- testing the same model (with the same neurons) in different but related assays (e.g. different experimental set ups)
- testing variants of the model (with some overlapping modules, but other distinct components, e.g completely different sensory cells)

It is my hope that a model generated through a more unified approach may be better constrained and, as such, more likely to capture essential cellular and circuit level mechanisms. In other words, such a model may be more explanatory and more predictive. By starting with a limited number of neurons, a strong grounding in a large body of experimental results and adding more neurons and experimental data over time, this model hopefully will be able to shed light on the cellular and circuit level mechanisms underlying sensory integration, decision making, and transitions between behaviors. Given the difficulty of this aim, it is vital that the model be created iteratively, in close collaboration with experimentalists.

Concretely, in this thesis I attempt to answer two methodological questions:

1. Can one create a generic model of *C. elegans* decision making, capable of rapid reproduction and incorporation of new experimental findings as opposed to the

specialized one off models of today (chapter 1 and 2).

2. Would a generic model be capable of producing testable hypotheses? Or alternatively, would such a model prove untenable with conflicting experimental data pushing the model to become either too constrained (i.e. no feasible solution exists), or too unrealistic (a compromise between conflicting findings that satisfies has little in common with the actual animal)?

The second of these I answer by looking at several case studies, focused on the following substantive questions:

1. How well do sensory neurons encode sensory information?
    - How is this encoding affected by the animal's 'internal state'?
    - What other computation is sustained in sensory cells and circuits?
2. How does *C. elegans* integrate attractive and repulsive stimuli?

To answer the substantive questions, I have arguably used the most well studied sensory response: chemotaxis to sodium chloride (naive attraction and learned aversion). I have complemented this with established multi-sensory assays containing either copper or hyperosmotic fructose as repellent and diacetyl as attractant.

Looking back, I can say it is very much possible to create a highly customizable computational model with predictive power, which in one case fully reproduced a novel experiment in as little as a day. This was only possible due to the modular design of the model and the separation of the simulation from the model specification that fully described the neuron properties, connectivities, assay and metrics to be measured. Additionally, the final model is capable of reproducing all experimental results tested, done in five very different assays, with four different chemicals, changing only the

environmental parameters, and leaving the remaining simulation parameters (for the animal itself) unchanged.

When testing the model in close cooperation with several experimentalists, I was surprised by the extent of sensory-neuron computation. Specifically, multiple forms of sensory neuron adaptation resulted in neuronal states that were either 'on' (responding to stimuli) or 'off' (unresponsive), flipped the valence of stimuli (i.e. from attraction to aversion) and allowed for memory of prior stimuli in sensory neurons. The experimental and model results strongly suggest that sensory neurons show activity that correlates with internal state and behavior, integrating the representation of a stimulus with internal state already in the sensory layer, to directly determine behavioral states and to control exploratory behavior.

Being a part of the experimental phase allowed us to rapidly test model predictions, improving the model with every iteration. Using this approach the model could provide deep insight into the ramifications of a hypothesis and predict which experimental setup should provide the clearest evidence to distinguish multiple conflicting hypotheses. For instance, in chapter 5 the model showed a simpler hypothesis could fully explain the experimental results, which was then confirmed by further experimental results designed using the model output.

1.3 Outline

For those unfamiliar with the nematode *C. elegans* I have included a short introduction in **chapter 2**, giving the background to this remarkable animal. Since I have done this PhD in a computer science department, it should come as no surprise that I am not an experimentalist, nonetheless I strongly believe that to model an organism you have to understand the experimental methodology and results. Thus I start with a review of the experimental field, beginning with the methodology and finally a summary of the key

experimental findings, followed by an overview of the existing computational models, their strengths and limitations. One of these models is explored more deeply in **chapter 3**.

In **chapter 4**, I describe the computational model of *C. elegans* that I developed, starting with the motivation, assumptions and constraints.

The model is used in two case studies. In **chapter 5**, I use my model to probe contextual decision making in a fructose-diacetyl decision making assay. Finally, in **chapter 6**, I investigate the role of various forms of sensory adaptation in the salt sensing sensory neurons on decision making. These two case studies were done in collaboration with the Jansen lab of Erasmus University, Rotterdam and the Nitabach lab of Yale University respectively. Each of these chapters is written with the experimental results integrated to show the power of an integrative approach. The order of results reflects for the most part the actual order of discovery.

Chapter 2

Why we care about a little worm

"There is no spoon"

– Spoon boy

2.1 For those unfamiliar with *Caenorhabditis elegans*

Before I started my PhD, I knew very little about the roundworm *C. elegans*. So for those readers who are unfamiliar with the mysteries that surround this remarkable animal, let me start with the story behind the nematode.

2.1.1 Finding the 'perfect' species

Sometime around 1965 the biologist Sydney Brenner was seeking to understand how genes give rise to complex structures such as an eye or a brain [14]. Brenner believed nervous systems were key in understanding how genes drive development. This was not just because of the complexity of a nervous system, but also because genetic mutations that affect the nervous system could be found by looking at the behavior of an animal.

Figure 2.1: A Caenorhabditis elegans N2 hermaphrodite pictured to scale, to the right of a 50 pence and 50 euro cent coin for comparison. Adults are approximately 1 millimeter long and 0.08 millimeter thick. All hermaphrodites consist of 959 somatic cells (excluding eggs and sperm), of which 302 are neurons.

At the time the fruit fly had already been established as a model organism but Brenner felt its nervous system was too large to allow a study of its structure. Then, but also today, nematodes were primarily studied because they tend to be parasitic, reducing crop yield and infecting livestock. For instance, the half a meter long nematode *Ascaris suum* spends most of its live in the intestines of a pig. In the mid fifties, Ellsworth C. Dougherty tried to obtain a strain[1] of nematodes usable for genetic studies: one that could survive in culture on only bacteria [77]. By chance, a few years earlier another biologist, Lancelot N. Staniland, had isolated a *C. elegans* strain from some mushrooms close to his office in Bristol, England. It was this strain, dubbed "Bristol N2" or N2 for short, which turned out to survive very well on a petri dish, with minimal requirements [77]. Traveling from Bristol via Germany, the N2 strain made it to Dougherty's lab in California, after which Brenner took them back to England in 1968 (the MRC lab in Cambridge).

The reason Dougherty and Brenner chose *C. elegans* as a genetic model organism is multifaceted: first, the species has a life cycle of only 3 days, second, it has a small

[1]Individuals of a species (e.g. *C. elegans*) show a wide variation in their genes (genotype), form and behavior (phenotype), a strain is defined as a family of individuals who express a particular genetic variation. For instance, in *C. elegans osm-9* are the family of worms (all cloned from the same original animal that first introduced the mutation) who have a particular developmental defect making them insensitive to hyperosmolarity. In humans, the word strain is typically not used, instead the term haplogroup is more common.

and fixed number of cells, third, it can be kept alive using only very basic ingredients, and last, *C. elegans* can reproduce sexually and asexually (making cloning and hybrid strain creation trivial). From Sydney Brenner's lab the N2 strain was further distributed to new labs over the years. First his former group members set out to start their own labs, later entirely new groups formed. Today there are hundreds of research groups all over the world studying this one strain and its many mutants. However, one limitation of using almost exclusively N2 is that it might not be representative for the species and nematodes in general. This potential limitation is supported by the difficulty Dougherty had in finding a strain that could survive in laboratory conditions.[2] Luckily, this is not a problem when trying to understand generic principles of genetics, neuroscience, behavior and their interaction [31], but it does limit the interpretation of behavior (e.g. why a certain behavior could have evolved).

2.1.2 Experimental techniques

To understand the strengths and limitations of the experimental data referenced in this work, I will briefly summarize the experimental tools most used in the field. Starting with a generic description of how behavior is measured and quantified, followed by ways to measure and influence neuronal activity.

Measuring behavior

For *C. elegans* when we talk about behavior, we either talk about what happens on the population level, counting for instance how many animals have moved into a particular region of space, or we talk about individual animal behavior, for instance when we compare locomotion trajectories.

[2] Out of the many strains from several *Caenorhabditis* species that Dougherty tested, Bristol N2 was the only strain that could survive in culture. Today several strains have been successfully grown in laboratories, allowing some comparisons to be made.

A metric that is often used to measure behavior is the chemotaxis index (CI), which is redefined for each assay but always measures the response strength to a chemical gradient (for instance the percentage of animals that are found within a region close to the peak concentration). Similarly an aversion index measures how strongly animals are repelled by a noxious stimulus. While population averages can diminish the effect of noise and increase the visibility of phenotypes, averages can be hard to interpret without taking individual behavior into account. For this reason, many studies now use automated tracking of many worms at the same time, storing the trajectory of each animal. This allows researchers to reuse the same dataset with changing analyses, giving greater explanatory power. In this thesis I rely on both population and individual metrics.

Measuring neural activity

There are roughly three ways to measure the activity of individual neurons, first stick an electrode into the neuron, second use a dye whose fluorescence indicates neuronal activity (calcium concentration or voltage), and last genetically modify the animal such that specific neurons express a fluorescent calcium indicator. While the intracellular electrode always measures electrical activity (the voltage across the cell membrane), fluorescence signals can be used as indicators of electrical activity (in the case of voltage-sensitive dyes) or of a proxy such as the calcium concentration in the cell. For *C. elegans*, but other organisms as well, it is usually not feasible to use electrophysiology on a large number of animals. *C. elegans* has the added difficulty that the body is pressurized and puncturing the animal makes its innards flow out.

While calcium dyes have been used extensively in many larger animals, the short life span, and great genetic amenability of *C. elegans* has led to a large number of strains expressing genetically encoded calcium indicators (GECIs) in individual or groups of neurons. While some of the earlier GECIs suffered from slowness and poor dynamic range, over time very fast highly contrasting GECIs have been developed, some even

matching the generally faster calcium dyes. Though still significantly slower and less precise than electrophysiology, the benefits are numerous. Most importantly, GECIs allow a researcher to study neuronal activity in freely behaving [64], and recently even freely moving animals [25].

Controlling neural activity

There are several ways to test for the function of a neuron in a particular context. The simplest of these involves 'disabling' a neuron, to see the resulting defect, and sometimes re-enabling the neuron, which should return the behavior to normal as a control. The targeted silencing of a neuron can be achieved using a brief but powerful focused laser beam to physically ablate a neuron or using several genetic techniques to prevent a neuron from developing. For instance, one could activate an apoptosis[3] pathway under influence of a cell specific promoter[4], or insert a mutation in a gene known to be involved in the cell's development.

There are some caveats to studies using laser or genetic ablations. For instance, some manipulations only partially silence a neuron, or silence the neuron but have secondary effects. Conflicting results can be further produced by the strong redundancy and robustness of neural processing in *C. elegans*. The effect of disruptions is often masked and only visible if multiple neurons are ablated simultaneously [41].

Besides ablation it is now possible to change the membrane potential using optogenetics. Typically animals are genetically modified to express light sensitive ion channels in specific neurons. By shining light on the animal, the light sensitive ion channels open, allowing positively or negatively charged ions (depending on the channel type) to rush into the cell, changing the neuron's activity in real time. Strongly hyperpolarizing a neuron can, in simple circumstances, be equivalent to ablation (with some caveats,

[3] programmed self-destruction of a cell

[4] a regulatory region in an organism's DNA that can drive a gene to be expressed

e.g. electrical connections between neurons cause currents to reverse direction), while depolarizing a neuron can provide an input directly into the animals' nervous system. This has been successfully used to steer animals by presenting them with a changing virtual chemical gradient inserted directly into the interneurons, or by directly controlling the motor neurons that drive its muscles [65].

2.1.3 Anatomy

In this work I focus strongly on the nervous system, for the most part treating the body of the worm as a point in space. Because of this I will only briefly describe the anatomy, insofar as it is necessary to understand how the animal moves and how the nervous system drives its behavior.

C. elegans can be found in two sexes, hermaphrodites and males. The vast majority of work has been done on the hermaphrodite and since I rely heavily on experimental work, I looked exclusively at hermaphrodites in this study. Adult hermaphrodite are approximately 1 millimeter long and under 0.1 millimeter thick consisting of 959 cells of which 302 are neurons [23, 109]. *C. elegans* suck up their food, bacteria, through their mouth using the pharynx. Surrounding the pharynx is the nerve ring, where most of the neuron's cell bodies are. Next to the mouth are two sensory endings, the amphids, which the worm uses to taste, smell and to sense several other modalities (further discussed in 2.1.5). The muscles are arranged along the dorsal and ventral side of the body.

2.1.4 Behavior

Perhaps surprisingly given its compact nervous system, *C. elegans* has a large and diverse behavioral repertoire. In my PhD I focus on decision making and sensory integration, so I will not go to deeply into the precise mechanics of *C. elegans* locomotion. I will present

the basics as far as they are required for this thesis, and recommend the PhD thesis of Jordan Boyle [12] for those wishing to dive deeper into the subject.

When moving about *C. elegans* crawl on their left or right side (switching occasionally) while bending in the dorsoventral plane to generate thrust. The wavelength and frequency of the undulations depend on the viscosity of the medium, with long wavelength rapid thrashing in liquids and slower, snake like, short wavelength crawling on more solid media [10]. In this study I only use the latter motion as most studies have been done with animals placed on a high viscosity solidified agar solution in a petri dish.

To find food and maintain suitable environmental conditions, *C. elegans* uses at least two strategies to follow or avoid concentration gradients, temperature gradients, brightness gradients, electromagnetic gradients and pH gradients: random reorientation where the probability of a reorientation depends on the direction of the gradient sensed over time (*klinokinesis*) and gradual reorientation to a gradient by sampling in space (*klinotaxis*) [52]. Recently, complex multisensory assays have shown *C. elegans* capable of dynamic decision making choosing between attractants [50, 51, 58, 80], whether to cross an aversive barrier depending on strength of an attractant on the other side [54, 93], or navigating complex environments.

I will describe the specific behaviors seen in several behavioral assays a bit further down in the section on behavioral assays (section 2.1.7).

2.1.5 The nervous system

With the publication of *'The mind of a worm'* in 1986 for the first time ever the full nervous system of an organism was described down to the synaptic level [109]. This Herculean task forced the authors to come up with a concise way to group and name the individual neurons. At the time the function of many neurons was not yet known, so grouping was done based on morphology and connectivity. This resulted in 118 classes

of similar neurons, most consisting of two (the left and right neuron). The incredible quality of this work became evident later on when the function and genetics of neurons aligned almost perfectly with the handpicked classes. In 2006 the connectome of the ventral nerve cord was revisited and in 2013 the circuit diagram for the anterior nervous system was further improved by re-analyzing the old serial section slides [23, 114].

The *C. elegans* nervous system can be divided into two parts, the pharyngeal and the somatic nervous system, which are connected by a single gap junction (one or more porous channels creating an electric coupling between two cells). Out of the 302 neurons, 282 are part of the somatic nervous system and 20 are pharyngeal [109]. In this work I will only look at (a part of) the somatic nervous system[5]. The name of each neuron tends to follow the same general principle. For instance the sensory neuron ASEL, which primarily senses increases in the sodium concentration, the first two letters indicates the type of neuron (A for amphid, S for sensory), the third letter is used to differentiate similar neurons in the same group (this is the fifth amphid sensory neuron pair, thus after A,B, etc. we have E), and finally the last letter(s) give the position along one or more body axes (here the L for left).

In contract to mammalian nervous systems, the *C. elegans* neurons are somewhat odd. For instance, unlike mammalian nervous systems, neurons can be both excitatory and inhibitory. Also, most *C. elegans* neurons do not spike but show graded potentials and graded synaptic release. People have speculated that this might be because of the small physical size of the neurons. As the neurons only have space for several tens of ion channels, thermal fluctuations of individual channels begin to play a role, which would make all or nothing action potential very unreliable.

For the model I created in this thesis I focus on several sensory neuron classes, interneuron classes and some abstract motor circuits, the latter of which are based on actual motor

[5]The 279 connected somatic neurons (CANL/R and VC06 do not make any connections to other neurons) form a network to each other through 6393 chemical synapses and 890 gap junctions [104]

motifs but not individual motor neurons. I will describe the key findings on these neurons and motifs below.

2.1.6 The sensory neurons

I have included three classes of amphid sensory neurons in my model that are involved in many of the multisensory integration and decision making assays. The main sensory organs of *C. elegans* include the amphids in the head, and the phasmid in the tail, though there are other sensory neurons, both in the head and along the body. In addition, other neurons (that are not classified as sensory, such as some interneurons and motor neurons involved in locomotion) may have additional sensory functions, such as stretch receptors [108]. All amphid sensory neurons have their cell body (soma) in the nerve ring, a dense ring of neuronal cell bodies and axons in the head of the animal. From there, each amphid sensory neuron has a cilium that extends to the left or right amphid, where the sensory endings are exposed to the environment.

To survive, *C. elegans* has to integrate multiple sensory modalities to gain sufficient information about its environment. Indeed, *C. elegans* can taste solubles [106], smell odorants [67], and sense pressure (touch) [45, 61], temperature [46, 75], nociception [31], light intensity (blue to ultraviolet) [18], pH [90], osmotic pressure [30], electromagnetic fields [95, 105] and body shape [71, 108]. Most of these are sensed by one or more amphids sensory neurons (some are also sensed by other neurons).

C. elegans appears to employ sparse coding: each neuron senses multiple stimuli (some even sense multiple modalities) and most stimuli are sensed by more than one neuron class. This introduces redundancy and allows multisensory integration to occur already in the sensory layer, allowing for a highly compact sensorimotor pathway. In fact, since the full connectome is known[6], a network analysis was done showing that on average it takes

[6]Varshney *et al.* estimates the connectome is 90% complete, with the last 10% missing due to 'missing data and technical difficulties' [104].

2.65 [107] to 4.0 [60] neurons to reach any neuron from any other neuron. For the sensory neurons I consider in this thesis there are one to three interneurons between the sensory neuron and the nearest ventral nerve cord motor neuron or neck motor neuron [104]. Clearly, compared to mammals this makes the nervous system very shallow and intuitively increases the amount of 'computational work' each neuron in the short sensorimotor chain must do.

One of the first studies to systematically identify which chemicals were attractants to *C. elegans* was by Ward [106]. Two of the most often used attractants are sodium chloride (NaCl) and diacetyl (DA). Both chemicals are highly attractive to naive animals. This is because the tastant sodium chloride (as well as other salts) tend to be present in higher concentrations around bacteria, the main food source of *C. elegans*. Similarly, the attractivity of the odor diacetyl is likely to be due to several diacetyl emitting bacterial strains.

Interestingly, the response to sodium chloride is plastic and can be reversed upon pre-exposure. Extensive research has shown that there are at least three different forms of plasticity in the salt response: gustatory plasticity, starvation enhanced gustatory plasticity and set point learning. The first occurs over time scales of ten minutes (with a reversal time of less than 5 minutes) upon pre-exposure to sodium chloride in the absence of food. Hence this is a form of associative learning [50, 51, 58]. Chemotaxis plasticity [52, 88, 101], occurs when animals are starved in the presence of NaCl over much longer timescales of an hour or longer and appears to be similar to starvation enhanced gustatory plasticity [51]. Finally, set point learning happens over several hours as well, but only in the presence of food, whereby animals learn to associate a specific concentration of NaCl with food, and will navigate to that specific concentration [73]. The presence of food makes it clear that a different mechanism must be in play for the latter. Additionally, all mutants that were defective in gustatory plasticity were normal in enhanced gustatory plasticity [51], suggesting that all three forms of NaCl adaptation use

independent pathways.

By ablating different classes of sensory neurons and testing chemotaxis behavior, several studies showed that NaCl attraction is mediated primarily by the ASE neuron pair, with a minor contribution from the ADF, ASG and ASI neuron classes [5, 52, 97]. Conversely, diacetyl is sensed primarily by the AWA sensory neuron pair, with high concentrations (1:10 dilution in 1μl ethanol) also sensed by the AWC pair [7, 24].

ASE sensory neuron pair

The amphid sensory E (ASE) class of neurons respond to a variety of tastants. Most importantly for this thesis, they detect sodium chloride (NaCl). In addition, ASE neurons sense cyclic AMP, biotin [5] and toxins such as cadmium and copper ions [89].

While most left-right neuron pairs in *C. elegans* are functionally identical, the ASE sensory neurons are one of the only functionally heterogeneous neuron pairs[7] [83, 97]. In fact bilateral (left-right) symmetry is seen throughout the animal kingdom, with identical gene expression for cells that are each other's left-right mirror sibling. For ASEL and ASER a novel genetic pathway has evolved just to break this symmetry [59], further suggesting something interesting - rather than chance - is happening here.

The sensory responses of ASEL and ASER neurons to salt differ by at least three factors: first, ASEL responds primarily to sodium, while ASER responds primarily to chloride [83]; second, the membrane potential of ASEL depolarizes (becomes less negative) in response to upsteps in the NaCl concentration, while ASER depolarizes to downsteps in the NaCl concentration [97]. Also, ASEL does not respond to NaCl concentration decreases, while ASER hyperpolarizes in response to NaCl concentration upsteps. Thirdly, upon pre-exposure in the absence of food, ASEL desensitizes, while

[7]The other functionally assymetric pair is AWC, which has an ON and an OFF cell which respond to different chemicals but both depolarize to odour removal. The identity of the ON and OFF cell (left or right) is determined stochastically during development [103]

ASER sensitizes [80]. Interestingly, there are no obvious distinctions between the functions of ASE and other amphid sensory neurons to suggest an advantage. Some hypotheses have been proposed, perhaps the most credible suggests that responding with opposite polarities increases the dynamic range downstream [3]. The opposite adaptation was only found recently and its function has not been examined yet. In chapter 6 I will address this question.

ASH sensory neuron pair

In contrast to the ASE pair, the ASH pair is symmetric. ASHL and ASHR appear to respond identically [100] and are electrically coupled by a gap junction[8] [23, 109]. ASH are also one of the few sensory neurons to be polymodal, responding to multiple sensory modalities (taste, touch, pH, osmotic shock) [6, 28, 47, 61, 89, 92, 100, 102]. While both ASH neurons respond with depolarizations to increases in nociceptive stimuli, the response to NaCl appears to be more complex. Specifically, ASH depolarizes to hyperosmotic increases in concentration [47], but ASH neurons also depolarize to decreases in NaCl from 40mM to 0 [100]. At first glance it seems odd that ASH would depolarize to both increases and decreases in the NaCl concentration. But earlier work comparing nose touch to osmotic shock showed that the ASH sensory neurons can change which neurotransmitter is released depending on the stimulus [86]. Even though ASH depolarizes to both nose touch and osmotic shock, the ASH effect on a key pair of downstream interneurons called RIM[9] has a complete opposite polarity, hyperpolarizing RIM in response to nose touch and depolarizing RIM in response to osmotic shocks.

[8] Gap junctions are believed to induce synchronization

[9] The RIM interneuron pair plays a central role in aversive responses, depolarizing RIM inhibits reversals, though in response to osmotic shock, ASH depolarizes RIM to produce a faster reversal where head oscillations are suppresed [86]

AWA sensory neuron pair

The AWA sensory neurons respond to several attractive odorants but it is the only pair known to respond to diacetyl (with minor contribution from AWC) [7, 24]. Like ASH, AWA respond with a depolarization to increases in the odor concentration but unlike ASH no hyperpolarization is seen in response to odor removal [67]. Recent calcium imaging has shown the extreme dynamic range of AWA to diacetyl [67]. A measurable response was detected over six orders of magnitude concentration change (0.001μM to 100μM). Additionally, the response profile to concentration steps changes markedly as the step size increases, suggesting there are different pathways for low concentration steps and high concentration steps.

Just like the ASH sensory neurons, it is assumed that the AWA sensory neuron pair are functionally identical as the left and right neuron are also coupled by a gap junction [23, 109], though to my knowledge no separate AWAL/AWAR calcium imaging has been done to confirm this.

2.1.7 Decision making assays

To give an overview of the different behavioral responses and assays used, I will list the key experimental findings in chronological order here. I will only focus on assays that used stimuli sensed by the ASE, ASH or AWA sensory neurons. Furthermore, I will focus on the most used stimuli: NaCl (ASE and ASH), copper (ASH), osmotic shock (ASH) and diacetyl (AWA). Early experimental studies did not include plasticity but instead focused on naive chemotaxis

2.1.8 Chemotaxis assay

Chemotaxis, the ability to follow chemical gradients, is tested in *C. elegans* by placing animals on an petri dish and measuring the response to a chemical gradient. Petri dishes invariably contain agar, and are typically prepared by depositing a chemical (attractant and/or repellent) in localized spots that are then left to diffuse for some time. The resulting chemical gradient then leads to a stochastic but goal-directed locomotion of the animals over time, either towards or away from the chemical peak. To assess the strength of chemotaxis, a region surrounding the chemical peak is defined, and the number of animals inside this region is counted after a certain duration. A ratio, typically called the chemotaxis index, can then be calculated in a variety of ways depending on the nature of the assay.

In the simplest case, the chemotaxis index is simply the ratio of the number of animals inside the peak concentration region versus the total number of animals put on the plate. The index set up this way, ranges from 0, no attraction to 1 full attraction. However, there are several issues with measuring chemotaxis in this way. First, the size of the region and the distance to the region are not controlled for. This means that the index does not tell you if the animals simply could not reach the region (too small, too far or not enough animals), or that animals were strongly repelled. Second, the number of animals is only counted once, at the end of the experiment. Thus if animals were attracted at some point but then left, the index would not distinguish this from a situation where no animal ever entered the region. Third, the chemotaxis index does not control for dead or non-moving animals. If for some experiments many animals were incapacitated during transfer or exhibit defective locomotion due to a genetic or other manipulation, this would incorrectly reduce the chemotaxis index.

Several solutions to the above mentioned issues with the chemotaxis index were found over the years. The most fundamental, and used in nearly every study, involves a control

region. Instead of having just a region for the concentration peak, a second region, equal in size and distance from the worms' initial location, is set at opposite ends of the plate. The chemotaxis index is then calculated as the difference in the number of animals between the control and test regions versus the sum of the number of animals in the two regions. This solves both the first and the third issue. Now the size of the test region and distance to the worm's initial location are taken into account, and non moving animals are excluded. Additionally, the chemotaxis index now ranges from -1 to 1, with -1 being full repulsion and 1 full attraction. A chemotaxis index of 0 is still ambiguous though, as it could mean no animal reached either region (i.e. a 'bad' assay), or simply no chemotaxis to the tested stimulus in question was found. This problem could be easily solved if papers published not just the chemotaxis index, but also the ratio of animals inside the control and test region versus all animals on the plate, giving the sensitivity of the assay. Unfortunately, I have not found any studies that do this.

The remaining issue of counting only at the end of the assay has been solved in two ways in several studies, but mostly has been taken for granted and even in recent studies has not been addressed. The first way to solve it is by adding an agent that renders the animals immobile in the test and control region (usually sodium azide). In doing this the researchers ensure no animal can enter and then leave the region. An obvious downside to this is the risk of saturation. Longer duration assays risk all animals getting stuck in either region. The second solution is better in my view, though requires more effort: simply count animals multiple times or continuously throughout the assay's duration. This way no saturation occurs, and both short term and long term changes in attraction and repulsion are captured.

Overall, the differences in the way chemotaxis is defined, the assay duration, chemical gradient and treatment of the animals ensure that great care must be taken when comparing results from multiple assays or studies. Often, assays look at different behavior with distinct molecular, cellular and circuit mechanisms.

NaCl assays

The attractiveness of NaCl was established in a study by Ward [106]. After letting sodium chloride diffuse on a 4cm plate, Ward placed approximately 100 worms around the edges and then counted the proportion of animals within 0.8 cm of the gradient peak at the center after varying times (from ten minutes to one hour). Using this setup the author found that *C. elegans* is attracted to solutions of sodium chloride of at least 2mM.

In a groundbreaking study by Iino and Yoshida [52], multiple discoveries regarding NaCl chemotaxis were made. The authors managed this feat by finding an assay that maximized the amount of chemotaxis data they could gather in a short amount of time. By using plates with twelve diffusing spots of NaCl in a grid layout, the animals perceived multiple gradient directions as they moved about. Also, the gradient slope was rather steep without the peak concentration becoming too high while ensuring there was a gradient across the full plate. The main results of the study are twofold: first, *C. elegans* uses both steering and biased random turns in NaCl chemotaxis, and second, ASEL and ASER have different contributions within this assay. Specifically, the authors found that ablating ASEL had no significant effect on any of their metrics. Additionally, the authors found a nearly linear relationship between gradient slope and steering strength[10].

The Plasterk lab and later the Jansen lab pioneered the use of assays looking at plastic responses to NaCl [50, 51, 58, 110]. Attraction was measured using a quadrant assay: in this assay, animals are placed in the center of a plate segmented in four quadrants, with alternating control and treatment regions containing a uniform stimulus concentration. The chemotaxis index is then calculated as the difference in the number of animals in the control and treatment quadrants divided by the total number of animals. Thus, if all animals go to the treatment quadrant the chemotaxis index has a value of 1 and conversely

[10]Though the effect is only demonstrated for the shallow end of gradients on the order of mM/cm (in contrast, in the assay animals were exposed to gradients of the order of mM/mm). This may therefore tell us more about the minimal salt sensitivity of the animal.

if all animals go to the control condition the chemotaxis index is -1. Similarly, if the treatment does not affect the animals' propensity to enter or leave the treated quadrant, the chemotaxis index is 0. This definition is consistent with the earlier use by the Bargmann group [27, 28], except that no sodium azide is used, such that assay can be run for longer durations while avoiding saturation of the metric. Furthermore, in the quadrant assay, animals are always either in the control or the treatment condition[11].

Using the quadrant assay the Jansen lab went on to discover a novel type of plastic behavior to NaCl that they called gustatory plasticity [50, 51]. The naive response, strong attraction to NaCl between 1mM and 200mM was found to turn to repulsion following a 10 minute pre-exposure in a buffer containing 100mM NaCl. Interestingly, they also showed that the reversal of the response depends on the concentrations used: pre-exposure to 10mM did not abolish attraction to 100mM, but did abolish attraction to 200mM.

At the same time the Iino lab studied salt plasticity in a slightly different way [1, 53, 80, 101]. This lab used a similar chemotaxis assay to the Bargmann lab. After letting an NaCl diffuse into the agar, they added sodium azide to the gradient peak and to a control spot on the opposite side of the plate. The chemotaxis index was calculated slightly differently from the Bargmann lab, excluding animals that did not move from their initial position: CI = (a-b)/(n-c), or the difference between the animals in the treatment (a) and control (b) regions divided by the number of animals (n-c) that moved from their initial position (c).

In contrast to the Jansen lab, the Iino lab kept animals in a buffer for one hour before testing the chemotaxis index. To see if the response after one hour of pre-exposure used the same mechanisms for plasticity the Jansen lab also kept animals in a buffer and compared several mutants in short and longer pre-exposure setups [51], the latter they dubbed *starvation enhanced* gustatory plasticity. Interestingly, while the chemotaxis indexes were similar between the two learning paradigms, the mutants results were very

[11]Though in practice the Jansen lab excluded a small region around the edges of the quadrant as some animals got stuck there.

different. In fact, none of the mutants that had disruptive learning behavior for gustatory plasticity showed any defect in starvation enhanced gustatory plasticity. This suggests that different forms of starvation enhanced NaCl plasticity use one or several separate molecular pathways. Furthermore, unlike the rapid time scale of gustatory plasticity, the long duration of the pre-conditioning and assay for starvation enhanced experiments allows ample time for changes in gene expression, circuit wide synaptic plasticity, etc. The apparent increased complexity introduced by such mechanisms have led me to focus on gustatory plasticity for this thesis.

Copper assays

There have been several studies looking at the responses of *C. elegans* to copper. Since many of the heavy metals are highly toxic, one would expect *C. elegans* to be strongly repelled by them. Indeed, a study by Sambongi et al. [89] found that *C. elegans* is aversive to copper and cadmium at low concentrations (0.01mM)[12]. Interestingly, this study also showed photographs of the tracks made by animals placed on a plate with a copper gradient applied to it. These tracks show a razor sharp edge at a specific distanced from the peak concentration beyond which almost no worms go. Similar photos were made by the same lab when testing acidic avoidance [90]. In chapter 3 these photos proved to be key in understanding how *C. elegans* ensures it does not enter lethal environments.

Around the same time several labs started investigating multisensory integration [54, 93]. Combining copper and diacetyl (as well as other combinations) in a single assay, allowed the authors to see how animals behaved in more challenging environments compared to unisensory assays. The assays were set up with a copper barrier across the center of the plate, the animals on one side and the attractant diacetyl on the other. The difficulty for the animals is that the conflicting sensory information should not lead to wavering

[12]Surprisingly, the same study did not find any response to nickel even though the concentration tested was lethal.

behavior; the animal must choose between crossing the barrier or not and cannot afford to show a hybrid of aversive and attractive behavior, lest it get stuck within the toxic area. Specifically, if the animal decides to go through the copper to reach the diacetyl, it must do so as quickly as possible otherwise it risks death. Conversely if the animal decides not go through the copper, it should inhibit its attractive behavior to the attractant on the other side in as much that there is no benefit to venture partially into the deadly copper.

Following the intuition that animals should not waver when presented with conflicting stimuli, the authors found that *C. elegans* appears to bias its behavior to either attraction or reversals [54, 93]. Specifically, several mutants were found to be identical to wild type in single stimulus assays but displayed abnormal behavior to assays with both stimuli. Using ablations, the authors concluded that AIA and AIY are involved in adjusting the balance between attraction and aversion in multisensory assays only. These results support the notion that some interneurons are primarily involved in multisensory assays.

Osmotic shock assays

Most osmotic shock assays use droplets containing a high concentration of fructose, NaCl or another chemical [45, 47, 86]. In some, animals are immobilized (either by gluing or in a microfluidic device); in others, they move freely, and the droplet is placed in their path. In addition, there have been two other types of assays, which were most influential for this thesis. The first, done by the Jansen lab, looked at the balance between NaCl attraction and repulsion at concentrations above 200mM in the quadrant assay. There, the authors found that wild type animals showed consistent repulsion to all concentrations above 200mM. Interestingly, animals with a genetic disruption of ASH (*osm-9*) showed attraction to the same concentrations, suggesting that osmotic shock as sensed by ASH overrides an attractive sensory signal. The second type of assay used in this thesis is developed by the Nitabach lab, where animals are placed inside a hyperosmotic fructose ring, with two spots of attractant (diacetyl) on either side of the ring. By counting the

number of animals crossing the barrier, the Nitabach lab found a novel mechanism that sets the balance between the attractant and the repellent (unpublished results). These two assays are described in greater detail in their respective chapters.

Diacetyl assays

The strong attractiveness of diacetyl to *C. elegans* has led to a variety of assays investigating the naive and conditioned response to this chemical. Diacetyl was first found to be attractive in the study by Bargmann et al. [7]. The focus there was to assess the attractiveness of odorants. The authors had two motivations, first to learn more about the response of *C. elegans* to odorants, and second to see if odorants can be used to perform chemotaxis assays quicker (due to their much faster diffusion). It turned out that many odorants are highly attractive. Out of the 154 odorants tested, 61 chemicals were attractants. However, only diacetyl and a few other odorants remained attractive across a broad range of concentrations (100 μM to $10^{-3}\mu$M). This has no doubt contributed to the popularity of diacetyl.

In addition to the studies mentioned earlier, there have been two key studies using diacetyl. The first is the Bargmann et al. [7] paper which adapted the assay developed by Ward [106]. The key differences between these two are the use of a larger plate and the introduction of the chemotaxis index as the difference between a treated and a control condition, as opposed to the unequal area comparison used by Ward. Also to increase the assay sensitivity, sodium azide was added to both the treatment and the control region. This chemical paralyzes the animals, ensuring that once an animal gets close to either region they can no longer leave. Naturally, this increases the sensitivity in short runs, but adds noise in longer runs, where more and more animals happen to enter one of the regions by chance.

The second key study was done by Larsch et al. [67]. This study looked at the

unusually broad range of the diacetyl response. In a microfluidic chamber where the diacetyl concentration could be very precisely controlled, the calcium activity of the AWA sensory neurons was measured in freely moving animals. This allowed high-throughput measuring behavior and AWA activity in response to diacetyl upsteps and downsteps of varying concentration, duration and slope. Interestingly, the authors found that the response to diacetyl upsteps was highly stochastic, with no clear correlation between the presence of a response in AWA and a behavioral response.

2.2 Previous computational models of C. elegans behavior

There have been several models of *C. elegans*, some highly detailed, some more abstract. Initial models focused mostly on locomotion, without any neurons at all, later models looked at either depending on the questions asked, and some recent models have combined locomotion with a neuronal model. As the aim of this thesis is to build a neuronal model, I will only cover the locomotion models superficially. Conversely, the neuronal models will be described in much greater detail. One of these I reproduced to show additional properties not available in the original paper.

2.2.1 Locomotion models

Some of the earlier models of *C. elegans* came from Niebur and Erdös. Their first model of *C. elegans* locomotion focused entirely on the method of locomotion [79]. The model includes a two dimensional body, its muscles and internal pressure. It follows from earlier work estimating the relevant forces (internal pressure, momentum, viscosity and friction) for *C. elegans* (and other microscopic nematodes) locomotion. The model does

not include a nervous system but instead assumes the head (or tail) follows a sinusoidal trajectory.

Later Niebur and Erdös extended their model by looking at how motor neurons drive the muscles to produce a propagating wave along the body [78]. Looking at larger nematodes they find that an electric waves passes synchronously with the muscle excitation wave. However, the small size of *C. elegans* makes the authors conclude this cannot be the case in *C. elegans*. They propose stretch receptors could be involved in the waveform propagation.

Later work by Bryden and Cohen showed stretch receptors could indeed reliably drive undulatory locomotion in *C. elegans* [16, 17], though the Bryden and Cohen models lacked the mechanics of the body and environment.

Building on the hypothesis from Niebur and Erdós [78], Berri *et al.* set out to test the role of physics in forward locomotion [10]. They did so by studying the transition between two very different looking behaviors that can be observed under different physical conditions - crawling in highly viscous gel and swimming in liquid, and found that these could in fact be described as extremes of a single gait. Using their positive findings, Boyle et al. [13] developed an integrated neuromechanical model of a single gait, modulated by the physics of the environment, that captured the entire range of behaviors (from swimming to crawling). Later experimental work further strengthened the single gait conjecture: swimming and crawling transition smoothly as a function the viscosity [10, 35, 68, 99]. The effect of stretch receptors was recently shown in an elegant paper that found motor neurons respond to exogenous bending of the worm's body [108]. This study also created a highly abstract model of the worm's body which independently confirmed that the characteristics of the stretch receptors support swimming and crawling as a single gait.

2.2.2 Chemotaxis models

There have been a wide variety of computational models capturing *C. elegans* chemotaxis. I will describe the most important here in detail. Some models I have chosen not to include in depth because they stray too far from the biology. While these models certainly have their merit, the predictive power is limited, and comparisons cannot be easily made.

Ferrée and Lockery, 1996

In 1996 a successful first attempt at modeling *C. elegans* chemotaxis was made. Recognizing that chemotaxis is about direction of locomotion rather than locomotion itself, the authors present a model of *C. elegans*, which in contrast to the earlier work of Niebur and Erdös, represents the worm's body as a single point in space moving forward with fixed speed along a direction θ. In doing this the authors assumed that the body follows the head. While this is not true [111], the center of mass of the second half of the body does follow the center of mass of the first half. Additionally, the chemical gradient is only detected by the nose of the animal, thus with respect to the chemical gradient, it is reasonable to argue that only the position of the nose is relevant. Finally, the authors argue for a plausible physical basis for their model transformation from muscle contraction to change in heading. Their minimal assumptions offer a powerful but computationally cheap framework for chemotaxis models and have been adopted by a large number of models since. Specifically, the recent model by Izquierdo and Beer [55] may offer a framework to validate the muscle-to-heading transformation of point models. The transformation itself handily comes out as proportional to the contraction difference between the dorsal and ventral muscles. In their model these dorsal and ventral muscles are collapsed into single units which are excited by a central pattern generator (CPG)[13]

[13] A central pattern generator is an intrinsically oscillating unit or in neuroscience typically a group of rhythmically firing neurons, for instance the lobster's stomatogastric ganglion contains CPG circuits that produce rhythmic activation of the stomach allowing the animal to chew its food.

and a single linear sensory neuron. The linear response of the sensory neuron poses a problem. In the absence of physiological recordings at the time, the authors reduced the computation to a minimal sequence of basic operations. Hence the neuron was taken to be linear, and to transform the linear response to a motor command that effects a change in heading, they introduced a derivative, subject to a capacitive filter, that imposes a slow timescale on the neuronal response. Nonetheless, the model is elegant in its simplicity of the descriptions and is used as a basis for future models and the model created in this thesis.

Pierce-Shimomura *et al.* 1999

This paper investigated the possible mechanism by which *C. elegans* navigates up a chemical gradient. They found no evidence for steering but did find that *C. elegans* modulates its pirouette probability in response to its bearing relative to the gradient, also known as tumble and run strategy or klinokinesis. To test their hypothesis the authors created a highly abstract model which only used klinokinesis and found that the model's trajectory characteristics matched the experimental results closely. However, the real animals produced a higher chemotaxis index than the model. This led the authors to speculate (rightly) that *C. elegans* might use a weak form of steering in addition to pirouette modulation.

The model falls into the class of behavioral models that lack explicit representations of neurons or neural circuits. In the spirit of minimalism, worms consisted of points that moved once every second, with a speed and direction sampled randomly from distributions determined experimentally. The pirouette probability was changed depending on the angle between the heading of the worm and the gradient, again by sampling randomly from an experimentally derived distribution. This first model of *C. elegans* chemotaxis produced quite realistic trajectories on first approximation, but naturally the absence of any detail precludes the use of the model beyond their research

question: whether *C. elegans* uses pirouette modulation to navigate.

Dunn *et al.* 2006

This study used simulated annealing to predict the basic network motifs for *C. elegans* chemotaxis. The authors explain their motivation to move beyond the sensory neuron and motor neurons into the then unexplored part of the nervous system: the interneurons. The work relied on two assumptions, first that the sensory neurons provide the absolute concentration of the current location, and second that the interneurons connect to a motor system that regulates the pirouette probability. We now know that the first assumption does not hold as most sensory neurons respond to changes in concentration [97, 100]. Nonetheless the general idea is interesting as an exercise in functionally analyzing a neural network. The network used by the authors was held constant, two sensory neurons (modeled after ASEL and ASER), a single interneuron and an output neuron. The weights between the neurons, the neuronal time constant and the 'bias' (a constant excitation or equivalently the resting activation) of each neuron were explored with simulated annealing.

After searching the parameter space, the authors grouped the resulting solutions into generic motifs using a technique called Neural Dynamic Clustering. This grouping was done purely based on parameter values, but was finally interpreted by the authors based on their circuit properties. Two distinct interpreted groups emerged, both with the same function: differentiation of the concentration over time. The first group used the interneuron as a slow delayed rectifier, the second motif used one slow and one fast sensory neuron with opposing polarities and did not use the interneuron. One alternative motif, dubbed trap and bounce was also found, where one sensory neuron suppressed pirouettes and the other neuron pushed the pirouette rate to its maximum, but this solution produced rather unnatural trajectories.

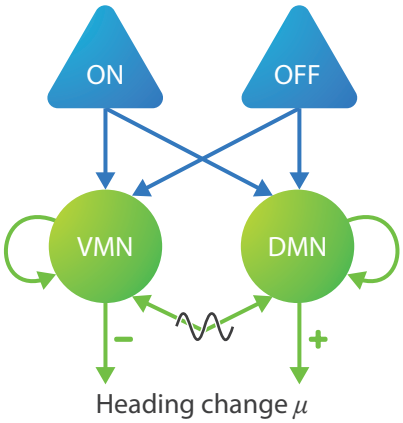

Figure 2.2: The neural network used in the study by Izquierdo and Lockery [57]. The network consist of two sensory neurons (blue triangles), ON and OFF, responding to increases and decreases respectively; two motor neurons, VMN and DMN (green circles), and an oscillator in the form of a sine wave (black wave). The difference between the two motor neurons drives the change in heading μ. Connections are shown with arrowheads, including self-connections for the two motor neurons.

Interestingly all circuits but the trap and bounce motif performed a derivative like computation. As mentioned earlier, we now have very clear evidence that this computation exists across sensory modalities, though not in the circuit but in the sensory neurons themselves.

Izquierdo and Lockery, 2010

Following up on the earlier steering model of Ferrée and Lockery, the authors extended the earlier model of ASE sensory neurons, now incorporating new evidence of their operation as derivative-like operators, to study their role in steering. The year before an experimental study by Iino and Yoshida [52] showed conclusively that *C. elegans* used not just pirouette modulation but also gradual steering. The minimal model structure and the methodological approach are essentially unchanged: a point body driven by a nervous system consisting of two opposing sensory neurons and two motor neurons (Figure 2.2),

where the parameters of the model are set using an evolutionary algorithm. However, after the work by Suzuki et al. [97] and Thiele et al. [100] the sensory neurons were seen as approximating derivative operators. To accommodate this, the sensory neurons were changed to have two opposing components producing a transient response to changes in concentration. Using this setup, the authors found they could produce highly efficient steering in a symmetric circuit if the two sensory neurons had opposite polarity and the motor neurons responded only during half of their duty cycle. The antisymmetry in the CPG driving the motor neurons then leads to input from the sensory system only affecting the motor neuron that is currently inactive (or active in another parameter regime).

As the model presented in this thesis is closest to the model by Izquierdo and Lockery, I will provide the inner workings of their model here in greater detail. The two motor neurons in the model are modeled using a first order linear ordinary differential equation (ODE) with a decay, a self-connection with weight w_s and a synaptic input I_i^{SI}:

$$\tau_m \frac{dV_i}{dt} = -V_i + w_s \sigma(V_i + \theta) + I_i^{\text{SI}} \,. \tag{2.1}$$

Where the sigmoid is defined as

$$\sigma(x) = (1 + e^{-x})^{-1} \,, \tag{2.2}$$

and the synaptic input as the weighted sum over the activity of the presynaptic neurons

$$I_i^{\text{SI}} = \sum_k w_{ki} V_k \,. \tag{2.3}$$

The sensory neurons used a time buffer of past concentrations ($C(t)$) to compute the instantaneous activation level (V_{SENSORY}). Their activity was set as the difference of the average concentration over a prior period with the average concentration of the period

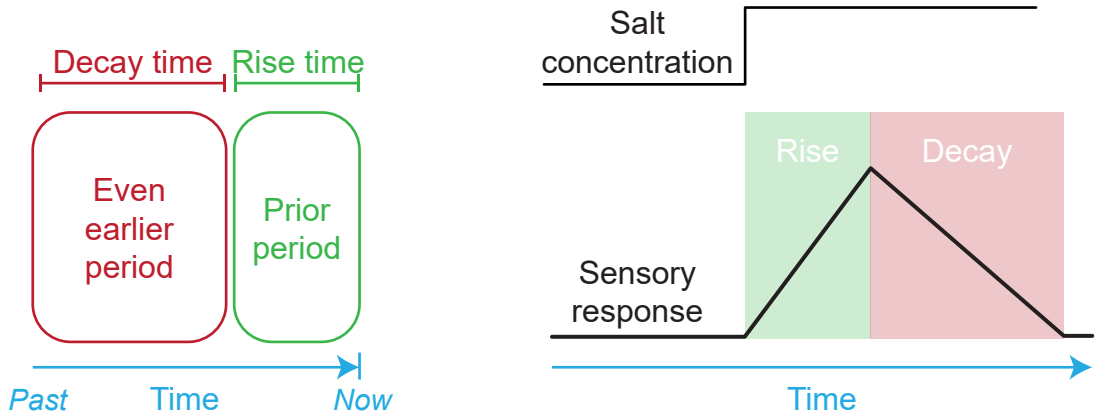

Figure 2.3: The sensory neurons used in the study by Izquierdo and Lockery [57]. The average concentration in the 'prior period' (in green) is compared to the average concentration in the 'even earlier period' (in red). This produces a response to a concentration step change (right). The duration of the increase is set by the 'rise time', τ_r while the relaxation to baseline lasts for as long as the 'decay time', τ_d.

even before the prior period:

$$V_{\text{SENSORY}} = \int_0^{\tau_r} C - \int_{\tau_r}^{\tau_r - \tau_d} C \,. \tag{2.4}$$

Thus the sensory neurons are governed by two key parameters called 'rise time', τ_r and 'decay time', τ_d (Figure 2.3). The precise values of these two parameters are very important as I will explain below.

The animal body is represented as a point in a two dimensional space moving with fixed speed $v = 0.022$cm/s along a heading μ. The change in heading depends on the difference between two sigmoids, and is subject to a further Gaussian noise ζ with a mean 0 and standard deviation 0.05. Each sigmoid transforms the activation level of one motor neuron (ventral or dorsal) into the activation of the corresponding (ventral or dorsal) 'muscle':

$$\frac{d\mu}{dt} = w_{\text{NMJ}} \left[\sigma(V_{\text{dmn}} + \theta) - \sigma(V_{\text{vmn}} + \theta)\right] + \zeta \,. \tag{2.5}$$

I have put muscles between quotes as the model does not describe muscles as a separate component but instead simplifies the muscles activation to a sigmoid over the motor neuron activation. Additionally a bias term θ is added to determine the sensitivity to sensory inputs as a function of duty cycle.

The virtual environment consists of a conical concentration gradient. Even though a Gaussian gradient would be more similar to experimentally used assays, the authors claim these would lead to unrealistic model worm trajectories. The concentration at (x, y) is thus simply the euclidean distance from the center or αr where r is the distance to the center in a radial coordinate system.

Appleby 2012

The model presented in Appleby [3], is similar to the model by Izquierdo and Lockery [57] but with a different, more detailed and physiological motivated model of the sensory neurons. Like Izquierdo and Lockery [57], this model included two sensory neurons (ASEL and ASER), an interneuron and two motor neurons. Additionally, an abstract pirouette command neuron was added to allow pirouette modulation. The latter was particularly unique as both the pirouette probability and the final turn angle are modulated. The aim of this model was somewhat different from the previous, looking not just at chemotaxis but also at associative learning.

The sensory neurons are modeled with two populations of ion channels driving the membrane potential (a depolarizing and a hyperpolarizing channel). The depolarizing channel's activation rate is proportional to the NaCl concentration with a threshold. The interneuron and motor neurons on the other hand are just instantaneous linear sums of the membrane potential of the pre-synaptic neurons.

While steering functions largely as in Izquierdo and Lockery [57], pirouette modulation is very different from Ferrée and Lockery [37]. First the final turn angle is randomly

picked from a modified Gaussian centered at π[14]. The Gaussian is calculated using two components, one pure Gaussian, and one bias term dragging the final turn angle to 2π. The balance between the two components is determined by the activity of the abstract pirouette command neuron. The pirouette probability is calculated using a Poisson process whose rate is linearly dependent on the same abstract pirouette command neuron.

To add associative learning a binary serotonin signal indicating food presence was added to model, together with dynamic weights between the sensory neurons and the interneuron. The weights were updated using a modified Hebb's rule. Additionally, an alternative learning rule is devised where the scaling parameters (maximum conductance) of the sensory neurons become plastic, changing as a function of the NaCl concentration and the serotonin state.

The author is careful to show agreement between the model sensory neuron's activity to up and downsteps and experimentally measured calcium imaging data, though the same time scales for ASEL and ASER were used (averaging the experimentally obtained time scales for the two sensory neurons). Also, in agreement with all earlier modeling work, opposite polarities of the two sensory neuron's synaptic weights are required for the model to function. More interestingly, using the highly simplified circuit, the sensory neurons' output can drive the pirouette probability, the final turn angle, and steering to generate successful chemotaxis. The model also finds both sensory neurons and all three chemotaxis strategies contribute to navigation. Finally, both the Hebbian learning and the non-Hebbian intracellular learning both reproduce the form of salt learning tested.

[14]In Appleby [3], on average model animals turn 180 degrees during a pirouette, in reality the average is likely to be slightly less, around 150 degrees [42].

Chapter 3

Analysis of the Izquierdo and Lockery model

3.1 Introduction

In this chapter I will explore the existing computational model by Izquierdo and Lockery [57], reproducing the original model, and then continuing to do a deeper analysis, looking at its strengths and its limitations.

As mentioned in the previous chapter, the previously published model by Izquierdo and Lockery [57] has particularly interesting characteristics (its parsimony, accurate steering and circuit properties), making it a good starting point to assess what a generic model of *C. elegans* chemotaxis should look like.

To understand the limitations and complexities of the computational model of *C. elegans* chemotaxis, presented by Izquierdo and Lockery [57], I started my work by reproducing their model. I had two questions I wanted to answer: first, to see whether their model could be further simplified (i.e. whether it is the most parsimonious description that can reproduce their modeling results), and second to further explore their model and see where

it breaks down. I then used the answers I found to create my own model.

While all equations are given in the Izquierdo and Lockery [57] paper, the same is not true for the parameter values, since they present a group of high performing solutions with different parameter values. To choose the missing parameter values I opted to do a combination of sensitivity analyses and manual tweaking. I starting out by setting the rise and decay times to low values (all at 0.5 second) to fit the region of values found by Izquierdo and Lockery [57]. Then, I performed a parameter sweep of the muscle bias parameter θ to see if the high chemotaxis index (defined by the authors as the average distance from the concentration peak) of over 0.8 could be achieved. This first sweep showed my simulation could convincingly reproduce the original strength of the chemotaxis (Figure 3.1). Doing the parameter sweep also showed that the bias parameter has an important symmetry breaking function. For bias values of around -2 or +2, the steering strength is maximized (in opposite directions). This is due to a shift in the sigmoid as already shown by Izquierdo and Lockery. What was not clear from their work though, is how this shift in the sigmoid and the rise and decay time relates to steering. A hint of this relationship can already be seen in Figure 3.1, where the curve is asymmetric about the 0 chemotaxis index.

To show the effects of the bias parameter on steering I simplified equation 2.5 by leaving out the Gaussian noise and the neuromuscular weight. These can be safely removed since neither has a (mean) effect on the relationship between the bias parameter and steering strength or direction. Expanding V_{dmn} and V_{dmn} (omitting the self connection for simplicity) then gives:

$$\frac{d\theta}{dt} \propto \sigma(\sin(2\pi\frac{t}{T}) + I(t) + \theta) - \sigma(-\sin(2\pi\frac{t}{T}) + I(t) + \theta)\,. \tag{3.1}$$

Before looking closer at the bias parameter, it is useful to reflect on how the Lockery system steers. Using the simplified equation above, it is easy to see that the change in

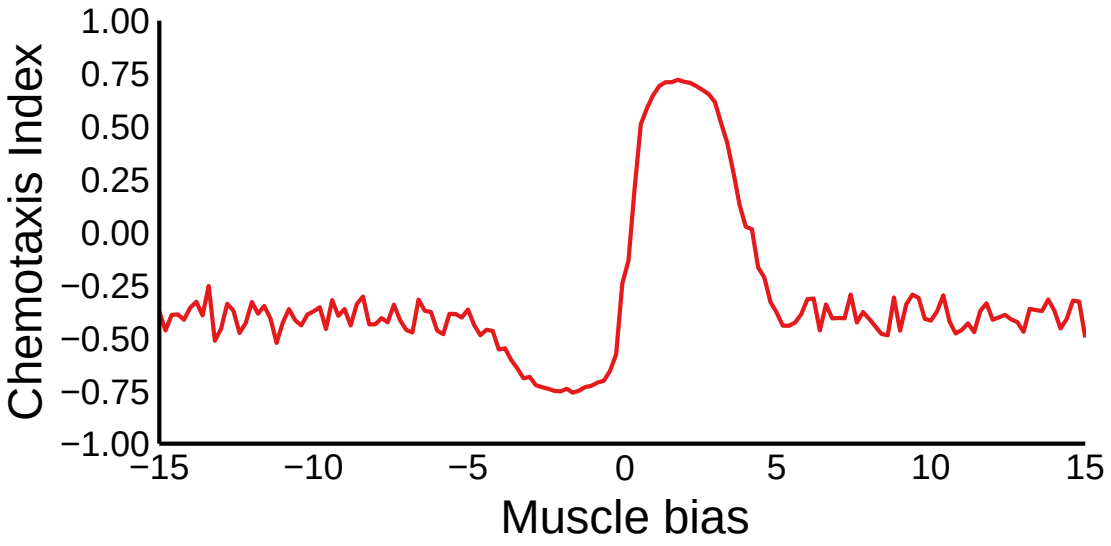

Figure 3.1: The chemotaxis index (normalized average distance from gradient peak over 500 seconds) as a function of the muscle bias ζ, or the shift in the sigmoid activation function of the two motor neurons.

heading over time is proportional to the difference between the activation of the dorsal and ventral motor neurons. Thus, to steer, there must be a net difference between the activity of these two motor neurons. In the absence of sensory input, the activation of the two motor neurons are two sine waves in antiphase (Figure 3.2A, bottom left panel). Because the activity of the two motor neurons are equal and opposite, there is a change in heading but no steering. After each undulation period the heading returns to the value of one undulation period earlier. This can be seen in the bottom left panel of Figure 3.2A where the net heading change (area under the curve, colored in purple) over one undulation period is 0.

Imagine that both motor neurons receive identical sensory input for an entire sine wave period. In this case both neurons would shift up or down an equal amount, which would change the shape of the undulations but would not steer the animal. If instead there is a difference in the sensory input between the two halves of an undulation, the bearing does not end up in the same point and the animal steers. To show this, a monotonously

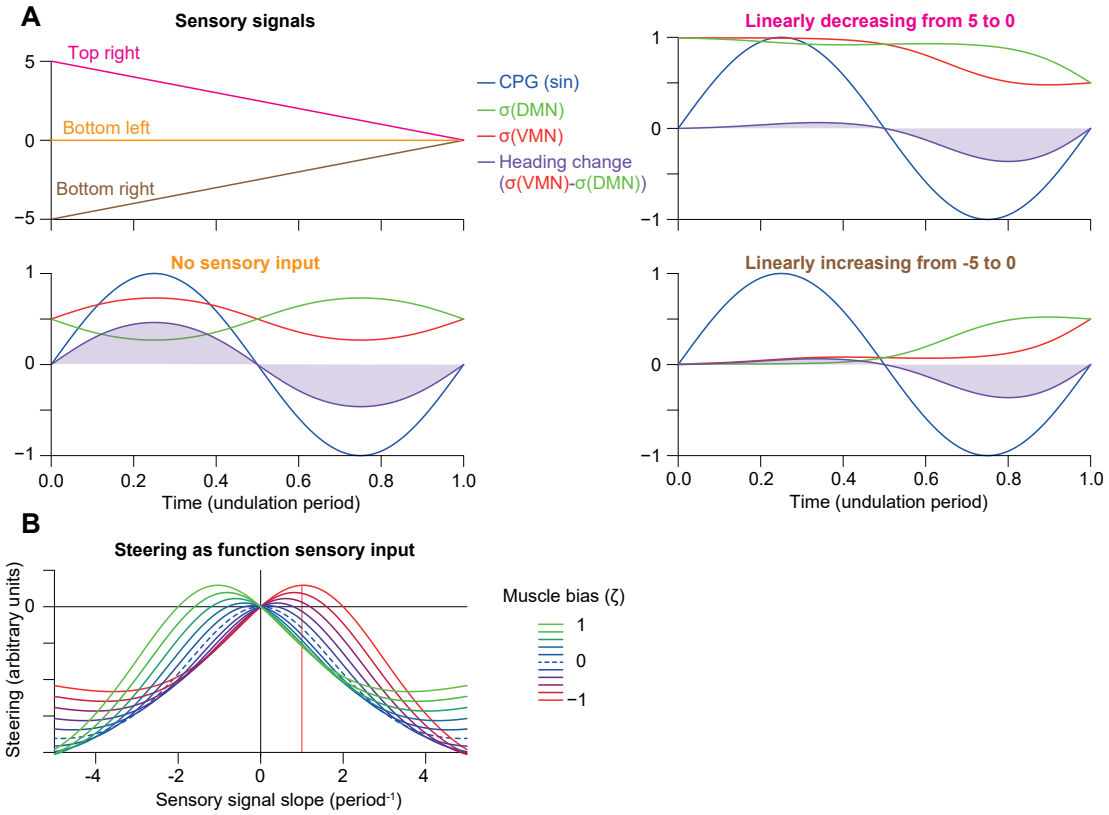

Figure 3.2: The effect of a monotonously changing sensory signal on the change in heading during a single period of an undulation. A, top left: Three sensory signals corresponding to the three top panels. A, bottom left: the change in heading in the absence of sensory input is symmetric between the two half periods causing the virtual worm to end up in the same heading after a full period as before (no steering occurs). A, top right & bottom right, linearly decreasing and increasing sensory signal respectively. The shaded area under the curve of the heading change shows the net change on the heading. If the integral is 0, no steering occurs. B: Steering strength (area under the curve of the heading change) as a function of the sensory signal slope and the muscle bias. For muscle bias of 0, the change in heading is identical for positive and negative sensory inputs (Equation 3.2). For other values steering can occur in both directions though not for all inputs.

changing sensory signal can be added to the motor neurons. In figure 3.2A the heading change is shown for sensory inputs changing from 5 to 0 or -5 to 0 over the course of one undulation. Both inputs produce symmetry breaking shifts in the motor neuron activities, leading to a strongly weakened heading change in the first half and a slightly weakened heading change in the second half. Interestingly, the heading change for the decreasing sensory input is equal to the increasing input, even though the activities of the motor neurons are different. Indeed, it turns out that, with a bias $\theta = 0$, for all sensory inputs I and central pattern generator inputs $S = \sin(2\pi\frac{t}{T})$, positive and negative sensory inputs produce identical changes in heading:

$$\frac{1}{1+\exp(S+I)} - \frac{1}{1+\exp(-S+I)} = \frac{1}{1+\exp(S-I)} - \frac{1}{1+\exp(-S-I)}\,. \quad (3.2)$$

In other words, the polarity of the downstream synaptic weights from ASEL and ASER is irrelevant for their ability to steer. However, all solutions of the evolutionary algorithm of Izquierdo and Lockery [57] used opposite polarities for the synaptic weights of ASEL and ASER. Closer inspection showed this to be due to the fact that their opposing responses summed cancel each other out (this is particularly true since ASEL and ASER have identical parameters and thus equal response times).

A more problematic consequence of identical steering resulting from positive and negative sensory inputs is that the steering system in the Izquierdo and Lockery model fails to distinguish between attractive and repulsive gradients (responding with similar orientations of steering to both). The bias term appears to have been added to break this symmetry and allow correct steering for animals moving up the gradient and down the gradient. To assess to what extend the bias term can alleviate this issue, I performed a sweep of the bias term and looked at the change in heading as a function of the slope of a monotonously changing sensory input (Figure 3.2B). With a bias of 0 (dashed line), we confirm the symmetric relationship of equation 3.2. With non zero values there is a shift in the curve which produces correct steering up to a limit. Beyond this limit the steering

direction reverses again, producing anti steering. Naturally, we expect the biological worm to steer up attractant gradients and down repellent gradients, and it is reasonable to assume that it responds robustly across a high range of gradients [67]. Hence, this is a major flaw in the model description of Izquierdo and Lockery [57], which prevents the model from showing correct chemotaxis across assays and concentration strengths.

While Izquierdo and Lockery created an elegant and parsimonious model, they did not set out explicitly to make it minimal (e.g. by penalizing model complexity in their fitness function). Minimal models may not necessarily offer greater biological realism, but they can help us tease out minimal system requirements, and to make the model analysis easier. While 'minimizing' the complexity of a model is not trivial to do in practice within an evolutionary search framework, manual tweaking of the model can often more easily achieve this aim. I therefore set out to identify the essential components of the Izquierdo-Lockery model. Interestingly, I quickly found that several features of their model could be removed without reducing the chemotaxis index (the performance metric used in Chapter 3). These include: the self-connections of the motor neurons and the presence of Gaussian noise. The last one is obvious, as the noise was only added to make the evolutionary algorithm more robust. In the paper, the self-connections are said to have been added to introduce a time scale as the model neurons themselves are instantaneous. By removing the self-connections in motor neurons, the motor system inherits the time scale of sensory neurons (i.e. their rise and decay times) and the undulations period. To explore this further, I ensured that my implementation of the Lockery model steered similarly by doing a sensitivity analysis on the rise and decay time. This was inspired by the pattern that could be seen from the data presented in the original paper. There, the authors find that all high performing solutions have a rise time less than half the undulation period, but additionally, a diagonal pattern can be seen, with a diagonal trough of repulsive chemotaxis and a peak of attractive chemotaxis[1] (figure 3.3). The dots show

[1] Attraction and repulsion, seen here as peaks and troughs respectively, can be flipped by swapping the sign of the bias parameter

the high performing values from the original study, the full view shows they all lie in the same region.

Further simulations for longer rise and decay times show a repeating pattern. From this figure it seems that the rise time must be synchronized to the undulation period, and to a lesser extent the decay time too. Changing the undulation period in the model confirms this hypothesis. In fact, the constraints imposed by the undulation period on sensory neuron parameters can be seen intuitively by reasoning about how the model steers. First, the circuit is symmetric. Second, steering can only happen because the motor neuron's sigmoid activation function have been shifted to make them amenable to input only half their duty cycle, in plain language, when one motor neuron is sensitive to input the other is not and vice-versa. Thus for steering to be effective, the input to the ventral and dorsal sides must have opposite polarity. Therefore, the sensory output (onto the motor neurons) must change sign between the half-undulations in which the dorsal and ventral motor neurons are sensitive to input. This requirement imposes strong constraints on the rise and (less so) the decay times of the sensory neurons. Specifically, the integral of the input must be different (i.e. the net increase or decrease in activity) as the activity is proportional to the change in heading. Now we can see why the sensory neuron's response must be synchronized, consistently in phase, or consistently out of phase, to the motor system: the time delay of the response determines which motor neuron is active (and sensitive or insensitive depending on the shift in the sigmoid), and thus increasing the delay moves the peak response away from the moment where the initial motor neuron is most sensitive. With a delay 1/4th of the undulation period, half way in between the maximum sensitivity of the two motor neurons no steering occurs. At half the undulation period the other motor neuron will be most sensitive to sensory input, producing anti steering.

Recently there was a study which seems to support this hypothesis of steering in the biological worm [62]. In this paper, a mutant was found which had a delayed response in one of the AWC sensory neurons. When testing the steering response as a function of

the angle between the heading of animals and the direction of the chemical gradient, the authors found the mutants anti steered for half the angles. While the authors do not make the link to the Izquierdo and Lockery model, I interpret their results to suggest that within the receptive field of the sensory neuron, the slowdown has pushed the sensory signal out of sync to the motor system, causing anti steering. In fact slowing down ASEL or ASER in my reproduction of the Izquierdo and Lockery model reproduces the experimental results strikingly.

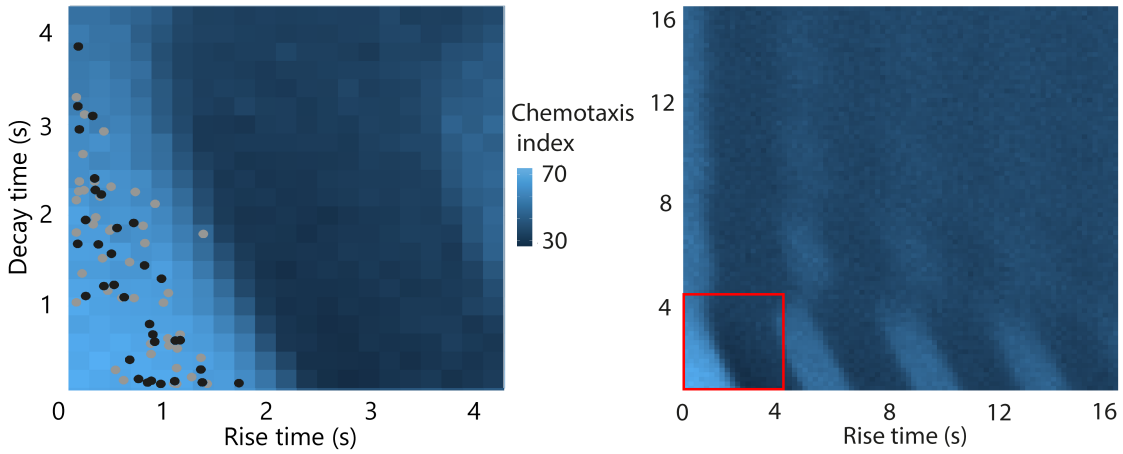

Figure 3.3: The chemotaxis index as a function of the rise time and the decay time over a single undulation period (left), and four undulation periods (right). The gray and black overlaid circles show the parameter values of high performing solutions found in [57]. All solutions lie within the same diagonal peak.

To better understand the effect of the self-connections I simulated the original model with varying strengths of w_s. Clearly, self-connections introduce feedback. For low values of w_s the same can be achieved using the neuronal time constant τ_m (τ in the original model). For higher values of w_s the motor neurons can get 'stuck' in high or low levels of activity, as the self-connection starts a feedback loop pushing the neurons to saturation. Once saturated, the dynamic range is severely limited (i.e. the change in activity in response to an input signal). Since the circuit ensures both motor neurons receive identical sensory input, and since they share a single self-connection strength parameter value, the ratio between and sum of the oscillating input, the sensory input and the self-connection

determine whether both motor neurons can become saturated simultaneously, only one, or none. If the parameter regime is such that both can become saturated, sensory input has very limited effect, thus severely hurting the chemotaxis index. When only one motor neuron can be saturated at a time, the chemotaxis index might actually increase. This is because the difference between the activity of the two motor neurons determines the change in heading. As both receive identical sensory input, their response to the sensory input needs to be different for steering to occur. Thus high values should reduce the chemotaxis index, while low values should increase the chemotaxis index. However, the careful reader should have noticed that there is another mechanism already capable of producing different input-output functions for the two motor neurons. The bias parameter ζ (θ in the original model) for instance can be used to change the sensitivity of the two motor neurons depending on their point in the their duty cycle.

Part II

Integrated model

Chapter 4

Creating my own model

The computational model presented here was built to simulate single worms in a variety of assays with the aim of studying sensory integration and decision making. Since this does not directly involve the physical constraints onto the body, and since biophysical models have a large computational cost [13, 56], I do not model the body. Instead, I assume that during locomotion, the body follows the head [57]. This allows us to represent animals as a point with coordinates $x(t),\ y(t)$ moving with bearing θ and fixed speed v. The direction of locomotion is driven by a simplified nervous system.

Neuronal properties and parameters of the motor system were constrained by calcium imaging data from the Jansen lab, previously published calcium imaging data [97, 100] and behavioral data from choice assays [50, 51, 58]. The motor output consists of steering and instant turning events, representing pirouettes. The ability to combine steering and pirouettes in a single model has proved essential in matching behavioral results under different conditions. Specifically, prior studies have shown that both pirouettes and steering play a role in navigation [3, 52]. Here we find that the relative contribution of both navigation strategies is strongly assay dependent, with steering more important in sharp gradients and pirouettes in shallow or noisy environments.

I start by describing all the model components and their assumptions. To ensure a solid grounding in experimental data, I will show the output of each component under different conditions and compare this to experimental data where possible. Once the full model has been described I will use several case studies to compare the model worm behavior with actual animals, and highlight multiple key predictions that helped inform experimental setups and led to increased understanding of the circuit functioning in unisensory and multisensory chemotaxis assays.

4.1 Model overview

Our model consists of a point worm moving at fixed speed in a two dimensional space (the arena). This point worm is controlled by a simplified *C. elegans* nervous system that consists of sensory neurons, either one or two interneurons, and an abstract motor system (Fig 4.1). The motor systems combines steering (superimposed on symmetric undulations) and stochastic 'omega' turns (in which the worm curves into an Omega-like shape and then proceeds in a new direction).

To create a predictive model of *C. elegans* chemotaxis we required a strong grounding in prior experimental data and close collaboration with experimentalists. The latter ensures we can use an iterative approach, improving the model and our hypotheses for each iteration. Additionally, we limited our scope to the circuit and cellular level, deliberately skipping (most) molecular details, as we felt not enough molecular details are known to create semi-complete molecular pathways. Also, given that most neuronal activity recorded in *C. elegans* to date come from calcium imaging data, and our collaborators used only calcium imaging we decided to model our neurons using abstract conductances and membrane potentials with arbitrary units. Finally, we assume three key neuronal properties: neurons are graded leaky integrators, neurons have rectified responses [97] and neurons respond with transient, derivative like operators [80, 100]. These assumptions

were done to be close to the biology, but we also felt these assumptions are key to understanding *C. elegans* chemotaxis. Specifically, transient responses suggests animals do not have a representation of absolute stimulus strength (e.g. not knowing the difference between a concentration increase from 10 to 20mM and 20 to 30mM), while the time scale of the transient suggests a coupling to the undulation period (as described in the previous section), and dynamic modulation hints at a Weber-Fechner like relationship (a relation between the absolute stimulus strength and the effect a given change in the stimulus strength has on the sensory response). While the first two have been modeled before, dynamic modulation has never been investigated computationally (though one study included threshold adaptation as a mechanism for adjusting dynamic range [3]).

As my PhD focuses on unisensory and multisensory integration, and in particular on the integration of chemical signals (in the context of chemotaxis behaviors), I have chosen to include sensory neurons that are known to be involved in a variety of multisensory integration assays. These include the ASE pair (sensing attractive soluble molecules, such as salt), the AWA pair (sensing attractive odorants, such as diacetyl) and the polymodal ASH pair (mediating avoidance). With this set of neurons, I will model a number of NaCl assays, as well as diacetyl-copper and diacetyl-fructose sensory integration assays. As the sensing of the presence of food (as distinct from chemical stimuli) is more complex and likely involves many more neurons, it will not be modeled here. The internal state of the animal (e.g. food deprivation) is likely encoded in a more distributed manner, and will be modeled more abstractly. The minimal motor system consists of two motor neurons (VMN and DMN) to support undulations and steering and a motor command unit (Ω) regulating the frequency of pirouettes (Fig. 4.1).

We model neurons as leaky integrators (with arbitrary units)

$$\tau_m \frac{dV_i}{dt} = -V_i + V_{0,i} + \sigma\left(I_i\right), \tag{4.1}$$

where V_i is a voltage like variable for neuron i, also referred to here as neuronal activation;

τ_m is a neuronal time constant; $V_{0,i}$ is the activation level at rest (set throughout to 0); and $\sigma(I_i)$ is a modified sigmoid function over the input (henceforth the index i is dropped for simplicity of notation)

$$\sigma(I) = \frac{1 - e^{-bI}}{1 - \frac{e^{-bI}}{I_{\min}}}, \tag{4.2}$$

where b is a gain parameter and $I_{\min} < 0$ is the most hyperpolarized value the neuron may take (relative to the rest state). The function $\sigma(I)$ varies smoothly and monotonically from $I_{\min}$ to 1, crossing 0 at $I = 0$. Thus, in response to a constant input I, a neuron's activation converges to $V_{0,i} + \sigma(I)$ with a timescale of τ_m. Applying a sigmoidal function over the sum of membrane and input currents is borrowed from the simplified rate neuron models, and naturally leads to thresholding and saturation of activation, as observed in *C. elegans* sensory neurons [97, 100]. Parameter values are given in a table in each section of the supplementary methods.

The input current I sums over all synaptic and sensory contributions $I = I_{\text{syn}}(t) + I_{\text{sens}}(t)$, where, assuming graded synaptic transmission, $I_{\text{syn}} = \sum_j W_{ij} V_j$ is a weighted sum over all presynaptic neuron activations (onto neuron j)[1] and, in sensory neurons, I_{sens} denotes the current response to the stimulus. Note that hyperpolarizing a neuron will effectively reverse the polarity of its synaptic transmission (with hyperpolarizing and depolarizing postsynaptic effects across excitatory and inhibitory synapses respectively).

Undulations and steering are modeled by a symmetric oscillator motif, consisting of reciprocal inhibitory and reciprocal delayed excitatory connections (Fig. 4.1F). We used *hidden* interneurons to create a delayed connection between motor neurons. Thus, the delayed excitatory connection from VMN to DMN is implemented as two connections, one from VMN to the hidden interneuron, and another from the hidden interneuron to DMN, using the neuronal time constant of the hidden interneuron, τ_m, as a synaptic delay.

[1] Where two connections exist from neuron i to j (specifically, between VMN and DMN), the weights are distinguished by a superscript indicating the polarity of the connection: $-$ for inhibitory and $+$ for excitatory.

The reciprocal connection from DMN to VMN is identical.

Neuronal parameters	**Value**	**Description**
τ_m	$0.5\ s$	Neuronal time constant
$V_{0,i}$	0	Resting potential
$I_{\min}$	-1	Maximum hyperpolarization (relative to rest)
b	4	Neuronal gain
Synaptic weights	**Value**	**Description**
$W_{\text{ASEL},m}$	-0.07	ASEL onto DMN and VMN
$W_{\text{ASER},m}$	0.07	ASER onto DMN and VMN
$W_{\text{ASH},m}$	0.07	ASH onto DMN and VMN
$W_{\text{ASEL},\Omega}$	-0.1	ASEL onto Ω
$W_{\text{ASER},\Omega}$	0.1	ASER onto Ω
$W_{\text{ASH},\Omega}$	1	ASH onto Ω
$W^{+}_{\text{D,V}}$	0.8, 0.9	DMN to VMN excitation (to, from hidden neuron)
$W^{+}_{\text{V,D}}$	0.8, 0.9	VMN to DMN excitation (to, from hidden neuron)
$W^{-}_{\text{D,V}}$	-1.4	DMN to VMN inhibition
$W^{-}_{\text{V,D}}$	-1.4	VMN to DMN inhibition

Table 4.1

4.2 Sensory neurons

For the three sensory neuron classes included in the model, the response profiles have been characterized relatively well using calcium imaging. Specifically, ASEL responds with a transient depolarization to an NaCl upstep between 10mM and 80mM [97]. ASER and ASH respond with a transient depolarization to NaCl decreases (between 1mM and 40mM) and with a transient hyperpolarization to increases in the NaCl concentration. Finally, AWA responds with a transient depolarization to diacetyl upsteps between 0.01 and 100 μM. All these responses (and likely other sensory neurons as well [20, 100]) can be viewed as approximations of derivative operators. What should be kept in mind, is that with few (recent) exceptions, behavioral assays are done on gradients, but calcium imaging is done in response to rapid concentration steps (increases and decreases) of fixed

magnitudes. In response to these steps, we see transients responses, above some threshold, and with smoothly increasing amplitude of response up to some saturation level. For this reason we have opted to focus on assays with sharp(er) gradients.

In contrast to the model by Izquierdo and Lockery (which uses finite time buffers with time spans to calculate the difference of the concentration over time), we propose to use a system with two opposing component. Across nature, two component systems are ubiquitous in driving excitability, neuronal activity in particular and transient responses more generally. In particular, neural membrane potentials (including graded potential neurons and calcium driven action potentials) are driven by opposing conductances with different time scales acting to depolarize and hyperpolarize the membrane potential. This is therefore the natural choice and is adopted here. Transient (derivative-like responses) in *C. elegans* sensory neurons have been modeled with various approaches, ranging from low level ion-channel models [3, 57] to minimal functional models using derivative-like operations [62]. The former are difficult to tune and lack experimental evidence to support assumptions. The advantage of the Izquierdo-Lockery framework is that it is easy to construct and tune, but, as shown before, it does not work for all concentration profiles, and the use of time-buffers is not based in physiologically. The alternative, more natural approach would be to consider leaky integrators over various gating or activation variables (here concentration or more generally stimulus intensity). In other words, rather than time-buffers, this approach uses activation and leak rates for different variables. This was the approach taken by Kato et al. [62] to model transient ASH responses. The main additional advantages of the Kato approach is that it is minimal, but as such it also lacks obvious properties such as thresholding and saturation that biological conductances and neurons exhibit. Most commonly (e.g. in Appleby [3], Izquierdo and Lockery [57], and Kato [62]), the opposing forces are both modeled as functions of the same sensory cue. The model presented here differs in that the delayed rectifying force is actually driven by the depolarizing force. This is both a strength and a limitation of my model. My approach for constructing the elementary transient response is in some ways most

similar to Kato's, but was derived independently and arose from different considerations. Namely, I attempted to link the kinetics of *C. elegans* chemotaxis neurons to processes in other eukaryotic cells (in uni- and multicellular organisms) that exhibit chemotactic responses. This has been modeled in detail for single celled amoeboids, where the change in concentration is calculated during chemotaxis using a fast signal and slow diffusing delayed rectifier [70]. A similar mechanism will be used here (though without diffusion). In addition, my model includes nonlinearities to account for thresholding and saturation.

The fast component simply changes proportional to the stimulus effect C:

$$\frac{dF}{dt} = -\alpha F + \beta C \,. \tag{4.3}$$

The effect of the stimulus on the sensory neuron, is set either proportional to the stimulus strength, or alternatively, as the log of the stimulus strength:

$$C_{\log}(x, y, t) = \log\left(\frac{C(x, y, t) + C_{\min}}{C_{\min}}\right) \,. \tag{4.4}$$

The slow delayed rectifier, responds proportional to the fast signal with rate γ:

$$\frac{dS}{dt} = \gamma(F - S) \,. \tag{4.5}$$

The sensory input to the sensory neuron is then the instantaneous difference between the fast component and the slow delayed rectifier:

$$I_{\text{se}} = F - S \,. \tag{4.6}$$

The activity of the sensory neurons V_i depends upon, similar to the motor neurons of the Izquierdo and Lockery [57] model, the sigmoid of the input. The input here being only the sensory input I_{se}:

$$\tau_m \frac{dV_i}{dt} = -V_i + \sigma(I_{\text{se}}) \tag{4.7}$$

The sigmoid function σ is an adapted sigmoid, set to go from -1 to 1 rather than 0 to 1, and $\sigma(0) = 0$:

$$\sigma(I) = \frac{1.5}{1 + 2\exp(-4x)} - 0.5, . \tag{4.8}$$

Assuming an instantaneous step change to the concentration, the solution for the fast signal is then:

$$F(t) = \frac{\beta C}{-\alpha}(e^{-\alpha t} - 1)\,, \tag{4.9}$$

and the slow signal:

$$S(t) = \frac{\beta C}{-\alpha}\left(\frac{\gamma}{\gamma - \alpha}e^{-\alpha t} - \left[\frac{\gamma}{\gamma - \alpha} - 1\right]e^{-\gamma t} - 1\right)\,. \tag{4.10}$$

In the model by Izquierdo and Lockery [57] the sensory neuron's rise and decay time are defined in terms of the response to a sustained increase or decrease in the stimulus strength. The time to peak depolarization was said to be the rise time, while the time to from peak depolarization to return to baseline was called the decay time. Due to the use of two sets of memories, the rise and decay time were free parameters of their model. In this model, the rise time can still be defined as the time to peak depolarization, but the decay time cannot, as the activity will get infinitely close to the baseline but will never reach it. Instead we use an arbitrary percentage. Thus we define the decay time as the time from peak depolarization until the activity has relaxed to below 1 percent of the peak depolarization amplitude. From our solution to the fast and slow components, we find that in our model, the rise time, t_r, is independent of the size of the stimulus increase and β but depends only on the decay of the fast signal, and the rate of the slow signal:

$$t_r = \frac{\log(\frac{\gamma}{\alpha})}{\gamma - \alpha}\,. \tag{4.11}$$

Equation 4.11 also shows that $\alpha$and γ are coupled in such a way that swapping the values of α and γ makes no difference.

While the the decay time, t_d, cannot be expressed in terms of elementary functions, the following relationship follows from my definition:

$$e^{-\alpha t_d} - e^{\gamma t_d} = 0.01 \left(e^{-\alpha t_r} - e^{-\gamma t_r} \right) . \tag{4.12}$$

Thus like the rise time, the decay time is symmetric in α and γ and independent of the stimulus and β, but also that $t_r < t_d$.

4.3 Motor system

The model contains two separate motor outputs: undulations and pirouettes. Both can be modulated by sensory inputs.

Motor output	**Value**	**Description**
v	0.11 mm s^{-1}	Forward speed
ω	0.8 s^{-1}	Steering strength/angular speed
V_{start}	0.001	Activity of oscillator start signal
τ_{start}	0.01 s	Duration of oscillator start signal
w_Ω	1 s^{-1}	$P_\Omega(V_\Omega)$ proportionality constant
$\overline{V}_\Omega$	0.035	Pirouette neuron modulation offset
ϵ	0.035	Pirouette neuron modulation range

Table 4.2

Undulations: Two motor neurons (VMN, DMN) in a half-center oscillator like configuration (Fig. 4.1) are shown to be capable of generating and maintaining stable oscillations as well as to steer the worm. The reciprocal connectivity pattern is reminiscent of connectivity found in several classes of head motor neurons in *C. elegans*. Compared to more compact models, e.g., Izquierdo and Lockery [57], our approach allows for the

modulation of the undulation frequency as well the amplitude, more closely matching observed trajectories of worms in the choice assay, especially in the vicinity of the quadrant boundaries.

In contrast, with a simpler model relying on a master pacemaker (adapted from Izquierdo and Lockery [57]) I was unable to account for a significant proportion of worm trajectories without changing the undulation amplitude to unrealistic levels (data not shown).

In the absence of sensory input, the motor circuit will produce stable oscillations, facilitated by fast reciprocal inhibition that is released by the delayed reciprocal excitation (Fig. 4.1). Any activity in one of the oscillating neurons will cause fast inhibition of the other followed by slower excitation and subsequently inhibition of the originally active neuron. Thus the frequency and amplitude of the oscillations are determined by the time scales of the neurons (τ_m), the connection strengths of the reciprocal inhibition, and delay in the delayed reciprocal connections. In our model, τ_m remained fixed, leaving the three pairs of reciprocal connection strengths as parameters to tune the oscillator. The circuit configuration and neuronal time constants set the minimum undulation period to $4\tau_m$.

Since the circuit configuration and all parameters are symmetric, symmetry breaking is required to set off the oscillations. Indeed, when VMN and DMN are equally active, the circuit does not oscillate. However, any small difference in activity (or initial conditions) is amplified by the mutual inhibition. In the model, a start 'signal' V_{start} is given for a short duration τ_{start} with opposite polarity to the two motor neurons VMN and DMN, causing them to diverge in activity. In the biological worm, environmental and physiological fluctuations will ensure small differences in activity even in a symmetric circuit.

Similar to other point models of *C. elegans* [16, 17, 57], the direction of locomotion (θ) changes as a function of the difference in activity of the dorsal and ventral motor neurons:

$$\frac{d\theta}{dt} = \omega \left(V_{\mathrm{VMN}} - V_{\mathrm{DMN}} \right), \tag{4.13}$$

where ω is the steering strength. Model worms move with constant velocity v along the direction vector θ according to

$$\frac{d(x,y)}{dt} = (v\ \sin\theta, v\ \cos\theta)\,. \tag{4.14}$$

Pirouettes. Instant turning events are executed by resetting the orientation of movement of the point worm. The probability of a pirouette per unit time P_Ω is encoded by the activation of the pirouette command unit V_Ω and given by a piecewise linear and monotonically decreasing function:

$$P_\Omega(V_\Omega) = \begin{cases} w_\Omega\ (\overline{V}_\Omega + \epsilon), & V_\Omega < -\epsilon \\ w_\Omega\ (\overline{V}_\Omega - V_\Omega), & -\epsilon \leq V_\Omega < \ \ \epsilon \\ w_\Omega\ (\overline{V}_\Omega - \epsilon), & \epsilon \leq V_\Omega\,, \end{cases} \tag{4.15}$$

where w_Ω converts the neuronal activation to a probability rate, such that $w_\Omega\,\overline{V}_\Omega$ is the base pirouette rate. The parameters were chosen such the base rate is approximately 2.1 pirouettes per minute, and suppression of pirouettes (for sufficiently hyperpolarized values of the neuron) is complete.

When a pirouette is executed, the heading, θ, is instantaneously set to a random value between 0 and 2π drawn from a uniform distribution.

4.4 Assays

The model simulation file supports several types of assay, plates can be bounded circular or square, or infinite in size. Additionally, virtual worms reaching the edge of a plate can be handled in three ways: the simulation can be stopped, reflection can be used, or a random reorientation can be done. The last option was used for all subsequent results

as it is closest to the real worms behavior[2]. There is no limit on the number of stimuli in a simulation, though in this thesis I never use more than two at a time. Stimuli can be selected by choosing built in options, such as a uniform strength, a linear gradient, a conical gradient or a Gaussian gradient. Alternatively a function of the coordinate and time can be specified for each stimulus in the simulation file allowing for more complex stimulus fields (for instance the hyperosmotic fructose and diacetyl assay used this option). In the current version of the model, sensory neurons can only respond to a single stimulus per simulation. While in principle the model could support more than one stimulus per neuron, more parameters would be needed if the sensory pathways for each of the stimuli in the sensory neuron had shared components.

Details of each assay used are given in the respective chapters.

4.5 Model framework

The model framework was written in Java, to allow it to run on multiple architectures (e.g. Windows, Linux, OS X) without compilation, hopefully lowering the hurdle to use the model.

Simulations are defined in an XML file, which is loaded by the framework. In the simulation file, end users can define the following:

- The assay
  - Plate properties such as size and shape (square or circular).
  - Stimuli using predefined settings or custom function of the form $S(x, y, t) = f(x, y, t)$.

[2]though worms also tend to get lost over time by escaping the plate, which would be somewhat equivalent to stopping the simulation when an animal reaches the edge

  - Metric to be measured, such as chemotaxis index, avoidance index, density plots etc.
  - where on the plate to place animals and if a fixed or stochastic placement should be used
  - Procedures, such as washing the worms, then placing them on a plate, or generally changing any parameter value during a simulation.
  - Assay duration, or trigger for ending the simulation (e.g. crossing a barrier)
  - Number of worms

- The nervous system
  - for every neuron a name, type and additional parameters
  - connections between the neurons (chemical synapses, gap junctions, and extra-synaptical neuropeptide release are supported).
  - whether neurons have sigmoidal activation functions, and whether chemical synapses are rectified (these can both be changed per neuron and connection as well).
  - the global neuronal membrane time constant
  - Pirouettes, u-turns and steering parameters
  - the speed of the animal

- general settings such as:
  - The save folder
  - the integration step size (the model uses Euler integration)
  - Parameter sweeps
  - The seed for the random number generator (each simulation saves the seed used, allowing users to investigate particular rare stochastic events, by entering a seed known to produce the event).

4.5.1 The model code

The code has been separated in clearly defined classes according to a model-view-controller separation. This allows the isolation of code that deals with data from code that deals with computation, output files and the user interface.

The structure of the framework is further separated into several packages:

- Model
  - environment, includes the current location and heading of the animal as well as the stimulus fields
  - metric, stores the aggregated data for all metrics (e.g. density over time, chemotaxis index, neuronal traces, position over time, etc.)
  - timehandler, stores all processes that need to occur during a simulation (e.g. washing of an animal moving to a different plate)
- View
  - view, handles user interface logic, builds up of output files (transforming several data structures to csv tables)
- Controller
  - circuit, builds up neural circuit, starts and ends simulation, integrates differential equations, calculates change in heading and new position of animal, initiates update of metrics
  - computation, dynamically builds up equations for stimuli and neuropeptides
  - network, handles all client server logic for distribution of work in a high performance cluster, and low level writing of files

- Helper, perform various functions, such as generic math functions, matrix operations, reference frame transformations, and includes a wrapper for the random number generator

Simulations can be run in a graphical interface, allowing the user to visualize the model nervous system, the assay, the locomotion trajectories of model animals, the corresponding neuronal traces, metrics such as the chemotaxis index (both for single animals, population statistics and parameter sweeps) and the model parameters. Simulations can also be run from the command line, either in local mode (on the current machine) or in a server client mode which can be used on high performance clusters where multiple computing nodes each run a part of the simulation. In this case, runs are split up over all nodes available. For instance, if a parameter sweep is done with 200 virtual animals per parameter value, and 50 computing nodes are available with four logical processors each, than all 200 animals are simulated in parallel, creating maximum speedup equal to the number of animals simulated. I tested this with a maximum of 500 nodes with 2 logical processors each on the University of Leeds high performance cluster, producing a near 1000 fold speedup over a fully serial simulation of each animal (some overhead is unavoidable). This shows that the server code scales excellently.

Model results, including trajectories, neuronal traces, metrics and stimulus fields can be saved in separate files in CSV format, allowing for quick import into Excel, R or Matlab.

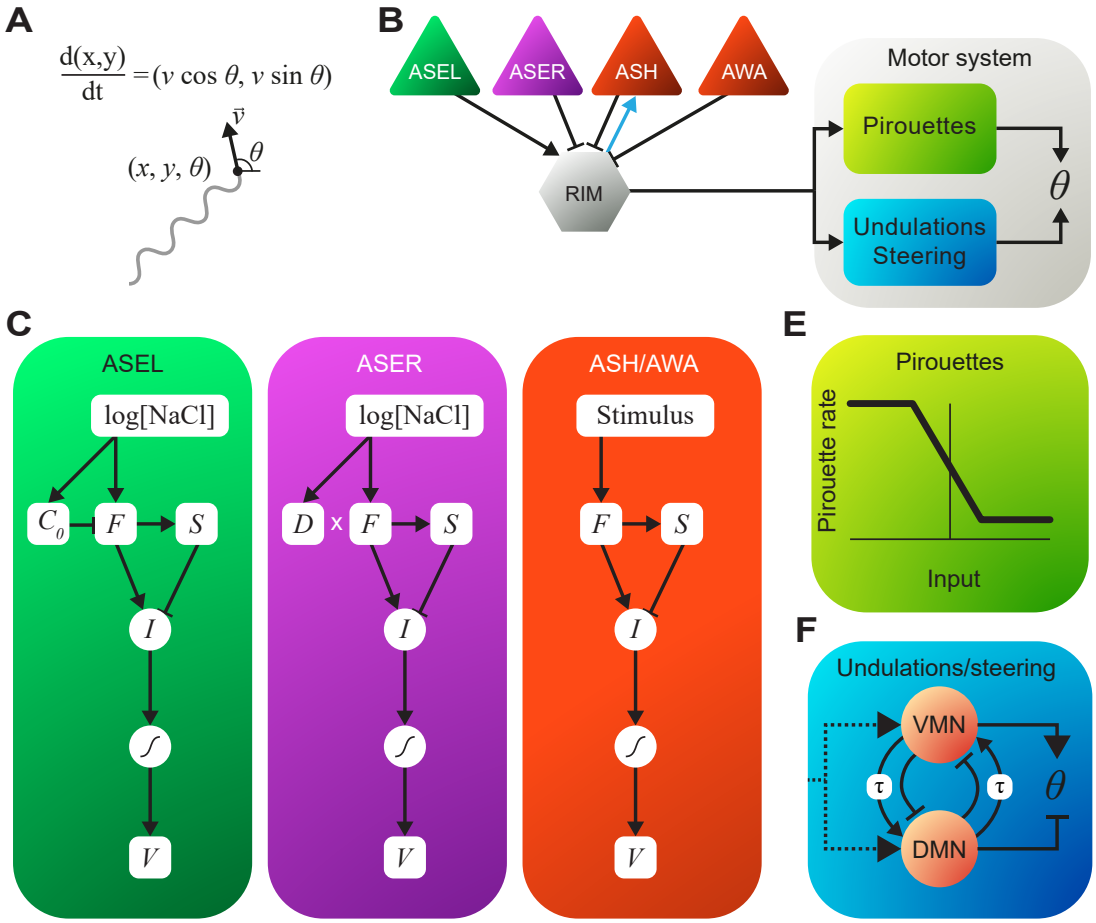

Figure 4.1: An overview of the model components. (A) the body is represented by a point moving along a vector with fixed speed. (B) the direction of locomotion, θ is modulated by a simplified nervous system consisting of a motor system directly innervated by several sensory neurons. The blue feed back connection from RIM onto ASH indicates tyraminergic modulation of ASH sensitivity by RIM (C) Sensory neuron activity is driven by the balance of a fast component and a slow delayed rectifier, constraint by a sigmoid function. ASEL has an adaptive baseline, C_0, ASER has a multiplicative gain, D (see chapter 6) (E) An abstract pirouette component sets the probability of instantaneous reorientations. (F) An oscillator generates undulations and smooth steering in response to sensory input.

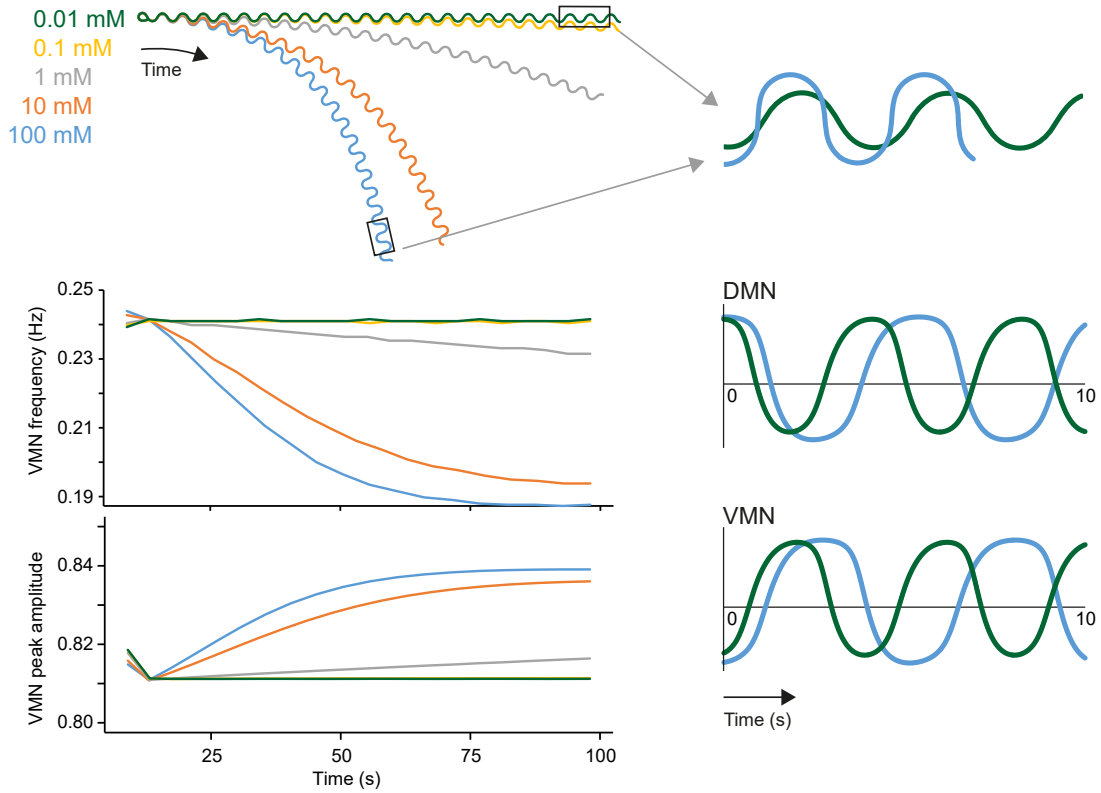

Figure 4.2: ***Top left****:Five 100 second trajectories of virtual worms in linear (downward facing) gradients increasing from 0 to 0.01, 0.1, 1, 10 or 100 mM over a distance of 4 cm.* ***Bottom left****: Modulation of frequency and amplitude of one of the motor neurons in the oscillator, VMN over the 100 second time course.* ***Right****: Overlaid blown up sections of final part of 0.01 and 100 mM trajectories, showing difference in shape (top) and corresponding activity in the oscillator neurons, VMN and DMN (bottom).*

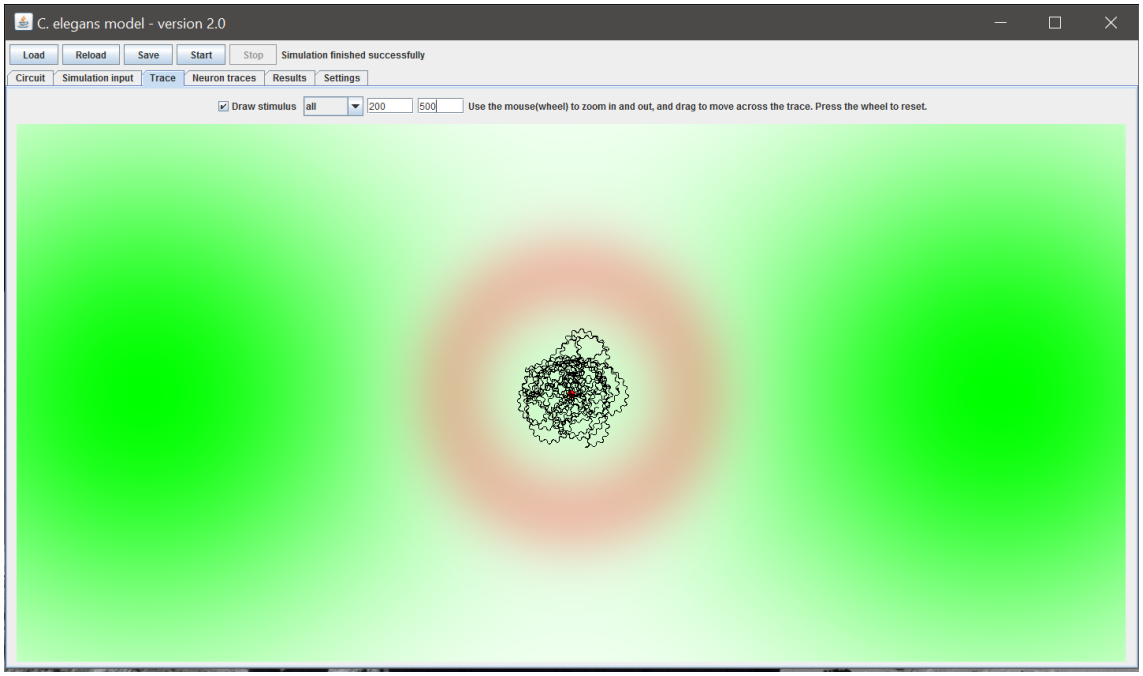

Figure 4.3: Screenshot of the model framework graphical user interface. The hyperosmotic fructose barrier is shown in red, diacetyl concentration in green, and the trajectory of a single worm is shown in black, simulated for 15 minutes of virtual time.

Chapter 5

Sensory integration 2

5.1 Introduction

For the first case study I looked at the sensory integration of an attractant (diacetyl) and a repellent (hyperosmotic concentrations of fructose) using unpublished behavioral and calcium imaging data from the Nitabach lab at Yale University.

Diacetyl is primarily sensed by the AWA sensory neurons [67, 93, 102], while hyperosmolarity is primarily sensed by the nociceptive sensory neuron pair ASH [6, 47, 61]. Both AWA and ASH connect to several downstream interneurons that integrate sensory signals from multiple modalities. ASH connects directly to RIM [23, 109], depolarizing RIM upon detection of hyperosmotic stimuli [86], while AWA connects indirectly [23, 109], hyperpolarizing RIM upon diacetyl exposure [72]. RIM, together with several other interneurons, connects to downstream command interneurons and motor neurons, promoting reversals upon activation [40, 42, 44, 86].

Prior to the start of our collaboration, the Nitabach lab had found several interesting mutants which showed aberrant behavior when diacetyl and fructose were presented together, but normal responses to diacetyl and fructose alone. Using a previously

established assay, where tens of animals are placed inside a hyperosmotic fructose ring with two diacetyl spots adjacent to the ring, the authors showed that several mutants exited the ring more readily than wild type. This behavior was found to be caused by the disruption of an ASH enhancing pathway. This pathway was activated by autocrine signaling of pigment dispersing factor 2 (PDF-2) in RIM followed by an extrasynaptic tyraminergic top-down signal to ASH, increasing its sensitivity to hyperosmolarity. Interestingly, disrupting this pathway only showed a phenotype when both diacetyl and fructose were present, and only at a fructose concentration of 3M (with no phenotype at 2M and 4M), and with normal chemotaxis to either stimulus on their own (Figure 5.4). These results led to the initial hypothesis that RIM was functioning as a coincidence detector of diacetyl and fructose.

Implementing the assay in the computational model, and constraining it using these data, the model showed an alternative hypothesis: we were looking at an edge cases of a thresholding mechanism. In the model the 2M fructose did not activate RIM sufficiently to cross the threshold and activate the aversion enhancing pathway, the 3M and 4M did but the 4M ring was so aversive no animal exited the ring regardless of the aversion enhancing pathway (Figure 5.4). In other words, the model suggested that what seemed like coincidence detection could in fact be a combination of thresholding and saturation effects. Interestingly, the model provided a testable prediction for this alternative hypothesis: it predicted that changing the experiment's parameters (e.g. concentration, diffusion time, starving the animals) should produce a phenotype even in the unisensory, fructose only, assay. Additionally, the model predicted that tyramine release and decay should be orders of magnitude slower than the neurons themselves. In the model, the slow tyramine induced heightened sense of aversion was shown to prevent animals from moving too close to the toxic region even if strongly attractive sources were present. While additional experiments did not show differences in the average distance to the gradient peak between wild type and mutants lacking the aversion enhancing pathway, when the Nitabach lab repeated the experiments with starved animals, the results now

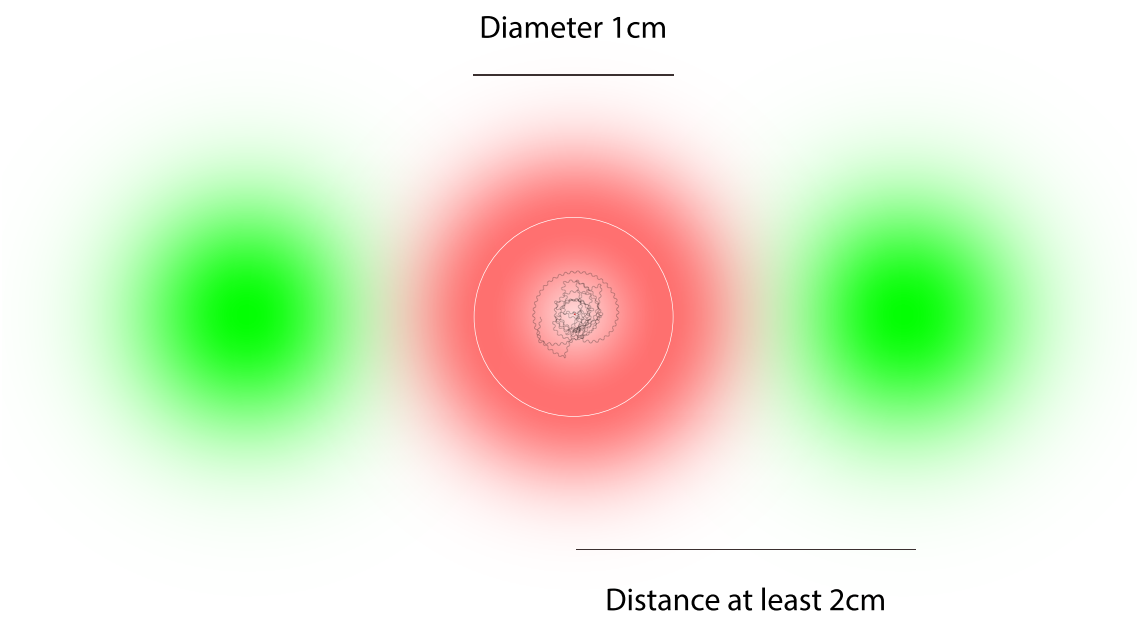

Figure 5.1: The ring assay used by the Nitabach lab, and the computational model consists of a 1cm diameter fructose ring, left to diffuse for 5 minutes prior to the assay start, and two diacetyl spots on either side of the ring, at least 2 cm (in the model exactly 2cm) from the center of the ring, spotted immediately prior to the start of the assay. Animals are left to roam the plate for 15 minutes, after which the number of animals that are outside the 1cm diameter of the ring are counted.

showed a phenotype in the fructose only assay, confirming the model's prediction that RIM uses a threshold rather than a coincidence detection.

5.2 Creating the model

Based on the initial data from the Nitabach lab, I started out by implementing the ring assay into the computational model (Figure 5.1). The assay consisted of a 1 cm diameter fructose ring (2, 3 or 4M), left to diffuse for 5 minutes, and two diacetyl spots on either side of the ring (1 μl of 1:350 dilution in water, 30mM), added immediately prior to the start of the assay. At the start, several animals are placed in the center of the ring, and left

to roam for 15 minutes.

The fructose ring, $F(x, y, t)$ was modeled by continuous diffusion from an initial delta peak ring with a 1cm diameter, placed in the center of the arena. The diffusion equation approximated the 2D Green's function:

$$F(x,y,t) = \frac{t_{FR}C_{FR}}{t_{FR}+t}\exp\left(-\frac{(\sqrt{(x-x_{FR})^2+(y-y_{FR})^2}-r)^2}{4D_{FR}(t_{FR}+t)}\right). \tag{5.1}$$

Here t_{FR} denotes the time of fructose diffusion prior to the start of the experiment, at $t = 0$, when virtual worms are added to the simulation. The fructose concentration and diffusion coefficient were set to match experimental results with different durations of fructose diffusion t_{FR}. Visual inspection of experimental worm traces showed animals moving towards diacetyl peaks even after 15 minutes. This is consistent with continuing evaporation of diacetyl, leading to a sustained concentration gradient throughout the assay. To capture this, we approximated the diacetyl concentration profile $DA(x, y, t_)$, by a two phased process: an initial rapid diffusion (to establish the concentration profile from two initial spots), followed by a static field:

$$DA(x,y,t) = C_{DA}\sum_{i=1}^{2}\exp\left(-\frac{(x-x_i^{DA})^2+(y-y_i^{DA})^2}{4D_{DA}}t_{DA}\right), \tag{5.2}$$

where (x_i^{DA},y_i^{DA}) are the coordinates for the i^{th} diacetyl spot and t_{DA} denotes the time of diacetyl diffusion. Simulations are prepared as described above. At $t = 0$ a single worm is placed at the center of the arena. As in the experimental assay, the balance of attraction and repulsion was quantified by the percentage of worms outside the ring after 900 seconds.

The diffusion coefficient for the fructose was set to 1e$-$6 cm^2 s^{-1} [21, 87] while the diacetyl gradient had to be kept time invariant because the very high rate of diffusion in air (D $\approx$ 0.1 cm^2 s^{-1}) would create a rapid equalization of the concentration across the

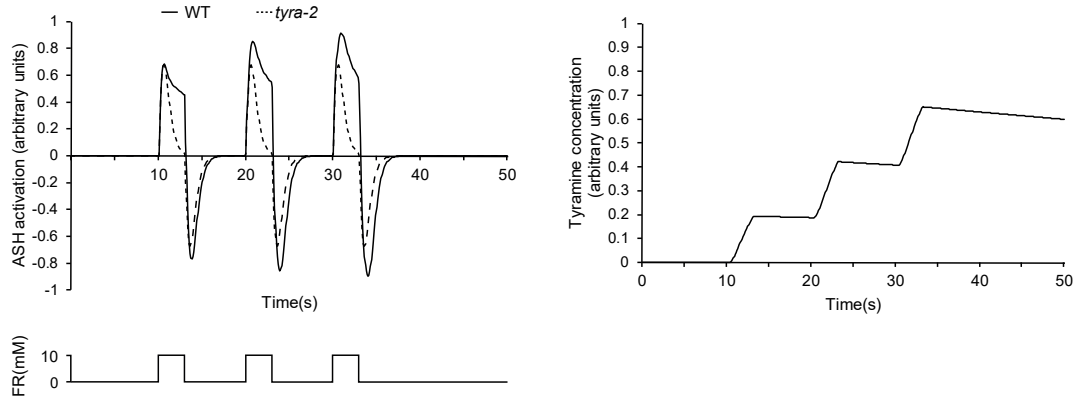

Figure 5.2: Left bottom, three three second 10mM upsteps are given. Left top, the ASH response for wild type (solid) and tyra-2 mutants. Right, tyramine concentration the 'extra cellular space'

plate. As we could not model this accurately, having only the behavioral data, we chose to use a static gradient. The parameters were chosen such that the gradient extends to every part of the dish, including inside the ring (Figure 5.3). Once set, we repeated the experiments with varying gradients to ensure the robustness of the model results, but did not tweak the gradient to produce correct data.

The model already included the ASH (copper) and AWA (diacetyl) sensory neurons, so assuming the response to hyperosmolarity was identical to copper, only the the tyra-2 neuropeptide need to be added.

Tyramine was set to increase linearly with the activity of RIM. To explain the absence of a phenotype in the 2M fructose ring condition, a threshold V_{tyr} was added:

$$\tau_{\mathrm{tyr}} \frac{dT}{dt} = \alpha_{\mathrm{tyr}} H(V_{\mathrm{RIM}} - V_{\mathrm{tyr}}) - \beta_{\mathrm{tyr}} \,, \tag{5.3}$$

where the function $H(x) = x$ for $x \geq 0$ and 0 otherwise. In other words, the tyramine level $T \geq 0$ at all times and increases only above the tyramine accumulation threshold V_{tyr}.

The physiological mechanism by which TYRA-2 modulates ASH excitability is

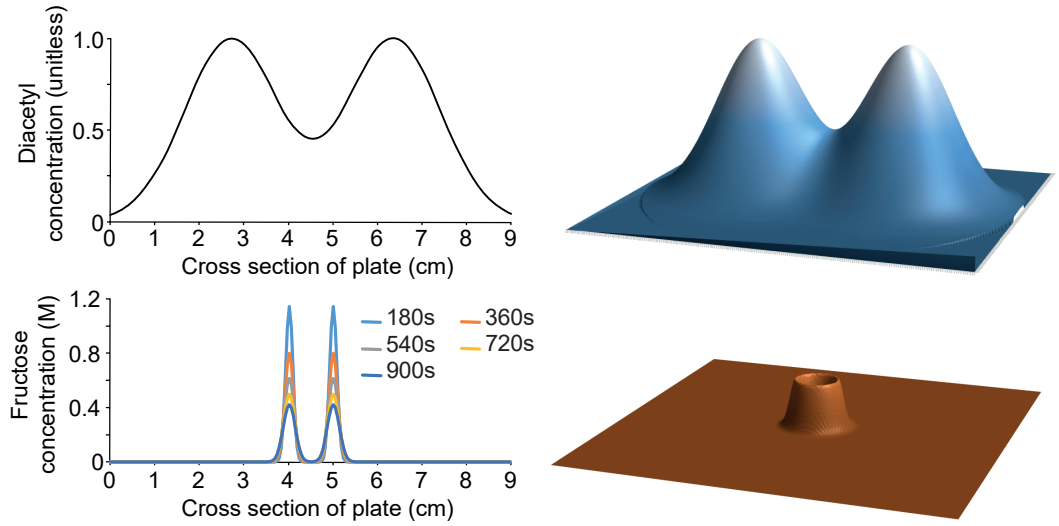

Figure 5.3: Profiles of the diacetyl and fructose concentration gradients. Left: cross section of the concentration gradient for diacetyl (top) and fructose (bottom) at different time points during the simulation. The diacetyl concentration is normalized to the peak concentration. Right full overview of the concentration profiles of diacetyl and fructose.

unknown. The application of tyramine did not appear to affect the ASH membrane potential. However, when a hyperosmotic stimulus was applied in the presence of tyramine, the ASH response seemed enhanced relative to the hyperosmotic stimulus without added tyramine (Figure 5.3B). Consistent with these observations, here the effect of TYRA-2 on ASH excitability is modeled as a contribution to the neuronal activation rate $\bar{\alpha}_{\text{ASH}}$ (Figure 5.2)

$$\alpha_{\text{ASH}}(t) = \bar{\alpha}_{\text{ASH}} + T(t). \tag{5.4}$$

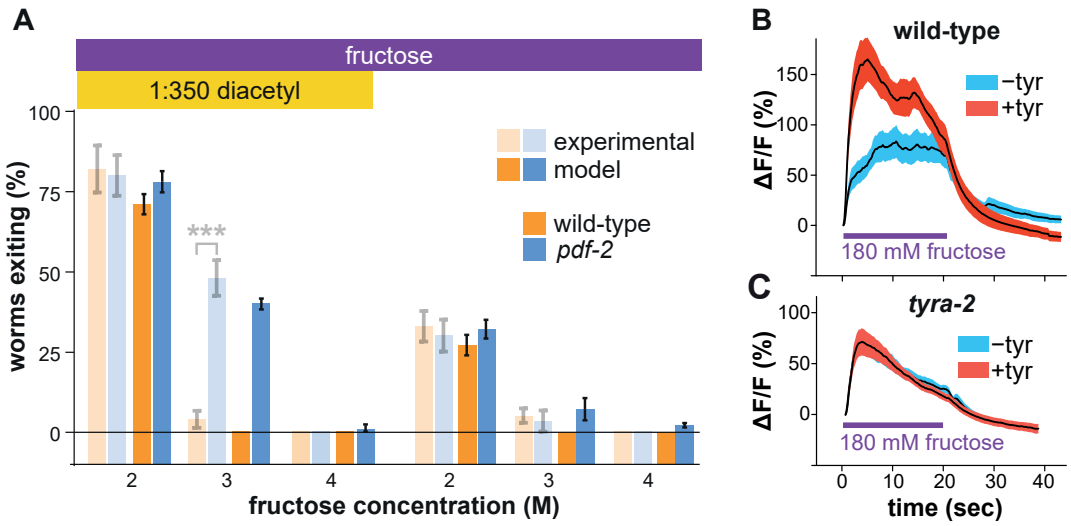

Figure 5.4: Experimental results and model reproduction of unisensory and multisensory fructose ring assay. (A) Opaque bars, experimental ring exiting rates, solid bars simulation results. Only for 3M fructose ring concentration, is a phenotype detected for pdf-2 null animals: significantly more pdf-2 mutants escape the ring compared to wild-type. (B and C) Average calcium response to 180 mM fructose presentation in ASH sensory neurons, in the absence (blue) and presence (red) of extraneously added tyramine, for wild-type (B) and tyra-2 null mutants (C).

5.3 Computational model predicts slow, non-linear tyramine regulation of threat-reward decision making

To characterize the interplay between neural activity, neuromodulatory activity, behavior, and the environment, we modeled each of these dynamic components in silico. Our model worms contain a highly simplified minimal nervous system sufficient for decision making (Figure 5.5). Neurons are modeled as "leaky integrators," such that each neuron integrates its input over time, while subject to continuous decay ("leak") of activity. In the absence of sensory input, the model worm's dorsoventral undulatory locomotion is driven by stable oscillations of a simplified central pattern generating circuit consisting of two reciprocally inhibited virtual motor neurons denoted DMN and VMN, which activate dorsal and ventral body bends, respectively. AWA and ASH sensory neurons respond with transient activation to changes in diacetyl or fructose stimuli, respectively. Activation of model sensory neurons AWA and ASH provides differentially weighted inhibitory and excitatory inputs onto RIM, respectively (Figure 5.5A). RIM integrates these sensory inputs and inhibits DMN and VMN to bias dorsal versus ventral bends, thereby inducing gradual steering of the worm (Figure 5.5A). Additionally, RIM activity positively increases the likelihood of pirouettes, which are modeled as instantaneous step changes in angular heading (Figure 5.5A). Importantly, in addition to the above previously established feed forward sensorimotor pathways, the simulation includes RIM-ASH tyraminergic positive feedback (Figure 5.5A). Tyraminergic potentiation of ASH in the model is only engaged above a threshold level of RIM activation as this non-linear relationship was required to reproduce experimental exiting rates. tyra- 2 null-mutant worms are modeled as lacking this tyraminergic feedback to ASH.

The virtual decision arena comprises a continuously diffusing fructose gradient ring and

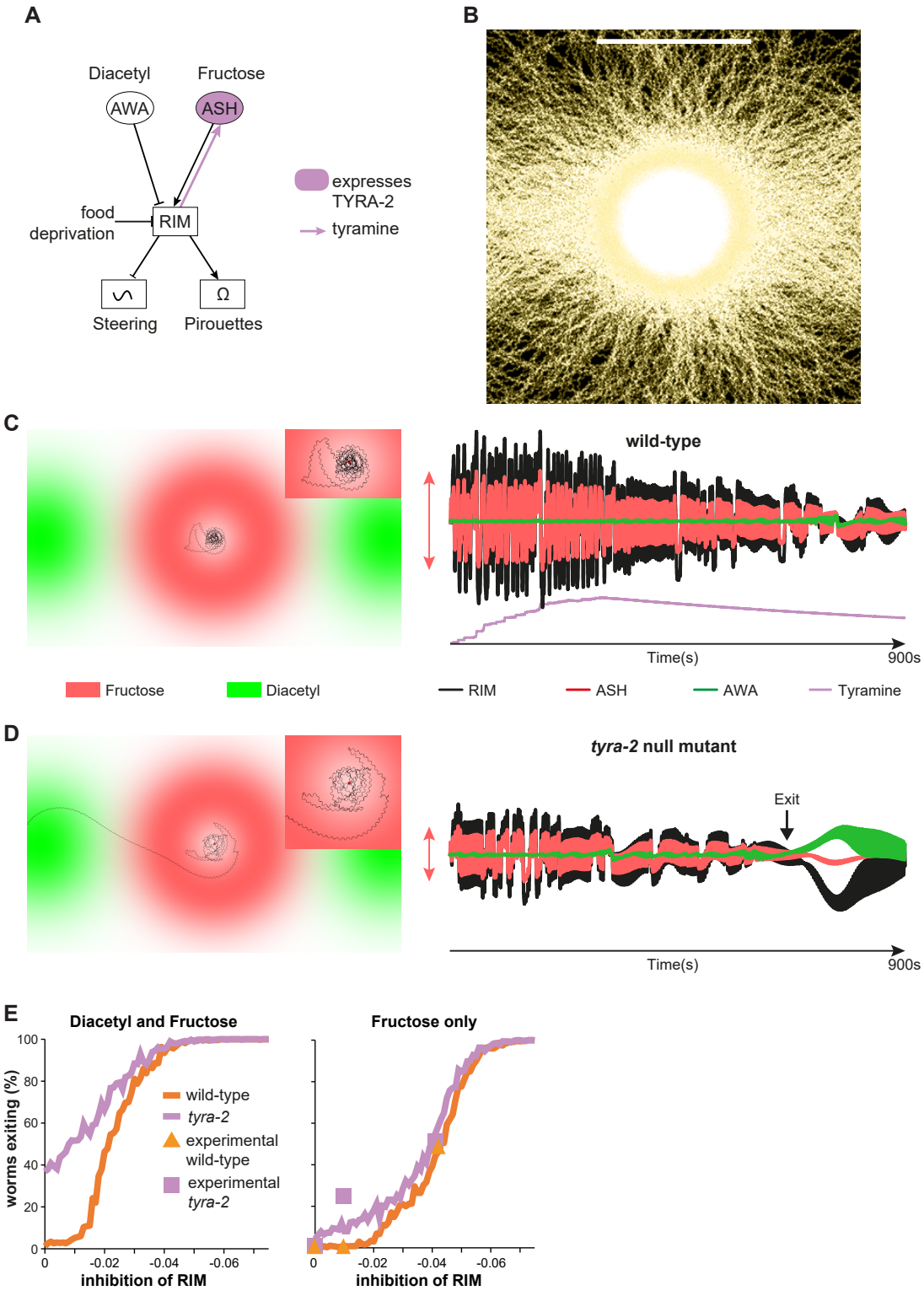

Figure 5.5: A) Schematic of the nervous system used in the ring assay. RIM releases tyramine which is sensed by the tyra-2 tyramine receptor in ASH (in purple). (B) trajectories of 1000 virtual animals, ring diameter shown with the white line at the top. (C and D) example trajectories and neuronal traces for a representative wild-type and tyra-2 worm. (E) Virtual RIM inhibition mimics starvation. Multisensory (left) and unisensory (right) exit percentages for virtual animals (lines) and experimental starvation (triangle and squares) for wild-type and tyra-2 animals.

time-invariant diacetyl gradients originating from two spots outside the ring. Modeling the fructose gradient as dynamically changing was essential, as the Nitabach results showed that continued diffusion of the fructose ring influences the time and probability of exit, and static fructose gradients failed to reproduce experimental exiting rates in our model. Each simulation begins with a single worm in the center of the virtual arena with a randomly selected initial heading, and the simulation is allowed to proceed for fifteen virtual minutes. Model parameters were manually calibrated until exiting rates of simulated wild-type and *tyra-2* null-mutant worms matched experimental exiting rates in multisensory and unisensory contexts for 2 M, 3 M, and 4 M fructose (Figure 5.4).

To illustrate the temporal evolution of the decision process, I plotted the locomotor trajectories and neural and neuromodulatory activity underlying the behavior of example simulated wild-type and *tyra-2* null-mutant worms (Figure 5.5C and D). This reveals that oscillatory changes in fructose and diacetyl concentration experienced by the worms as they undulate within the arena (Figure 5.5C) induces corresponding oscillatory changes in the activity of AWA, ASH, and RIM that are phase locked to the locomotor DMN-VMN pattern generator. In both wild-type and tyra-2 null-mutant worms, the magnitude of RIM and ASH oscillatory activity is larger than the AWA signal, and decreases over time. However, the magnitude of this oscillatory activity in RIM and ASH is higher in wild-type worms than in tyra-2 null-mutant worms (Figure 5.5D). Furthermore, in virtual tyra-2 null-mutant worms, the magnitude of RIM and ASH activity decreases over the course of the simulation until it matches AWA activity, which permits exiting of the ring. After exiting, the AWA signal dominates, ASH becomes silent, and RIM becomes inhibited as the worm continuously ascends the diacetyl gradient (Figure 5.5D). The model thus predicts that RIM activity above a particular threshold engages the RIM-ASH feedback loop, thereby decreasing threat tolerance and preventing exiting of the ring (Figure 5.5D). Importantly, the model also requires slow kinetics of accumulation and decay of the tyramine signal on a timescale of minutes to preclude exiting of wild-type worms even as the fructose barrier continues to diffuse and weaken (Figure 5.5D and

5.3). The reduced activation of ASH and RIM in simulated tyra-2 null-mutant worms, in which tyraminergic RIM-ASH feedback is absent, encodes increased threat tolerance underlying increased propensity to exit the ring (Figure 5.5D). Our computational model thus suggests that the slow, continuous, and self- reinforcing enhancement of RIM and ASH activity by top-down tyraminergic positive feedback determines threat tolerance that ultimately controls the decision balance.

5.4 Food deprived model worms now do show a *tyra-2* phenotype in the fructose only assay

To further test the hypothesis that food deprivation inhibits RIM, we simulated food deprivation as duration-dependent tonic inhibition of RIM, keeping all other model parameters unchanged. We modeled one hour of food deprivation as RIM inhibition of 0.02 (in arbitrary units), because this level of RIM inhibition increases exiting of simulated wild-type worms to 50%, the same as real worms food-deprived for one hour (Figure 5.5F). As RIM inhibition increases from 0 to 0.02, simulated wild-type worms increase exiting more steeply than tyra-2 null-mutant worms (Figure 5.5F). This qualitatively recapitulates the experimental results. As RIM inhibition increases to 0.03, both wild-type and tyra-2 null-mutant simulated worms increase exiting to 75%, the same as five hour food-deprived real wild-type and tyra-2 null-mutant worms. In the unisensory fructose-only context, as RIM inhibition increases from 0 to 0.02, simulated wild- type worms increase exiting less steeply than tyra-2 null-mutant worms (Figure 5.5F). This qualitatively recapitulates the unisensory experimental results (Figure 5.5F). Model parameters were selected solely to match simulated exiting rates to experimental exiting rates (Figure 5.4), without any consideration of the effects of food deprivation. It is thus remarkable that simulating food-deprivation as increasing inhibition of RIM qualitatively recapitulates the experimental effects of increasing food deprivation on both

wild-type and tyra-2 null-mutant worms in both multisensory and unisensory contexts. These computational results reinforce the conclusion supported by genetic manipulations in both the unisensory and multisensory contexts that food deprivation increases threat tolerance by inhibiting RIM and thereby suppressing RIM-ASH tyraminergic feedback.

5.5 Discussion

Our model predicts that integration of multisensory inputs in RIM determines the magnitude of the tyramine feedback signal and rules out a linear relationship between RIM activity and tyraminergic feedback. Using this model, we simulated the dynamic changes in neural and neuromodulatory activity that occur in freely moving worms during decision making, and determined the slow timescale at which RIM-ASH tyraminergic feedback must act to implement the decision (Figure 5.5). Our computational results suggest that food deprivation increases threat tolerance through suppression of RIM-ASH positive feedback (Figure 5.5F). These studies provide an integrated neuroendocrine circuit architecture for internal state control of multisensory threat-reward decision making.

I propose that tyraminergic feedback coordinately regulates and thereby links the excitability of RIM and ASH. Further, this coordinate regulation of RIM and ASH excitability operates on a time-scale of minutes to reflect internal hunger state. On a shorter time-scale (sub- seconds to seconds), inherent stochasticity within the network determines instantaneous activity [40]. Thus I propose that multisensory decision making depends on two linked mechanisms operating on different time-scales. On a longer time-scale, RIM excitability is modulated by internal physiological state and activation of the PDF-2-PDFR-1 autocrine positive feedback loop. This stable, long-term state is unaffected by instantaneous oscillations in network activity, such as those previously observed in RIM [40]. The level of RIM excitability then determines via tyraminergic

feedback the probability of neural processing events occurring on shorter time-scales during the decision task. These short time-scale events are subject to dynamic, stochastic changes in network activity but unaffected by changes in internal physiological state. Functional alteration of either of these mechanisms informs this dynamic, probabilistic decision making process at each behavioral contingency as the worm evaluates and explores the multisensory arena. Indeed, though inclusion of other feedback pathways and interneurons could potentially increase the accuracy of our computational modeling, our minimal model that incorporated only a single RIM-ASH feedback signal was sufficient to qualitatively recapitulate all experimental results (Figure 5.4 and 5.5).

Interestingly, this modeling study predicts that the extrasynaptic tyramine signal accumulates and decays slowly, modulating ASH sensitivity over long time-scales of multiple minutes (Figure 5.5C and D). The computational model is agnostic to how the slow kinetics of tyramine signaling are implemented, though there are multiple plausible biological mechanisms: either through the autocrine PDF-2-PDFR-1 feedback loop that modulates RIM excitability, or the time taken for tyramine to diffuse extrasynaptically to bind to TYRA-2 on ASH and then be cleared. Tyraminergic RIM-ASH positive feedback could determine the worm's tolerance to a variety of threats, as the ASH neuron is polymodal and senses multiple noxious cues [6, 47]. We propose that this slow tyramine signaling functions as a type of memory for the worm by suppressing sensory adaptation to dangerous stimuli, a feature which could be advantageous for worms navigating changing environmental conditions.

Chapter 6

Return of the salt

6.1 Introduction

In this chapter I extend my computational model to answer what mechanisms underlie gustatory plasticity. We collaborated closely with the Jansen lab who provided us with calcium imaging data and performed behavioral experiments. The behavioral experiments were strongly guided by the outcome of the computational model.

Naive *C. elegans* are attracted to NaCl concentrations up to 200mM and repelled by higher concentrations [30, 50, 106]. Attraction is primarily mediated by the ASE sensory neurons [5, 83] while avoidance is mediated by the ASH sensory neuron class [6]. Interestingly, ASH defective *odr-3* mutants remain attracted to NaCl up to 1M [50], suggesting that the ASE sensory neurons mediate attraction up to much higher concentrations.

After 15 minutes pre-exposure to 100 mM NaCl in the absence of food, *C. elegans* strongly avoids all NaCl concentrations. This response is called gustatory plasticity [50, 51, 58]. The association of the absence of food with the presence of NaCl is reversible, lasting less than 5 minutes [58].

Previous studies have shown that the ASE and ASH neuron classes play a role in gustatory plasticity [9, 50, 51, 58]. Building on these data the Jansen lab measured the responses of these sensory neurons to NaCl in naive animals and animals that were pre-exposed to NaCl of varying concentrations and durations.

The Ca^{2+} imaging results show several new forms of adaptation (going beyond Oda et al. [80]): ASEL is desensitized upon pre-exposure to NaCl whereas ASER is initially insensitive to NaCl changes and sensitizes upon NaCl pre-exposure. In addition, ASH nociceptive neurons become sensitized to considerably lower (non-toxic) levels of NaCl upon pre-exposure. Interestingly, all these forms of adaptation occur over similar time scales as gustatory plasticity (around 10 minutes).

Using these calcium imaging data in my computational model, I show that the different responses of ASEL and ASER mediate different locomotion strategies. Interestingly, the model strongly suggests that the primary effects of adaptation in ASEL and ASER are not related to gustatory plasticity even though they occur over the same time scale as gustatory plasticity. Conversely, the model suggests that ASH recruitment is the key driver to gustatory plasticity.

I then show the model requirements that account for the range of observed behaviors and deduce a number of testable model predictions, including the dominance of ASH-mediated avoidance over ASE-mediated attraction, the dynamic range of the sensitivities of the gustatory neurons and that (de)sensitization most likely occurs downstream of the receptor. The experimental data used to create the model are summarized in Appendix A.

6.2 Extending the model

The model consists of three sensory neurons ASEL, ASER, and ASH (representing ASHL and ASHR by a single computational unit), a single downstream interneuron and an

abstract motor system driving a point worm. ASEL was modeled to show desensitization over the course of 10 minutes to mimic experimental results. Similarly, in our model ASER becomes sensitized over 10 minutes. Since the nature of the recruitment signal from ASE to ASH is unknown, I modeled the recruitment of ASH as a two state Markov chain, with dynamic switching rates dependent on the history of the salt concentration. Specifically, in the sustained presence of salt, ASH has a high rate of switching on, while in the absence of salt there is a high rate of switching ASH off. For simplicity, I implement a 'drowning' mechanism whereby the ASH input to the interneuron is taken to be much stronger than the input from ASE. However, it is easy to see that an alternative "blocking" mechanism whereby ASH would actively disrupt signaling along the ASE sensorimotor pathway is equally tenable. In fact, Oda et al. showed a complete loss of activity to NaCl downsteps in the AIB interneurons (one of the targets of ASER) after pre-exposure to NaCl in the absence of food [80]. All virtual assays, including pre-exposure, were done in the absence of food. Neuronal properties and parameters of the motor system were constrained by unpublished calcium imaging data from the Jansen lab, published calcium imaging data [97, 100] and behavioral data from choice assays [50, 51, 58].

Simulations are performed on a virtual two dimensional 9 cm plate, which animals cannot leave. Upon reaching the edge of the plate, virtual animals are reoriented to a random angle between 0 and 2π drawn from a uniform distribution. Reorientation can occur multiple times in succession if worms continue to hit the edge.

As in the experimental protocol, the choice of condition was quantified using a chemotaxis index (CI) by counting the number of worms after 600 seconds in each quadrant

$$\mathrm{CI} = \frac{A - B}{A + B}\,, \tag{6.1}$$

where A is the number of worms located in quadrants with NaCl and B, the number of worms located in quadrants without NaCl. In the experiments, worms that remained stuck near a border between quadrants were excluded, and not counted towards the CI.

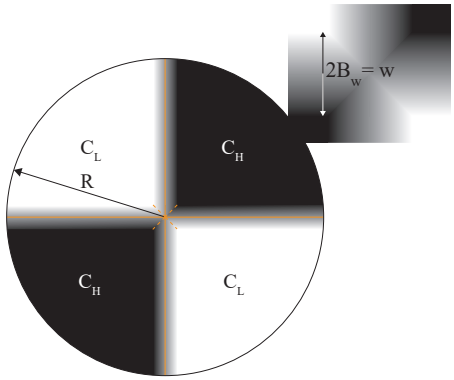

Figure 6.1: View from above of the choice assay used in our simulations. A plate of radius R is prepared with alternating quadrants of uniform high C_H (black) and low, C_L (white), NaCl concentrations. Quadrants are separated by intermediate regions of width $2B_w$ described by a linear concentration gradient.

As virtual worms cannot get stuck I do not exclude any region of the plate. To ensure that this does not alter our results, I verified that excluding a region around the borders produces statistically identical CIs.

For a coordinate system (x, y) whose origin is at the intersection between the four quadrants (at the centre of the arena), I approximate the concentration field $C(x, y)$ over the domain $x^2+y^2 \leq R^2$. $C(x, y)$ is uniformly high (C_H) or low (C_L) within the quadrants and changes linearly in narrow regions of width $2B_w$ between the quadrants:

$$C(x,y) = \begin{cases} C_H\,, & xy > 0 \text{ and } |x|, |y| \geq B_w \\ C_L\,, & xy < 0 \text{ and } |x|, |y| \geq B_w \\ \dfrac{C_H + C_L}{2} + \dfrac{C_H - C_L}{2B_w} \times \begin{cases} \text{sgn}(x)\, y\,, & |y| \leq B_w \text{ and } |y| \leq |x| \\ \text{sgn}(y)\, x\,, & |x| \leq B_w \text{ and } |x| \leq |y|\,. \end{cases} \end{cases}$$

Here $\text{sgn}(x) = \pm 1$ depending on whether x is positive or negative, respectively.

The choice assay was performed with both naive animals and with conditioned animals. In the experiments, animals were washed in either salt-containing or in salt-free M9 buffer for 15 minutes before being placed on the assay plate. To mimic pre-exposure in our model, I simulated animals on a plate with uniform concentration of salt for 15 minutes,

Initialization (naive)	Value	Description
τ_{end}	600 s	Duration of the assay
Δt	0.01 s	Time step of the simulation
$\theta(0)$	[0,2π)	Initial direction drawn from uniform distribution
C_{high}	100 mM	NaCl concentration in NaCl quadrants
C_{low}	0 mM	NaCl concentration in control quadrants
B_w	0.2 cm	Half width of boundary region with NaCl gradient
V_i	0	Initial activity for all neurons
F_i	0	Initial value for fast component of all sensory neurons
S_i	0	Initial value for slow component of all sensory neurons
C_0	0 mM	Initial value for the baseline of ASEL
D	0	Initial value for fast component of I_{hyp} in ASER
E	0	Initial value for slow component of I_{hyp} in ASER
C_{wash}	100 mM	Concentration of NaCl in buffer used for conditioning

Table 6.1

and then virtually transferred them to the center of the quadrant plate.

6.2.1 Model sensory neurons

Ca^{2+} imaging has shown that many *C. elegans* sensory neurons, including ASE and ASH, integrate over time to produce an approximation of the change in stimulus strength [97, 100]. Such responses are well modeled by two opposing components, F (fast) and S (slow), with a separation of timescales (Figure 6.2). In our model, ASEL exhibits a rectified depolarizing response to NaCl concentration increases, whereas ASER exhibits an unrectified response to NaCl concentration changes, allowing a single current to capture the depolarizing response to NaCl concentration decreases, and the hyperpolarizing response to concentration increases. Since ASHL and ASHR appear to respond identically to NaCl [100] and are gap-junctionally coupled [109] I collapsed them into a single model neuron (ASH, Figure 4.1).

To account for our Ca^{2+} imaging data, I first considered the rise and decay times of the depolarizing responses of ASEL and ASER. To this end, I focused on fully sensitized responses, i.e. on the ASEL response in naive animals and on the ASER responses following 10 minutes of pre-exposure. Analyzing the Jansen lab calcium imaging data, I found that both the rise and decay of the responses were consistently and significantly faster in ASEL than in ASER: Peak Ca^{2+} responses in ASEL were reached on average after 1.9 seconds, compared to a rise time of 5.7 seconds in ASER ($p<0.001$). Similar rise times were observed after exposure to other NaCl concentrations in ASEL or after shorter pre-exposure times in ASER. The difference between ASEL and ASER Ca^{2+} response times is further supported by previous work [97]. In particular, the difference in decay time between ASEL and ASER seen in the calcium imaging traces by us and others [97] is much larger than would be expected by a calcium imaging lag alone [19]. To investigate the consequences of a slow ASER I used the calcium imaging rise and decay times as upper bounds in our computational model.

6.2.2 Modeling sensory adaptation

In the calcium imaging data from the Jansen lab (supported by Oda et al. [80]) a slow desensitization of ASEL and a slow sensitization of ASER can be seen. Specifically, ASEL failed to respond to an increase in [NaCl] after a pre-exposure of 600 s. However, a response was seen to larger increases in [NaCl]. This response hints at an adaptive threshold and, together with the wide dynamic range of responses, is reminiscent of Fechner's law, typically expressed as $r \propto \log s$, where r and s denote the response and signal, respectively. The incremental form of the law $\Delta r \propto \Delta s/s$ describes the minimal stimulus change needed to evoke a reponse, relative to some baseline [26].

Jansen's Ca^{2+} imaging data suggest that when ASEL is sensitized, ASER would not be, and vice versa. Additionally, the consequences of ASEL and ASER adaptation are

further masked by ASH sensitization, which occurs over similar timescales. To better understand why ASEL, ASER and ASH have such different but overlapping (in time) forms of adaptation I modeled each form separately.

ASEL was modeled to show desensitization over the course of 10 minutes to mimic experimental results. The presence of a response to higher concentrations when desensitized by pre-exposure, e.g. to 100 mM, led us to model ASEL desensitization as baseline (or threshold) adaptation 6.2. Accordingly, the slow sensory adaptation of ASEL to NaCl is implemented with a slowly evolving concentration sensitivity threshold C_0 (Fig. 4.1, 6.2)

$$\frac{dC_0}{dt} = \delta_i^{\mathrm{ON}} C_{\log} - \delta_i^{\mathrm{OFF}} C_0 \,.$$

In addition, the fast component F integrates over the log of the NaCl concentration field, capturing the wide dynamic range of behavioral responses to NaCl

$$C_{\log} = \log\left(\frac{C(x,y,t) + C_{\min}}{C_{\min}}\right) , \tag{6.2}$$

where $C_{\min}$ is a cutoff required to ensure a positive definite value and representing the cutoff sensitivity of the cell; its value (1 mM) was set conservatively to match behavioral evidence, in the literature as well as in our own data. Note that in our model, threshold adaptation only applies to ASEL, thus only for $i = \{\mathrm{ASEL}\}$: $\delta_i^{\mathrm{ON}} \neq 0\,,\ \delta_i^{\mathrm{OFF}} \neq 0$.

In contrast to the slow desensitization of ASEL, Jansen and Oda et al. [80] have shown that ASER *sensitizes* over time: longer NaCl pre-exposure results in a stronger depolarizing response to downsteps. This sensitization is captured in our model with a multiplicative gain parameter D_{ASER}: a slowly evolving measure of the presence of NaCl such that the fast component F increases with the pre-exposure duration, as measured experimentally (Fig 6.2).

$$\frac{dD_{\mathrm{ASER}}}{dt} = -\lambda^{\mathrm{OFF}}(D_{\mathrm{ASER}} + D^0_{\mathrm{ASER}}) + \lambda^{\mathrm{ON}} C_{\log}(1 - D_{\mathrm{ASER}}) \,. \tag{6.3}$$

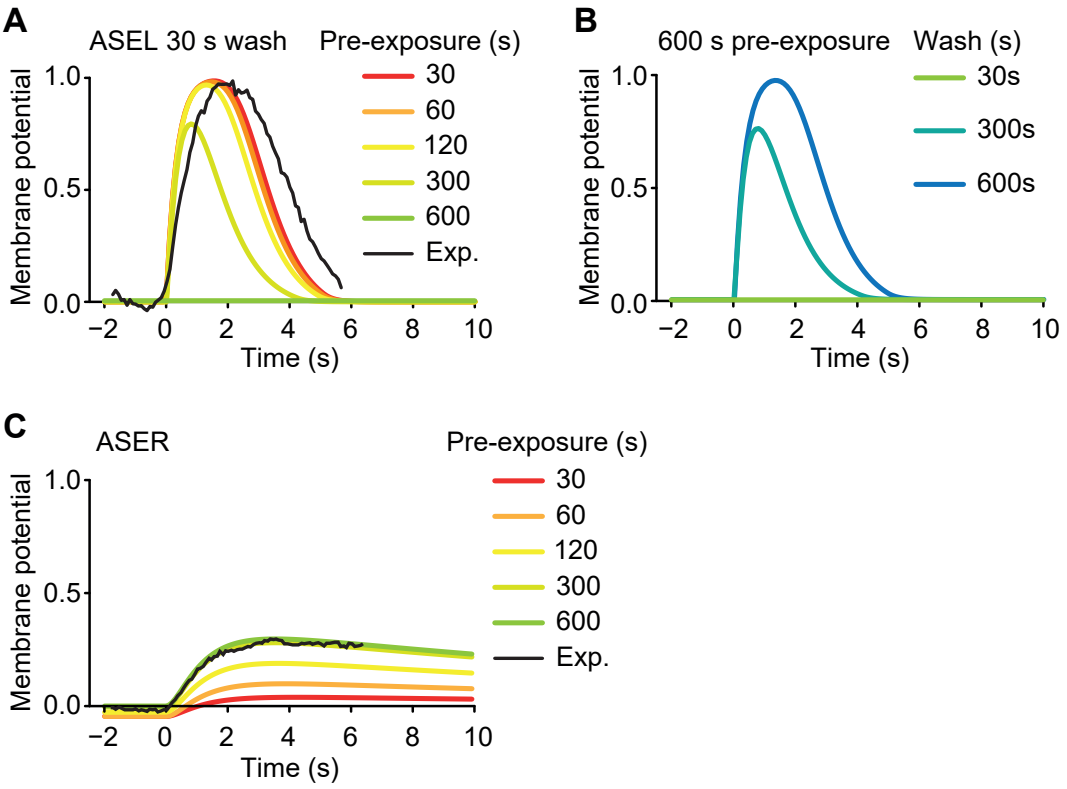

Figure 6.2: (A) Model ASEL responses to a 3 seconds exposure to 100 mM NaCl (starting at 0 seconds) after pre-exposure of varying durations to 100 mM NaCl and a 30 seconds wash. A representative calcium imaging trace (30 seconds pre-exposure to 100 mM NaCl, 30 seconds wash) is overlaid in black with vertical scaling to the amplitude of the corresponding model trace. (B) ASEL responses to a 3 seconds exposure to 100 mM NaCl after 600 seconds of pre-exposure to 100 mM NaCl and a wash of varying durations. (C) ASER responses to a decrease in NaCl from 100 to 0 mM after pre-exposure to 100 mM NaCl of varying durations. A representative calcium imaging trace (600 seconds pre-exposure to 100 mM NaCl) is overlaid in black with vertical scaling to the amplitude of the corresponding model trace.

Sensory neuron parameters	**Value**	**Description**
α_{ASEL}	$1\ s^{-1}$	ASEL depolarization rate
β_{ASEL}	$0.8\ s^{-1}$	ASEL leak rate
γ_{ASEL}	$1\ s^{-1}$	ASEL rectification (repolarization) rate
$\delta^{\text{ON}}_{\text{ASEL}}$	$0.006\ s^{-1}$	ASEL desensitization rate
$\delta^{\text{OFF}}_{\text{ASEL}}$	$0.004\ s^{-1}$	ASEL desensitization relaxation rate
D_{ASEL}	1	ASEL gain adaptation factor
α_{ASER}	$0.3\ s^{-1}$	ASER activation rate
β_{ASER}	$1\ s^{-1}$	ASER leak rate
γ_{ASER}	$0.05\ s^{-1}$	ASER rectification rate
$\delta^{\text{ON}}_{\text{ASER}}$, $\delta^{\text{OFF}}_{\text{ASER}}$	$0\ s^{-1}$	ASER desensitization rate
λ^{OFF}	$0.01\ s^{-1}$	ASER gain adaptation relaxation rate
λ^{ON}	$6 \cdot 10^{-6}\ s^{-1}$	ASER gain adaptation rate
α_{ASH}	$0.1\ s^{-1}$	ASH activation rate
β_{ASH}	$0.60\ s^{-1}$	ASH leak rate
γ_{ASH}	$0.01\ s^{-1}$	ASH rectification rate
$\delta^{\text{ON}}_{\text{ASH}}$, $\delta^{\text{OFF}}_{\text{ASH}}$	$0\ s^{-1}$	ASH desensitization rate
D_{ASH}	1	ASH gain adaptation factor
$C_{\min}$	1 mM	Stimulus resolution limit

Table 6.2

6.2.3 In silico animals reproduce neuronal response and behavior of naive real animals

Before I looked at adaptation, I compared the responses of virtual ASEL and ASER with our calcium imaging data. Model results showed very close agreement with Ca^{2+} traces in ASEL and ASER from naive animals (Figure 6.2). Visual inspection of trajectories of experimental naive animals showed they predominantly use steering to orient themselves in the quadrant assay. The model animals exhibited similar motor behavior to those of actual animals (Figure M4 in Supplemental information).

Next, we tested if the resulting virtual behavior also matched our experimental data. We simulated 500 wild type naive worms, with ASEL, ASER and ASH adaptation/recruitment dynamics, for ten minutes of virtual time in the quadrant assay. This simulation yielded a similar in silico chemotaxis index to experimental naive results (wild type in Figure 6.3).

6.2.4 ASE (de)sensitization reduces robustness of attraction in our computational model

Lowered responsiveness of sensory neurons almost invariably implies loss of sensory information. In fact, the opposite action of ASEL and ASER adaptation suggests only one of the ASE pair is fully sensitized at any one time. Thus, I expected a particularly severe performance penalty in our simulations (relative to a model with no adaptation), which is supported by previous computational models where both ASE neurons were always fully sensitized [55, 57]. In our simulations, worms with always fully sensitized ASEL and ASER and unrecruited ASH achieved very similar performance to wild type animals (Figure 6.3). To understand this unexpected result, I performed a sensitivity analysis on the key sensory parameters (ASEL/R rise and decay times). This revealed that for

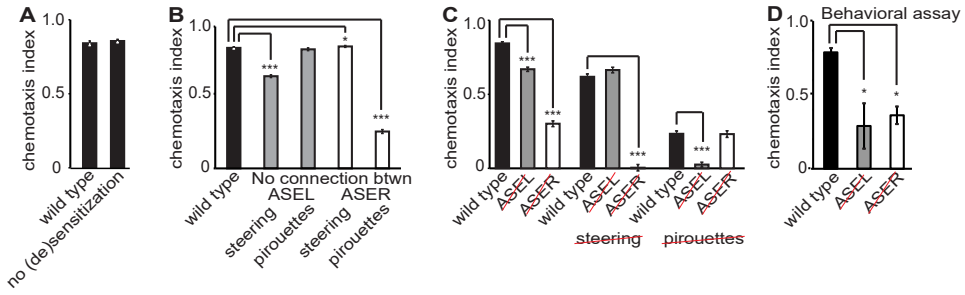

*Figure 6.3: ASEL and ASER drive steering and klinokinesis respectively in our computational model. Chemotaxis index of model WT versus mutant animals in the simulated quadrant assay. (A) Our model shows no difference in attraction in the quadrant assay between wild type and animals with always fully sensitized ASEL and ASER. (B) Ablating the synaptic connection from ASEL to the steering motor neuron or from ASER to the pirouette neuron significantly reduced the chemotaxis index. Ablating the connection from ASER to steering very slightly increased the chemotaxis index. (C) Double mutants with ablated ASEL and no steering, or ablated ASER and no pirouettes achieved the same chemotaxis index as single mutants. (D) Experimental validation: animals with genetically ablated ASEL (OH8585) and genetically ablated ASER (OH8593) exhibit a strong reduction in the chemotaxis index in the quadrant assay. *: p¡0.05, ***: p¡0.0005.*

all possible timings of ASE left and right, animals with ASE adaptation had lower or equal chemotaxis indices, with the vast majority of parameters resulting in a significantly lower chemotaxis index (data not shown). If this reflects limitations on the physiological parameters of the biological worm, it hints at selective pressure to recover ASE responses in the presence of information loss due to ASE adaptation.

6.2.5 Sensitization of ASH is sufficient to reproduce gustatory plasticity in a computational model

Next, I incorporated stochastic ASH recruitment (and release) into our computational model and simulations.

Since the nature of the recruitment mechanism of ASH is unknown, it was modeled as a stochastic switch, with dynamic rates dependent on the history of the salt

concentration. In its off or *unrecruited* state, ASH is assumed to respond only to dangerous concentrations of NaCl (> 300 mM), whereas in its on or *recruited* state, it responds to low concentrations of NaCl as well. Specifically, in the recruited state, the ASH sensory neuron is modeled as identical to ASER, up to a sign reversal.

NaCl avoidance after pre-exposure to NaCl was achieved by setting the synaptic weight between ASH and the pirouette command neuron significantly higher than the weight from ASE. Indeed, the strong attraction to 300 or 500 mM in ASH deficient *odr-3* animals, in contrast to the strong avoidance by wild type animals, suggests that ASE-mediated attraction is overridden by ASH [50]. This is further supported by avoidance of 300 and 500 mM NaCl, despite ASEL showing a strong calcium imaging response in wild type animals. Thus, in this model, ASH sensitization is likened to a recruitment of ASH into the (non-hyperosmotic) NaCl sensing circuit.

Let ρ denote the propensity of ASH to be recruited, which varies from 0 (no NaCl) to 1 (saturated exposure to NaCl):

$$\frac{d\rho}{dt} = \kappa \left(\frac{C_{\log}}{C_{\max}} - \rho \right) . \tag{6.4}$$

Thus, ρ converges to the ratio of the current concentration and a 'maximum' concentration. Let the transition rates α_{rec} and β_{rec} denote the recruitment and unrecruitment rates respectively, such that

$$\text{OFF} \underset{\beta_{\text{rec}}}{\overset{\alpha_{\text{rec}}}{\rightleftharpoons}} \text{ON}$$

with $\alpha_{\text{rec}} = \dfrac{\rho}{\tau_\alpha}$ and $\beta_{\text{rec}} = \dfrac{1-\rho}{\tau_\beta}$.

The steady state probabilities $P(\text{on})$ and $P(\text{off})$ for occupying the on (recruited) and off (unrecruited) states (Figure 6.4) are then given by

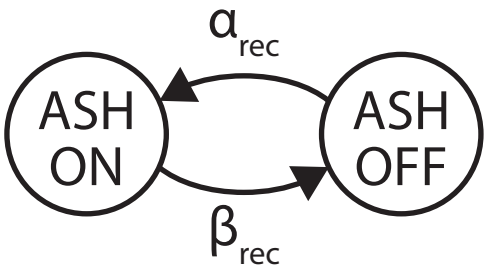

Figure 6.4: Diagram showing the two state Markov chain, used to model ASH recruitment. ASH switches on with rate α_{rec} and off with rate β_{rec}.

$$\begin{aligned} P^*(\mathrm{on}) &= \frac{\alpha_{\mathrm{rec}}}{\alpha_{\mathrm{rec}} + \beta_{\mathrm{rec}}} \\ P^*(\mathrm{off}) &= \frac{\beta_{\mathrm{rec}}}{\alpha_{\mathrm{rec}} + \beta_{\mathrm{rec}}} . \end{aligned}$$

For simplicity and parsimony, the above general formulation can be simplified by collapsing the two time scale parameters into one, such that $\tau_\alpha = \tau_\beta = 1/\kappa$. In this case $P^*(\mathrm{on}) = \frac{C_{\log}}{C_{\max}}$ and $P^*(\mathrm{off}) = 1 - \frac{C_{\log}}{C_{\max}}$.

ASH recruitment	**Value**	**Description**
$C_{\max}$	100	NaCl saturation level for recruitment ($\rho \to 1$)
κ	0.001 s^{-1}	Integration rate for [NaCl] history

Table 6.3

We first asked whether our model of ASH recruitment is sufficient to account for the balance of attraction and aversion over time. To ground our model in experimental data I performed the quadrant assay for a significantly longer time (one hour) and analyzed the chemotaxis index of naive animals and those pre-exposed to NaCl for 15 minutes. Interestingly, the chemotaxis index dropped to 0 over the course of 60 minutes for naive animals as well as for pre-exposed animals with similar but opposite time courses (Figure

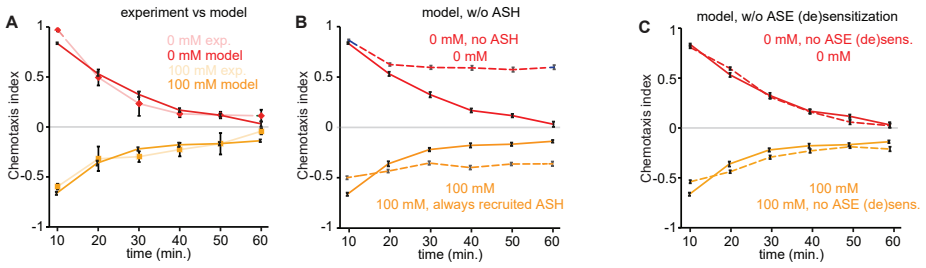

Figure 6.5: Recruitment of ASH drives gustatory plasticity in our computational model. Chemotaxis index over time in experiments and simulations of the quadrant assay. (A) Chemotaxis index for naive (0 mM) and pre-exposed (15 minutes, 100 mM NaCl) animals. The behavioral results (light lines) and the modeling results (dark lines) show a monotonic decay towards a chemotaxis index of 0, for both naive and pre-exposed animals. (B) Virtual chemotaxis index for animals with unrecruited ASH (dashed line) and with recruited ASH (solid line). Without ASH state dynamics the chemotaxis index does not decay to 0. (C) Comparison of chemotaxis index for model with ASE (de)sensitization (solid lines) and with fully sensitized ASEL and ASER (dashed lines).

6.5, dashed lines). Chemotaxis indices obtained from simulations of our model for 60 minutes closely reproduced the experimental data (Figure 6.5A, solid lines).

We next asked why the chemotaxis index decayed to 0 over time (indicating roughly equal numbers of animals in the salt and no salt quadrants). To determine if this may be due to two sub-populations (with ASH on and off) or to a detailed balance scenario (in which animals continually and stochastically switch between recruited and unrecruited ASH states), I disabled changes in ASH recruitment during simulations. This allowed us to run simulations with two subpopulations of animals, one having ASH completely disabled and the other fully recruited throughout the simulation. Now the chemotaxis index decayed only partially, reaching a plateau around 0.5 and -0.3 respectively (Figure 6.5B). These results suggest that the recruitment kinetics obey a law of detailed balance: Our simulations confirm that ASH becomes recruited in animals that stay within a salt quadrant for some time, but not in animals that remained in a no-salt quadrant. Stochastic navigation of animals allows for quadrant-crossing resulting in stochastic switching of ASH states. This ensures that over time the number of animals with ASH in either state

will be equal.

To determine whether ASE (de)sensitization plays a role other than in the recruitment of ASH, I disabled adaptation in the ASE sensory neurons and reran our simulations. When comparing pre-exposed animals with and without ASE (de)sensitization, I find no change in the strength or time course of the chemotaxis index (Figure 6.5C).

In summary, our simulations, for both naive and pre-exposed animals, suggest that the experimental response of animals to NaCl in the quadrant assay requires dynamic ASH state-switching. Desensitization of ASEL or sensitization of ASER does not seem to be required, although it is very well possible that these processes play a role in recruitment of ASH. Unfortunately, it is currently not possible to genetically disable ASE (de)sensitization. Our results demonstrate how experience dependence (here, of a spatially heterogeneous environment) can rapidly (here, within one hour) randomize the internal states of a population of animals with initially identical internal state.

6.2.6 Sensory neuron timing strongly influences navigation strategies in our computational model

Previous models of salt navigation considered ASEL and ASER as having opposite, complementary roles during positive chemotaxis, an assumption that relies on these neurons responding over similar timescales (e.g., Izquierdo and Beer [55], Izquierdo and Lockery [57]), despite some indications to the contrary in calcium imaging experiments [80, 97]. Experimental evidence has shown that the relative contributions of ASEL and ASER to NaCl navigation is assay dependent: some show ASER is sufficient and drives both steering and pirouette modulation [52], others show that ASEL and ASER contribute equally [1].

When I ablated the in silico synaptic connection from ASEL to the pirouette motor program or the in silico synaptic connection from ASER to the steering circuit, the

chemotaxis index remained unchanged relative to wild type model animals (Figure 6.3B). Conversely, virtually severing the connection from ASEL to the steering circuit or from ASER to the pirouette motor program severely reduced the chemotaxis index (Figure 6.3B). These results strongly suggest that in our model, ASEL controls steering, but has little effect on the modulation of the pirouette rate, whereas ASER modulates pirouettes, but has little control over steering.

To confirm this interpretation, I disabled steering in wild type and ASEL-ablated animals in our computational model; as expected, I found that the chemotaxis index was equally reduced in single (steering) versus double (ASEL and steering) virtual mutants (Figure 6.3C). Together these results show that in our model ASEL almost fully drives steering, having a negligible effect on pirouette modulation (klinokinesis). Similarly, disabling pirouette modulation in wild type or ASER ablated double mutants resulted in an equally reduced chemotaxis index (Figure 6.3C). Finally, ablating ASEL in animals where pirouette modulation was disabled, or ablating ASER in animals where steering was disabled almost fully abolished the response to NaCl in our model (Figure 6.3C).

Thus, in our model, both steering and pirouettes contribute to the chemotaxis index in the quadrant assay, but these distinct motor programs are separately controlled by ASEL and ASER, respectively. The distinct roles of ASEL and ASER in our computational model are a direct result of the timescales of their responses. To steer, sensory signals must be detected on the timescale of a half-undulation: O(1-2 sec) or faster [41, 52, 57]). The slower rise time in ASER in our model precludes this. The contribution of ASER to steering in different assays [1, 52] may indicate a faster rise time in ASER. Pirouettes occur with a mean rate of 2.1 events per minute [83]. Therefore, to effectively modulate this rate requires a memory of salt exposure over commensurate (or longer) timescales. The fast decay time of ASEL in our model precludes this. Conversely the slow decay time of ASER is ideally suited to modulate the pirouette rate effectively. Should ASER lack this slow timescale, the modulation of pirouettes would appear to require a slow

integration elsewhere in the circuit.

To rule out any contribution of desensitization of ASEL and sensitization of ASER to the above analyses, I re-ran our simulations with all forms of adaptation disabled such that both ASE neurons are fully sensitized and ASH recruitment is disabled. These analyses gave very similar results as our previous analyses (Figure 6.3C), confirming that in our model the separate roles of ASEL and ASER can be attributed to the differences in the time courses of ASEL and ASER responses.

Unfortunately, it is currently not possible to disable either of the two navigation strategies in *C. elegans* in vivo. To test whether ASEL and ASER are indeed both required for successful navigation in the quadrant assay, as predicted by our model (Figure 6.3C), the Jansen lab genetically ablated either ASEL or ASER, using animals that express Caspase-3 in either the left (OH8585) or right (OH8593) ASE neuron [82]. These animals showed a strong reduction in chemotaxis to NaCl (Figure 6.3D), confirming that both ASEL and ASER contribute to quadrant navigation in this assay.

6.3 Discussion

Based on our results I propose that the response of *C. elegans* to NaCl is regulated at multiple levels. Naive chemotaxis to NaCl is mediated by a core NaCl chemosensation machinery, comprised of the ASE neurons that mediate NaCl attraction and the ASH neurons that mediate avoidance of hyperosmotic stresses, resulting in a switch between attraction up to 200 mM NaCl and avoidance of higher concentrations (Figure 6.6). Pre-exposure to 100 mM NaCl in the absence of food results in an altered dynamic ranges in both the ASEL and ASH neurons. The ASEL neuron becomes desensitized to salt – up to the pre-exposure concentrations – whereas ASH become sensitized to low concentrations. Desensitization of the ASEL neuron is mostly cell-autonomous, but it involves serotonin

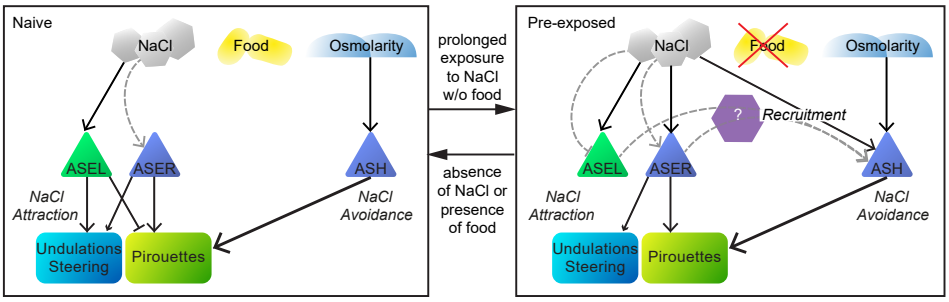

Figure 6.6: Schematic model of the NaCl navigation circuit. Schematic of the different forms of sensory adaptation and their downstream effects in response to NaCl exposure in the absence of food. Left: The naive state, in the absence of NaCl and/or the presence of food. ASEL is fully sensitized, ASER desensitized and ASH only responds to high NaCl concentrations (osmotic shock). Right: pre-exposed state, after 10-15 minutes of exposure to NaCl in the absence of food: ASEL becomes desensitized, ASER sensitized and ASH recruited to respond to lower NaCl concentrations. Recruitment of ASH depends on an absence of food signal and ASE, possibly via one or more intermediate neurons. ASEL/R mediate attraction to NaCl and ASH mediates avoidance of NaCl. NaCl dependent adaptation presented in gray dashed arrows. Solid arrows represent excitation (either via receptors or synapses), solid bars inhibition.

and thus signals from one or more other neurons. ASER also sensitizes following salt-exposure, exhibiting enhanced responses to concentration decreases.

While other sensory neurons and contributions from the downstream circuitry most likely contribute to the behavioral response, our simulations demonstrate the feasibility of a parsimonious model in which recruitment of ASH by a food and an ASE (NaCl) derived signal underpin gustatory plasticity. While ASER plays a role in NaCl attraction, counterintuitively, its sensitization timescale hints at a possible contribution to NaCl avoidance. In our model, ASER mediates attraction only, and its effect is masked when ASH is recruited. An alternative scenario may be suggested based on a recent study showing evidence for ASER flipping its synaptic sign to a downstream interneuron [73]. Thus, ASER could mediate avoidance in gustatory plasticity if the synaptic sign flip was starvation dependent. Future work will need to address what the direct function of ASE (de)sensitization is, beyond a possible role in ASH recruitment.

One question that immediately comes to mind when studying the ASE sensory neurons is why ASEL and ASER exhibit such different responses. These neurons were already known to exhibit bilaterally asymmetric kinetics, in which ASEL and ASER depolarize in response to concentration increases and decreases, respectively [97]. One attractive conjecture is that this functional differentiation, with opposite polarities of responses in the two neurons, allows the animal to double its dynamic range (from {0,x} to {-x,x}), thus enhancing its resolution. However, the apparent timescale separation in the (fully sensitized) responses suggests otherwise.

Our computational modeling results demonstrate how such a separation of timescales in the processing of sensory inputs leads to distinct pathways for the control of different motor programs: Fast sensory processing (as observed in ASEL) controls steering whereas slow sensory processing (potentially in ASER) has the capacity to modulate motor programs such as pirouettes over tens of seconds or minutes. Therefore, I conjecture that *C. elegans* has evolved distinct sensory processing pathways with distinct characteristic timescales to drive separate navigational strategies: steering and pirouette modulation. If indeed, such timescale separation is confirmed already at the level of sensory neurons (in ASEL and ASER response kinetics), it would be, to our knowledge, the first example of sensory neurons encoding and directly controlling motor actions.

We modeled ASEL desensitization as an adaptive threshold and ASER sensitization as a multiplicative gain adaptation. While this was mathematically the most natural choice, and appears biologically plausible, I cannot exclude other forms of adaptation. Future experiments will have to look closer at the mechanism underlying ASE (de)sensitization to provide evidence as to the molecular nature of adaptation.

While one would expect some forms of adaptation in sensory neurons (such as photo receptor adaptation to light intensity levels), our results point to severe information loss, causing a potentially considerable impediment in salt sensing. The bilaterally asymmetric responses mean that when ASER is desensitized, for example, the animal's ability to

respond to concentration decreases is all but abolished. It is therefore natural to ask whether these forms of adaptation should be considered purely as limitations (perhaps resulting from metabolic or other constraints), or whether they may prove beneficial in the animal's natural habitat.

Our model predicts a number of behavioral consequences for these distinct forms of adaptation off food. In our model, naive worms (with sensitized ASEL only) will move up gradients, but if the salt regions explored are insufficient to sensitize ASER, some level of dispersion from these regions will occur. Desensitization of ASEL promotes dispersion from a salt region that has been explored for some time. Conversely, if ASER is sufficiently sensitized, a downward trajectory will suppress dispersion by promoting turning (and a return to the salt rich region). Thus, ASER sensitization would ensure that ASER only responds to sufficiently large salt regions, ignoring small fluctuations. In summary, salt-adaptation of ASE neurons could serve to balance exploration and exploitation navigational strategies in complex, heterogeneous environments. In addition, if ASEL predominantly controls steering towards gradient peaks when navigating up the gradient, desensitization would reduce steering only after entering a salt region (promoting broader exploration within the salt-rich region). Conversely if ASER predominantly modulates pirouettes, then leaving a salt patch will likely induce a pirouette. In our model, I have not included preferential exit angles from a pirouette, which may play a further role in such scenarios.

The intuition presented here suggests that, in the case of a neutral signal such as NaCl, the compactness of the nervous system in *C. elegans* may benefit from enhanced computation in sensory neurons at the price of considerable information loss. Taken together, our computational model and experimental data point to a highly complex set of distinct forms of plastic sensory computation in the NaCl sensing circuit, indicating that, compared to higher animals, *C. elegans* has seen a shift of computation from the inter- to sensory layers over its evolutionary history.

The behavioral response of *C. elegans* is strikingly similar to the responses of mice, rats and humans to salt, which show attraction to low NaCl concentrations (100-150 mM NaCl and lower) and avoidance of high NaCl concentrations [4, 8, 15]. Recent analyses of the response of mice to NaCl using genetic and imaging techniques has revealed that appetitive NaCl taste involves different taste receptor cells than avoidance of high NaCl concentrations [22, 81]. Interestingly, mice in which avoidance of high NaCl concentrations is inactivated are strongly attracted to very high NaCl concentrations [81]. Moreover, in mice, rats and humans, the response to NaCl can be modulated by for example the internal sodium balance [4, 8, 15]. Whether the response to NaCl can be manipulated in these mammals to the same extent as in *C. elegans* remains to be seen.

Chapter 7

Discussion

The work presented in this thesis explores the role of sensory computation in decision making. Across the animal kingdom, sensory systems have evolved to encode sensory inputs. Some of the complexities of sensory systems, including their architectures, dynamic range adaptation and modulation, can be explained by better understanding the signals they encode, or by a more introspective examination of their limitations due to speed-accuracy trade-offs, their limited bandwidth of neural processing and constraints due to various metabolic costs, to name a few. None of these considerations change the basic premise that the role of sensory systems is to encode sensory inputs.

This view has been confirmed time and again in *C. elegans*. In particular, a recent study by Gordus et al. [40] has specifically asked this question and concluded that whereas *C. elegans* sensory neurons encode sensory information, downstream neurons (even first layer interneurons) encode behavioral decisions or motor behavior. This view is also consistent with a number of studies that consider switching between different behaviors, such as forward and backward locomotion [63], roaming and dwelling [38], attraction and repulsion [54], and more. In all of the above, the decision making occurs downstream of the sensory layer, or equivalently, the behavior cannot be predicted form looking at activity in the sensory layer.

In this thesis, I proposed that the computation performed by sensory systems in *C. elegans* is much more extensive. My model of copper-diacetyl integration follows conventional thinking, by considering a minimal feed forward pathway and assigning the interesting computation to the postulated site of sensory integration, the AIY interneurons. While useful in highlighting model requirements, the proposed mechanisms are not surprising. In fact, these are well understood in the computational neuroscience and adaptive behavior communities. My study of diacetyl-fructose sensory integration was more powerful as I had the opportunity to test the model, through iterations of data and modeling. The result was a model that can be likened to top-down attention modulation in other animals. An interneuron RIM serves as a slow integrator to modulate the excitability of ASH sensory neurons. The decision to cross the barrier, or not, is then modulated by the level of ASH activation.

Turning my attention to salt navigation and gustatory plasticity, my model and simulations suggest that the sensitization and desensitization of the ASE and ASH sensory neurons directly encodes the behavioral state of the animal. Furthermore, the modulation of the sensory neurons, which for ASE appears to be largely cell-autonomous, regulates the balance of attraction and avoidance, and more subtly – exploration and exploitation (presumably of food). Thus surprisingly, here, the internal state and animal behavior can be gleaned from sensory neuron activity alone!

In this chapter, I summarize these findings in turn, and discuss the limitations of my models. Finally, I briefly mention future directions.

7.1 Preliminary findings

When preparing to create my model, I decided to first do a more detailed investigation of the computational model proposed in the study by Izquierdo and Lockery [57]. Reproducing their model, I found that a more parsimonious variant could be created

by removing the self-connections, Gaussian noise, and muscle bias parameter. This last parameter, I showed to be important for steering. Specifically, the equations used, do not allow a full symmetry in steering, such that animals cannot steer towards attractants and away from repellents for all concentrations. This suggests, that for a model capable of assays with a wider variety of stimuli (attractive and repulsive), a new steering system is needed. It also shows that two key parameters of the sensory neurons, the rise time and decay time, or equivalently the time to peak depolarization in response to a step change, need to be matched to the motor program, and stimulus encoding. For instance, the model predicts that slowing down a sensory neuron to more than 1/4th of an undulation period (approximately 1 second) should change an attractive stimulus into an aversive and vice versa. Interestingly, a result highly reminiscent of this effect was reported in an experimental study (Kato et al. [62], figure 6F of their publication), where animals with a slowed down AWC response (*odr-3* null mutants) showed anti-steering, or as phrased in their study: 'when moving away form the odor source, *odr-3* animals curve in the wrong direction' [62].

7.2 Iterations of the model

In building a computational model, I wanted to address a number of requirements. First, to link neural computation with behavior, I required an integrated simulation framework, including sensory neurons, downstream circuits, motor outputs and physical environments. Second, I set out to make this framework generic, easily specifiable, and modular. In so doing I was motivated by three considerations: (i) to allow me the flexibility to study different neurons, circuits and assays, and to easily modify my own models; (ii) to be able to constrain my models by testing them under a variety of conditions and even different assays; and (iii) to provide a friendly and powerful tool for similar modeling endeavors by the community.

The aim of my PhD was to create a generic integrated model, capable of capturing several forms of sensory integration and decision making. Naturally, the model should not just reproduce experimental findings, but should provide testable predictions and guide experiments in an iterative approach. The latter being especially important. Indeed, creating a model that can reproduce several different assays is challenging and risks becoming under constrained (by including too many features) or over constrained (if the assays were performed under different conditions that are not accounted for in the model). I believe the model presented in this thesis has achieved all this, while striking an appropriate balance between the level of abstraction and biological grounding.

I used a case study based on an assay from the literature – the copper and diacetyl assay [54, 93] (including a copper only assay [89]) – to build my model framework and to consider model requirements. This model was in many ways similar to salt chemotaxis models developed by Izquierdo and Lockery [57], and extended by Izquierdo and Beer [55, 56]. The model successfully accounted for the results in the literature and made a number of interesting predictions. First, to quantitatively account for the results, model sensory neurons had respond to the log of concentration gradients. Additionally, in the model, copper avoidance triggers reversals with a final turn angle distribution that is narrower than stochastic reversals, producing something like a u-turn. This feature, modeled by a distinct motor program in my model prevents model animals from continuing in the same direction as before a pirouette, when avoiding an immediate threat in front of them.

In the process of building and iterating the model, several of the assumptions I had made early on had to be revisited. One such assumption was that the sensory neurons respond with an (imperfect) approximation of a time derivative of the stimulus strength [57, 100]. While it is clear that many sensory neurons respond to changes in stimulus strength rather than absolute strength, my model has showed me that it is likely that much more computation occurs in the sensory layer. First, the time period over which the sensory

neurons integrate matters. Too slow or too fast and no steering or anti-steering occurs. Additionally, slower sensory neurons produce better pirouette modulation, while faster sensory neurons are better for steering.

In a full sensorimotor system, bi-directional constraints are imposed between the sensory system and motor programs (in particular steering). This was later evident by observations in the quadrant assay, in which (unlike gradient assays) worms need to choose quadrants based on sensory information gathered in only a very narrow region of space. My observations that worms performed successful, very strong steering near the quadrant interfaces required further adjustment of my steering circuit model. While my model does not capture the detailed embodiment, or even speed modulation and modulations of the strength of steering that likely exist in the worm, it does contain a steering circuit that can modulate both wavelength and amplitude in a way that enhances the sensory perception during sharp turns, allowing the model worm to more closely match behavioral observations.

7.3 Model limitations

The price of parsimony is that many aspects are missing or simplified. Only minimal circuits were considered and embodiment was neglected. Thus the worm was modeled as a point, moving at fixed speed. While the models of steering appear to capture *C. elegans* more realistically than some of the existing published models, it does not capture the richness of *C. elegans* actual coordination and movement. Many other motor programs such as reversals and omega turns were neglected as well (though adding actual reversals or a duration to our pirouettes was not found to make a difference for any of the results tested). In addition, the model used average parameters (from calcium imaging and behavioral metrics) to model a fictional *averaged C. elegans*. It does not attempt to capture the details of individual behavior correctly, but only to capture the essential

features necessary to capture the same high level behavioral metrics (such as various chemotaxis indices).

At the methodological level, the key limitation of the model is its speed. Speed was the main consideration in excluding embodiment from the model framework (as this would substantially slow down the simulations)[13, 56]. However, the situated nature of experiments, especially when chemical diffusion is included, remains prohibitive.

In many ways, this model is a first step, incorporating a small number of neurons and a small number of assays. It is hoped that further iterations and extensions of the model, on the basis of additional studies, will offer validation for the framework, its usability and the validity of the biological mechanisms proposed.

7.4 Future directions

Two separate branches of follow up work can be distinguished. First, the model predictions point to specific experiments that can be done to test them. Second, the model can be further extended in several (non-exclusive) ways.

7.4.1 Testing model predictions

My model makes several testable predictions. First, the model predicts that sensory neurons' response lag must be in sync with the motor system, and that ASEL and ASER steer optimally with different response lags. Second, ASEL, ASER and AWA appear to respond to a log like function of the change in concentration, thus producing a Weber-Fechner like response. Third, in the model, naive animals move towards salt spots already in their path (mediated by naive ASEL) but do not move towards NaCl spots behind them (mediated only by ASER after pre-exposure to NaCl), this allows model animals to ignore small salt patches. Fourth, the model predicts that gustatory deficient mutants would have

reduced exploration of a plate with a grid of salt patches, visiting less patches than wild type animals. I will briefly describe a possible experimental setup for each prediction.

Other than the *odr-3* mutant, there are currently no strains that allows precise control of sensory neurons' response lag. Changing the speed of the undulations however is trivial. Since the sensory neurons response lag must be in sync to the motor system an increase in the undulation frequency should break steering (the model indeed shows this). Since, swimming *C. elegans* have a much higher undulation frequency, one could simply test if swimming animals use pirouette modulation exclusively. Another interesting experiment that could be done, but which would be much more challenging and costly, is to use optogenetics to drive the calcium concentration in ASEL and ASER in real animals according to model sensory neurons' activation in a virtual assay. In the study by Kocabas et al. [65], an animal's nose was tracked such that the interneuron AIY could be excited according to the gradient change in a virtual assay. This procedure produced real world animals that followed virtual gradients. Adapting this study to use my model, and changing the rates of the sensory neurons (i.e. response lag), you could show that slower sensory neurons produce anti steering, and that if ASEL and ASER have different response lags, the chemotaxis index is higher, than if they are the same. Interestingly, the Kocabas et al. [65] study already noticed that a delay needed to be included in their activation of the interneuron. Unfortunately, no systematic sweep of delays was reported.

I ended up using a Weber-Fechner like response for ASEL, ASER and AWA in the model because the model required it to reproduce calcium imaging and behavioral data (calcium imaging data [67, 97] and (Appendix A, behavioral data [50, 51, 54, 93]). This model result has been partially tested for AWA by Larsch et al. [67] by systematically changing the step size, duration and gradient, and measuring the calcium response with GCaMP. Though longer diacetyl exposures would be needed to exclude a response to the removal of diacetyl. For ASEL and ASER a similar setup could be used, where the response of both neurons (for ASEL naively, and ASER pre-exposed) to a variety of step sizes,

durations and gradients could be measured with a sensitive calcium indicator (Yellow Cameleon is not sensitive enough to detect responses to low concentration steps).

Testing if *C. elegans* does not steer towards NaCl spots behind the worm in the first two minutes of exposure can be done using a linear gradient (see wormbreeder's gazette volume 18, number 3, Making linear chemical gradients in agar) and a worm tracker, one could see if in the first two minutes after placement, animals with an original heading away from the gradient peak steer less well than those after the first two minutes.

The third prediction, that gustatory plasticity deficient animals will explore more areas, can be tested using a multi spot assay, as used in Iino and Yoshida [52] and allowing animals to roam freely for at least an hour (allowing multiple cycles of ASH sensitization and desensitization). If the model prediction holds up, wild type animals should visit more spots within the hour than mutants such as *gpc-1* and *odr-3*. Additionally, the model predicts that the cycle of moving towards an NaCl peak, leaving and then visiting another peak, should be around 15 minutes (the 10 minutes it takes to sensitize ASH and the 5 to relax).

7.4.2 Model extensions

I can see several model extensions that follow logically from the current state. First, the framework of the model allows it to be linked to biophysical models of the worm body (such as those used in Boyle et al. [13], Xu and Deng [112] and Szigeti et al. [98]) making it possible to ask more locomotion oriented questions on the role of sensory processing. Second and more closely related to the questions asked in the case studies of this thesis, the model can be extended to look closer at the NaCl sensing circuit, adding the downstream first layer interneurons, AIA, AIB, AIY, AIZ, as well as adding ADL and ASI, both known to be involved in gustatory plasticity [50].

Other avenues that have not been explored yet, but where a large body of experimental

work is available are AWC mediated chemotaxis and thermotaxis. The latter of which, like NaCl chemotaxis, is known to involve several forms of adaptation and conveniently involves the sensory neuron classes AFD, AWC and ASI [11, 66, 76]. Adding sensory neurons should also allow the model to look more at multiple modalities overlapping in one neuron class (e.g. chemotaxis and thermotaxis in AWC, hyperosmolarity and toxicity in ASH, food and thermotaxis in ASI).

7.5 Reflections

Looking back, I hope I have shown the important contributions that computational models of *C. elegans* behavior can make when integrated with experimental work. Additionally, I hope the model itself will prove its value beyond this work, and that its ease of adaptation will entice non-computational labs to use it for rapid testing of assays and ablations that would be too time-intensive or not yet possible in real world experiments. Having a tool like this can help guide experiments, potentially providing non-trivial hypotheses and clues as to the function of neuronal and circuit mechanisms.

Bibliography

[1] Takeshi Adachi, Hirofumi Kunitomo, Masahiro Tomioka, Hayao Ohno, Yoshifumi Okochi, Ikue Mori, and Yuichi Iino. Reversal of salt preference is directed by the insulin/pi3k and gq/pkc signaling in *Caenorhabditis elegans*. *Genetics*, 186(4): 1309–1319, 2010. doi: 10.1534/genetics.110.119768.

[2] Dirk R. Albrecht and Cornelia I. Bargmann. High-content behavioral analysis of *Caenorhabditis elegans* in precise spatiotemporal chemical environments. *Nature Methods*, 8(7):599–605, 2011. doi: 10.1038/nmeth.1630.

[3] Peter A. Appleby. A model of chemotaxis and associative learning in *C. elegans*. *Biological Cybernetics*, pages 373–387, 2012. doi: 10.1007/s00422-012-0504-8.

[4] Alexander A. Bachmanov, Gary K. Beauchamp, and Michael G. Tordoff. Voluntary consumption of nacl, kcl, cacl(2), and nh(4)cl solutions by 28 mouse strains. *Behavior Genetics*, 32(6):445–457, Nov 2002. 12467342[pmid].

[5] Cornelia I. Bargmann and H. Robert Horvitz. Chemosensory neurons with overlapping functions direct chemotaxis to multiple chemicals in *C. elegans*. *Neuron*, 7:729–742, 1991. doi: 10.1016/0896-6273(91)90276-6.

[6] Cornelia I. Bargmann, James H. Thomas, and H. Robert Horvitz. Chemosensory cell function in the behavior and development of *Caenorhabditis elegans*. *Cold Spring Harbor Symposia on Quantitative Biology*, 55:529–538, 1990. doi: 10.1101/SQB.1990.055.01.051.

[7] Cornelia I. Bargmann, Erika Hartwieg, and H. Robert Horvitz. Odorant-selective genes and neurons mediate olfaction in *C. elegans*. *Cell*, 74:515–527, 1993. doi: 10.1016/0092-8674(93)80053-H.

[8] Gary K. Beauchamp, Mary Bertino, Darlene Burke, and Karl Engelman. Experimental sodium depletion and salt taste in normal human volunteers. *The American Journal of Clinical Nutrition*, 51(5):881–9, 1990.

[9] Isabel Beets, Tom Janssen, Ellen Meelkop, Liesbet Temmerman, Nick Suetens, Suzanne Rademakers, Gert Jansen, and Liliane Schoofs. Vasopressin/oxytocin-related signaling regulates gustatory associative learning in *C. elegans*. *Science*, 338(6106):543–545, 2012. doi: 10.1126/science.1226860.

[10] Stefano Berri, Jordan H. Boyle, Manlio Tassieri, Ian A. Hope, and Netta Cohen. Forward locomotion of the nematode *C. elegans* is achieved through modulation of a single gait. *Human Frontier Science Program Journal*, 3(3):186–193, 2009. doi: 10.2976/1.3082260.

[11] Matthew Beverly, Sriram Anbil, and Piali Sengupta. Degeneracy and neuromodulation among thermosensory neurons contribute to robust thermosensory behaviors in *Caenorhabditis elegans*. *The Journal of Neuroscience*, 31(32):11718–11727, 2011. doi: 10.1523/JNEUROSCI.1098-11.2011.

[12] Jordan H. Boyle. C. elegans *locomotion: an integrated approach*. PhD thesis, School of Computing, University of Leeds, 2009.

[13] Jordan H. Boyle, Stefano Berri, and Netta Cohen. Gait modulation in C. elegans: An integrated neuromechanical model. *Front. Comput. Neurosci.*, 6(March):1–10, 2012. ISSN 1662-5188. doi: 10.3389/fncom.2012.00010.

[14] Sydney Brenner. The genetics of *Caenorhabditis elegans*. *Genetics*, 77(1):71–94, 1974.

[15] Paul A. Breslin, Joshua M. Kaplan, Alan C. Spector, Christine M. Zambito, and Harvey J. Grill. Lick rate analysis of sodium taste-state combinations. *American Journal of Physiology - Regulatory, Integrative and Comparative Physiology*, 264 (2):R312–R318, 1993.

[16] John Bryden and Netta Cohen. Neural control of *Caenorhabditis elegans* forward locomotion: the role of sensory feedback. *Biological Cybernetics*, 98(4):339–351, 2008. doi: 10.1007/s00422-008-0212-6.

[17] John A. Bryden and Netta Cohen. A simulation model of the locomotion controllers for the nematode *Caenorhabditis elegans*. In S. Schaal, A.J. Ijspeert, A. Billard, S. Vijayakumar, J. Hallam, and J-A. Meyer, editors, *From Animals to Animats 8: Proceedings of the Eighth International Conference on the Simulation of Adaptive Behavior*, pages 183–192, July 2004.

[18] Arthur H. Burr. The photomovement of *Caenorhabditis elegans*, a nematode which lacks ocelli. proof that the respons is to light not radiant heating. *Photochemistry and Photobiology*, 41(5):577–582, 1985. doi: 10.1111/j.1751-1097.1985.tb03529.x.

[19] Victoria J. Butler, Robyn Branicky, Eviatar Yemini, Jana F. Liewald, Alexander Gottschalk, Rex A. Kerr, Dmitri B. Chklovskii, and William R. Schafer. A consistent muscle activation strategy underlies crawling and swimming in *Caenorhabditis elegans*. *Journal of The Royal Society Interface*, 12(102), 2015. doi: 10.1098/rsif.2014.0963.

[20] Sreekanth H. Chalasani, Nikos Chronis, Makoto Tsunozaki, Jesse M. Gray, Daniel Ramot, Miriam B. Goodman, and Cornelia I. Bargmann. Dissecting a circuit for olfactory behaviour in *Caenorhabditis elegans*. *Nature*, 450:63–70, 2007.

[21] Dominique Champion, Hubert Hervet, Genevieve Blond, and Denise Simatos. Comparison between two methods to measure translational diffusion of a small

molecule at subzero temperature. *Journal of Agricultural and Food Chemistry*, 43 (11):2887–2891, 1995. doi: 10.1021/jf00059a022.

[22] Jayaram Chandrashekar, Christina Kuhn, Yuki Oka, David A. Yarmolinsky, Edith Hummler, Nicholas J. P. Ryba, and Charles S. Zuker. The cells and peripheral representation of sodium taste in mice. *Nature*, 464(7286):297–301, 2010. doi: 10.1038/nature08783.

[23] Beth L. Chen, David H. Hall, and Dmitri B. Chklovskii. Wiring optimization can relate neuronal structure and function. *Proceedings of the National Academy of Sciences of the United States of America*, 103:4723–4728, 2006.

[24] Joseph H. Chou, Cornelia I. Bargmann, and Piali Sengupta. The *Caenorhabditis elegans* odr-2 gene encodes a novel ly-6-related protein required for olfaction. *Genetics*, 157(1):211–224, 2001.

[25] Damon A. Clark, Christopher V. Gabel, Harrison Gabel, and Aravinthan D. T. Samuel. Temporal activity patterns in thermosensory neurons of freely moving *Caenorhabditis elegans* encode spatial thermal gradients. *The Journal of Neuroscience*, 27(23):6083–6090, 2007. doi: 10.1523/JNEUROSCI.1032-07.2007.

[26] Netta Cohen and Tom Sanders. Nematode locomotion: dissecting the neuronal–environmental loop. *Current Opinion Neurobiology*, 25:99–106, 2014. doi: j.conb.2013.12.003.

[27] Heather A. Colbert and Cornelia I. Bargmann. Odorant-specific adaptation pathways generate olfactory plasticity in *C. elegans*. *Cell*, 14:803–812, 1995.

[28] Heather A. Colbert, Tracy L. Smith, and Cornelia I. Bargmann. Osm-9, a novel protein with structural similarity to channels, is required for olfaction,

mechanosensation, and olfactory adaptation in *Caenorhabditis elegans*. *The Journal of Neuroscience*, 17(21):8259–8269, 1997.

[29] Shane R. Crandall, Scott J. Cruikshank, and Barry W. Connors. A corticothalamic switch: Controlling the thalamus with dynamic synapses. *Neuron*, 86(3):768–782, 2015. doi: 10.1016/j.neuron.2015.03.040.

[30] Joseph G. Culotti and Richard L. Russell. Osmotic avoidance defective mutants of the nematode *Caenorhabditis elegans*. *Genetics*, 90(2):243–256, 1978.

[31] Mario de Bono and Andres V. Maricq. Neuronal substrates of complex behaviors in *C. elegans*. *Annual Review of Neuroscience*, 28(1):451–501, 2005. doi: 10.1146/annurev.neuro.27.070203.144259.

[32] Nathan A. Dunn, Shawn R. Lockery, Jonathan T. Pierce-Shimomura, and John S. Conery. A neural network model of chemotaxis predicts functions of synaptic connections in the nematode *Caenorhabditis elegans*. *Journal of Computational Neuroscience*, 17:137–147, 2004.

[33] Nathan A. Dunn, Jonathan T. Pierce-Shimomura, John S. Conery, and Shawn R. Lockery. Clustered neural dynamics identify motifs for chemotaxis in *Caenorhabditis elegans*. In *Neural Networks, 2006. IJCNN '06. International Joint Conference on*, pages 547–554, 2006. doi: 10.1109/IJCNN.2006.246730.

[34] *C. elegans* Sequencing Consortium. Genome sequence of the nematode *C. elegans*: A platform for investigating biology. *Science*, 282(5396):2012–2018, 1998. doi: 10.1126/science.282.5396.2012.

[35] Christopher Fang-Yen, Matthieu Wyart, Julie Xie, Risa Kawai, Tom Kodger, Sway Chen, Quan Wen, and Aravinthan D. T. Samuel. Biomechanical analysis of gait adaptation in the nematode *Caenorhabditis elegans*. *Proceedings of the National*

Academy of Sciences of the United States of America, 107(47):20323–20328, 2010. doi: 10.1073/pnas.1003016107.

[36] Robert P. Feldman and T. Goodrich, James. The edwin smith surgical papyrus. *Child's Nervous System*, 15(6-7):281–284, 1999. doi: 10.1007/s003810050395.

[37] Thomas C. Ferrée and Shawn R. Lockery. Computational rules for chemotaxis in the nematode *C. elegans*. *Journal of Computational Neuroscience*, 6:263–277, 1999.

[38] Steven W. Flavell, Navin Pokala, Evan Z. Macosko, Dirk R. Albrecht, Johannes Larsch, and Cornelia I. Bargmann. Serotonin and the neuropeptide PDF initiate and extend opposing behavioral states in *C. elegans*. *Cell*, 154(5):1023–1035, 2013. doi: 10.1016/j.cell.2013.08.001.

[39] Wesley T. Frazier, Eric R. Kandel, Irving Kupfermann, Rafiq Waziri, and Richard E. Coggeshall. Morphological and functional properties of identified neurons in the abdominal ganglion of *Aplysia californica*. *Journal of Neurophysiology*, 30(6):1288–1351, 1967.

[40] Andrew Gordus, Navin Pokala, Sagi Levy, Steven W. Flavell, and Cornelia I. Bargmann. Feedback from network states generates variability in a probabilistic olfactory circuit. *Cell*, 161(2):215–227, 2015. doi: 10.1016/j.cell.2015.02.018.

[41] Jesse M. Gray, David S. Karow, Hang Lu, Andy J. Chang, Jennifer S. Chang, Ronald E. Ellis, Michael A. Marletta, and Cornelia I. Bargmann. Oxygen sensation and social feeding mediated by a *C. elegans* guanylate cyclase homologue. *Nature*, 430:317–322, 2004. doi: 10.1038/nature02714.

[42] Jesse M. Gray, Joseph J. Hill, and Cornelia I. Bargmann. A circuit for navigation in *Caenorhabditis elegans*. *Proceedings of the National Academy of Sciences of the United States of America*, 102:3184–3191, 2005.

[43] Charles G. Gross. *Brain, Vision, Memory: Tales in the History of Neuroscience*. A Bradford book. MIT Press, 1999. ISBN 9780262571357.

[44] Zengcai V. Guo, Anne C. Hart, and Sharad Ramanathan. Optical interrogation of neural circuits in *Caenorhabditis elegans*. *Nature Methods*, 6(12):891–896, 2009. doi: 10.1038/nmeth.1397.

[45] Anne C. Hart, Jamie Kass, Jonathan E. Shapiro, and Joshua M. Kaplan. Distinct signaling pathways mediate touch and osmosensory responses in a polymodal sensory neuron. *The Journal of Neuroscience*, 19(6):1952–1958, 1999.

[46] Edward M. Hedgecock and Richard L. Russell. Normal and mutant thermotaxis in the nematode *Caenorhabditis elegans*. *Proceedings of the National Academy of Sciences of the United States of America*, 72(10):4061–4065, 1975.

[47] Massimo A. Hilliard, Alfonso J. Apicella, Rex Kerr, Hiroshi Suzuki, Paolo Bazzicalupo, and William R. Schafer. *In vivo* imaging of *C. elegans* ash neurons: cellular response and adaptation to chemical repellents. *EMBO Journal*, 24.

[48] Alan L. Hodgkin and Andrew F. Huxley. A quantitative description of membrane current and its application to conduction and excitation in nerve. *The Journal of physiology*, 117(4):500–544, 1952.

[49] Jonathan Hodgkin. Male phenotypes and mating efficiency in *Caenorhabditis elegans*. *Genetics*, 103(1):43–64, 1983.

[50] Renate K. Hukema, Suzanne Rademakers, Martijn P. J. Dekkers, Jan Burghoorn, and Gert Jansen. Antagonistic sensory cues generate gustatory plasticity in *Caenorhabditis elegans*. *EMBO Journal*, 25:312–322, 2006.

[51] Renate K. Hukema, Suzanne Rademakers, and Gert Jansen. Gustatory plasticity in *C. elegans* involves integration of negative cues and nacl taste mediated by serotonin, dopamine, and glutamate. *Learning and Memory*, 15:829–836, 2008.

[52] Yuichi Iino and Kazushi Yoshida. Parallel use of two behavioral mechanisms for chemotaxis in *Caenorhabditis elegans*. *The Journal of Neuroscience*, 29:5370–5380, 2009.

[53] Daisuke D. Ikeda, Yukan Duan, Masahiro Matsuki, Hirofumi Kunitomo, Harald Hutter, Edward M. Hedgecock, and Yuichi Iino. Casy-1, an ortholog of calsyntenins/alcadeins, is essential for learning in *Caenorhabditis elegans*. *Proceedings of the National Academy of Science of the United States of America*, 105(13):5260–5265, 2008. doi: 10.1073/pnas.0711894105.

[54] Takeshi Ishihara, Yuichi Iino, Akiko Mohri, Ikue Mori, Keiko Gengyo-Ando, Shohei Mitani, and Isao Katsura. Hen-1, a secretory protein with an ldl receptor motif, regulates sensory integration and learning in *Caenorhabditis elegans*. *Cell*, 109(5):639–649, 2002.

[55] Eduardo J. Izquierdo and Randall D. Beer. Connecting a connectome to behavior: An ensemble of neuroanatomical models of *C. elegans* klinotaxis. *PLoS Computational Biology*, 9(2):e1002890, 2013. doi: 10.1371/journal.pcbi.1002890.

[56] Eduardo J. Izquierdo and Randall D. Beer. An integrated neuromechanical model of steering in *C. elegans*. In *Proceeding of the European Conference on Artificial Life*, pages 199–206. MIT Press, 2015.

[57] Eduardo J. Izquierdo and Shawn R. Lockery. Evolution and analysis of minimal neural circuits for klinotaxis in *Caenorhabditis elegans*. *The Journal of Neuroscience*, 30:12908–12917, 2010.

[58] Gert Jansen, David Weinkove, and Ronald H. A. Plasterk. The g-protein gamma subunit gpc-1 of the nematode *C. elegans* is involved in taste adaptation. *EMBO Journal*, 21:986–994, 2002. doi: 10.1093/emboj/21.5.986.

[59] Robert J. Johnston and Oliver Hobert. A microrna controlling left/right neuronal asymmetry in *Caenorhabditis elegans*. *Nature*, 426(6968):845–849, 2003. doi: 10.1038/nature02255.

[60] Marcus Kaiser and Claus C. Hilgetag. Nonoptimal component placement, but short processing paths, due to long-distance projections in neural systems. *PLoS Compututional Biology*, 2(7):e95, 2006. doi: 10.1371/journal.pcbi.0020095.

[61] Joshua M. Kaplan and H. Robert Horvitz. A dual mechanosensory and chemosensory neuron in *Caenorhabditis elegans*. *Proceedings of the National Academy of Sciences of the United States of America*, 90(6):2227–2231, 1993. doi: 10.1073/pnas.90.6.2227.

[62] Saul Kato, Yifan Xu, Christine E. Cho, Laurence F. Abbott, and Cornelia I. Bargmann. Temporal responses of *C. elegans* chemosensory neurons are preserved in behavioral dynamics. *Neuron*, 81(3):616–628, 2014.

[63] Taizo Kawano, Michelle D. Po, Shangbang Gao, George Leung, William S. Ryu, and Mei Zhen. An imbalancing act: Gap junctions reduce the backward motor circuit activity to bias *C. elegans* for forward locomotion. *Neuron*, 72(4):572–586, 2011. doi: 10.1016/j.neuron.2011.09.005.

[64] Rex Kerr, Varda Lev-Ram, Geoff Baird, Pierre Vincent, Roger Y. Tsien, and William R. Schafer. Optical imaging of calcium transients in neurons and pharyngeal muscle of *C. elegans*. *Neuron*, 26(3):583–594, 2000. doi: 10.1016/S0896-6273(00)81196-4.

[65] Askin Kocabas, Ching-Han Shen, Zengcai V. Guo, and Sharad Ramanathan. Controlling interneuron activity in *Caenorhabditis elegans* to evoke chemotactic behaviour. *Nature*, 490(7419):273–277, 2012. doi: 10.1038/nature11431.

[66] Atsushi Kuhara, Masatoshi Okumura, Tsubasa Kimata, Yoshinori Tanizawa, Ryo Takano, Koutarou D. Kimura, Hitoshi Inada, Kunihiro Matsumoto, and Ikue Mori. Temperature sensing by an olfactory neuron in a circuit controlling behavior of *C. elegans*. *Science*, 320(5877):803–807, 2008. doi: 10.1126/science.1148922.

[67] Johannes Larsch, Donovan Ventimiglia, Cornelia I. Bargmann, and Dirk R. Albrecht. High-throughput imaging of neuronal activity in *Caenorhabditis elegans*. *Proceedings of the National Academy of Sciences of the United States of America*, 110(45):E4266–E4273, 2013. doi: 10.1073/pnas.1318325110.

[68] Félix Lebois, Pascal Sauvage, Charlotte Py, Olivier Cardoso, Benoît Ladoux, Pascal Hersen, and Jean-Marc Di Meglio. Locomotion control of *Caenorhabditis elegans* through confinement. *Biophysical Journal*, 102(12):2791–2798, 2012. doi: 10.1016/j.bpj.2012.04.051.

[69] SooHyun Lee, George E. Carvell, and Daniel J. Simons. Motor modulation of afferent somatosensory circuits. *Nature Neuroscience*, 11(12):1430–1438, 2008. doi: 10.1038/nn.2227.

[70] Herbert Levine and Wouter-Jan Rappel. The physics of eukaryotic chemotaxis. *Physics Today*, 66(2):10.1063/PT.3.1884, 2013. doi: 10.1063/PT.3.1884.

[71] Wei Li, Zhaoyang Feng, Paul W. Sternberg, and X. Z. Shawn Xu. A *C. elegans* stretch receptor neuron revealed by a mechanosensitive trp channel homologue. *Nature*, 440(7084):684–687, 2006. doi: 10.1038/nature04538.

[72] Zhaoyu Li, Yidong Li, Yalan Yi, Wenming Huang, Song Yang, Weipin Niu, Li Zhang, Zijing Xu, Anlian Qu, Zhengxing Wu, and Tao Xu. Dissecting a central flip-flop circuit that integrates contradictory sensory cues in *C. elegans* feeding regulation. *Nature Communications*, 3:776, 2012.

[73] Linjiao Luo, Quan Wen, Jing Ren, Michael Hendricks, Marc Gershow, Yuqi Qin, Joel Greenwood, Edward R. Soucy, Mason Klein, Heidi K. Smith-Parker, Ana C. Calvo, Daniel A. Colón-Ramos, Aravinthan D. T. Samuel, and Yun Zhang. Dynamic encoding of perception, memory, and movement in a *C. elegans* chemotaxis circuit. *Neuron*, 82(5):1115–1128, 2014. doi: 10.1016/j.neuron.2014.05.010.

[74] Henry Markram, Eilif Muller, Srikanth Ramaswamy, Michael W. Reimann, Marwan Abdellah, Carlos Aguado Sanchez, Anastasia Ailamaki, Lidia Alonso-Nanclares, Nicolas Antille, and Selim Arsever *et al.* . Reconstruction and simulation of neocortical microcircuitry. *Cell*, 163(2):456–492, 2015. doi: 10.1016/j.cell.2015.09.029.

[75] Ikue Mori. Genetics of chemotaxis and thermotaxis in the nematode *Caenorhabditis elegans*. *Annual Review of Genetics*, 33:399–422, 1999. doi: 10.1146/annurev.genet.33.1.399.

[76] Ikue Mori and Yasumi Ohshima. Neural regulation of thermotaxis in *Caenorhabditis elegans*. *Nature*, 376:344–348, 1995.

[77] Warwick L. Nicholas, Ellsworth C. Dougherty, and Eder L. Hansen. Axenic cultivation of *Caenorharditis briggsae* (nematoda: Rhabditidae) with chemically undefined supplements; comparative studies with related nematodes. *Annals of the New York Academy of Sciences*, 77(2):218–236, 1959.

[78] Ernst Niebur and Erdós. Theory of the locomotion of nematodes: Control of the somatic motor neurons by interneurons. *Mathematical Biosciences*, 118(1):51–82, 1993. doi: 10.1016/0025-5564(93)90033-7.

[79] Ernst Niebur and Paul Erdós. Theory of the locomotion of nematodes: Dynamics of undulatory progression on a surface. *Biophysical Journal*, 60(5):1132–1146, 1991.

[80] Shigekazu Oda, Masahiro Tomioka, and Yuichi Iino. Neuronal plasticity regulated by the insulin-like signaling pathway underlies salt chemotaxis learning in *Caenorhabditis elegans*. *Journal of Neurophysiology*, 106(1):301–308, 2011. doi: 10.1152/jn.01029.2010.

[81] Yuki Oka, Matthew Butnaru, Lars von Buchholtz, Nicholas J. P. Ryba, and Charles S. Zuker. High salt recruits aversive taste pathways. *Nature*, 494(7438): 472–475, 2013. doi: 10.1038/nature11905.

[82] Christopher O. Ortiz, Serge Faumont, Jun Takayama, Heidi K. Ahmed, Andrew D. Goldsmith, Roger Pocock, Kathryn E. McCormick, Hirofumi Kunimoto, Yuichi Iino, Shawn Lockery, and Oliver Hobert. Lateralized gustatory behavior of *C. elegans* is controlled by specific receptor-type guanylyl cyclases. *Current Biology*, 19(12):996–1004, 2009. doi: 10.1016/j.cub.2009.05.043.

[83] Jonathan T. Pierce-Shimomura, Serge Faumont, Michelle R. Gaston, Bret J. Pearson, and Shawn R. Lockery. The homeobox gene lim-6 is required for distinct chemosensory representations in *C. elegans*. *Nature*, 410(6829), .

[84] Jonathan T. Pierce-Shimomura, Thomas M. Morse, and Shawn R. Lockery. The fundamental role of pirouettes in *Caenorhabditis elegans* chemotaxis. *The Journal of Neuroscience*, 19(21), .

[85] Jonathan T. Pierce-Shimomura, Michael Dores, and Shawn R. Lockery. Analysis of the effects of turning bias on chemotaxis in *C. elegans*. *Journal of Experimental Biology*, 208(24):4727–4733, 2005.

[86] Beverly J. Piggott, Jie Liu, Zhaoyang Feng, Seth A. Wescott, and X. Z. Shawn Xu. The neural circuits and synaptic mechanisms underlying motor initiation in *C. elegans*. *Cell*, 147(4):922–933, 2011. doi: 10.1016/j.cell.2011.08.053.

[87] Ana C. F. Ribeiro, Ornella Ortona, Susana M. N. Simões, Cecília I. A. V. Santos, Pedro M. R. A. Prazeres, Arthur J. M. Valente, Victor M. M. Lobo, , and Hugh D. Burrows. Binary mutual diffusion coefficients of aqueous solutions of sucrose, lactose, glucose, and fructose in the temperature range from (298.15 to 328.15) k. *Journal of Chemical & Engineering Data*, 51(5):1836–1840, 2006. doi: 10.1021/je0602061.

[88] Satoshi Saeki, Massayuki Yamamoto, and Yuichi Iino. Plasticity of chemotaxis revealed by paired presentation of a chemoattractant and starvation in the nematode *Caenorhabditis elegans*. *Journal of Experimental Biology*, 204(10):1757–1764, 2001.

[89] Yoshihiro Sambongi, Takashi Nagae, Yanna Liu, Takao Yoshimizu, Kenji Takeda, Yoh Wada, and Masamitsu Futai. Sensing of cadmium and copper ions by externally exposed adl, ase, and ash neurons elicits avoidance response in *Caenorhabditis elegans*. *NeuroReport*, 10(4):753–757, 1999.

[90] Yoshihiro Sambongi, Kenji Takeda, Tokumitsu Wakabayashi, Ikuo Ueda, Yoh Wada, and Masamitsu Futai. *Caenorhabditis elegans* senses protons through amphid chemosensory neurons: proton signals elicit avoidance behavior. *NeuroReport*, 11(10):2229–2232, 2000.

[91] Hiroyuki Sasakura, Yuki Tsukada, Shin Takagi, and Ikue Mori. Japanese studies on neural circuits and behavior of caenorhabditis elegans. *Frontiers in Neural Circuits*, 7(187), 2013. doi: 10.3389/fncir.2013.00187.

[92] Toshihiro Sassa, Takashi Murayama, and Ichi N. Maruyama. Strongly alkaline ph avoidance mediated by ash sensory neurons in *C. elegans*. *Neuroscience Letters*, 555:248–252, 2013. doi: 10.1016/j.neulet.2013.06.001.

[93] Yoichi Shinkai, Yuta Yamamoto, Manabi Fujiwara, Takashi Tabata, Takashi Murayama, Takaaki Hirotsu, Daisuke D. Ikeda, Makoto Tsunozaki, Yuichi

Iino, Cornelia I. Bargmann, Isao Katsura, and Takeshi Ishihara. Behavioral choice between conflicting alternatives is regulated by a receptor guanylyl cyclase, gcy-28, and a receptor tyrosine kinase, scd-2, in aia interneurons of *Caenorhabditis elegans*. *The Journal of Neuroscience*, 31(8):3007–3015, 2011. doi: 10.1523/JNEUROSCI.4691-10.2011.

[94] Greg J. Stephens, Bethany Johnson-Kerner, William Bialek, and William S. Ryu. Dimensionality and dynamics in the behavior of *C. elegans*. *PLoS Computational Biology*, 4:1–10, 2008.

[95] Nirmal C. Sukul and Neil A. Croll. Influence of potential difference and current on the electrotaxis of *Caenorhaditis elegans*. *Journal of Nematology*, 10(4):314–317, 1978.

[96] J.E. Sulston, E. Schierenberg, J.G. White, and J.N. Thomson. The embryonic cell lineage of the nematode caenorhabditis elegans. *Developmental Biology*, 100(1): 64–119, 1983. doi: 10.1016/0012-1606(83)90201-4.

[97] Hiroshi Suzuki, Tod R. Thiele, Serge Faumont, Marina Ezcurra, Shawn R. Lockery, and William R. Schafer. Functional asymmetry in *Caenorhabditis elegans* taste neurons and its computational role in chemotaxis. *Nature*, 454(7200):114–117, 2008. doi: 10.1038/nature06927.

[98] Balázs Szigeti, Padraig Gleeson, Michael Vella, Sergey Khayrulin, Andrey Palyanov, Jim Hokanson, Michael Currie, Matteo Cantarelli, Giovanni Idili, and Stephen Larson. Openworm: an open-science approach to modelling caenorhabditis elegans. *Frontiers in Computational Neuroscience*, 8(137), 2014. doi: 10.3389/fncom.2014.00137.

[99] Josué Sznitman, Xiaohua. Shen, Prashant K. Purohit, and Paulo E. Arratia. The effects of fluid viscosity on the kinematics and material properties of *C. elegans*

swimming at low reynolds number. *Experimental Mechanics*, 50(9):1303–1311, 2010. doi: 10.1007/s11340-010-9339-1.

[100] Tod R. Thiele, Serge Faumont, and Shawn R. Lockery. The neural network for chemotaxis to tastants in *Caenorhabditis elegans* is specialized for temporal differentiation. *The Journal of Neuroscience*, 29(38):11904–11911, 2009.

[101] Masahiro Tomioka, Takeshi Adachi, Hiroshi Suzuki, Hirofumi Kunitomo, William R. Schafer, and Yuichi Iino. The insulin/pi 3-kinase pathway regulates salt chemotaxis learning in *Caenorhabditis elegans*. *Neuron*, 51(5):613–625, 2006. doi: 10.1016/j.neuron.2006.07.024.

[102] Emily R. Troemel, Joseph H. Chou, Noelle D. Dwyer, Heather A. Colbert, and Cornelia I. Bargmann. Divergent seven transmembrane receptors are candidate chemosensory receptors in *C. elegans*. *Cell*, 83(2):207–218, 1995. doi: 10.1016/0092-8674(95)90162-0.

[103] Emily R. Troemel, Bruce E. Kimmel, and Cornelia I. Bargmann. Reprogramming chemotaxis responses: sensory neurons define olfactory preferences in *C. elegans*. *Cell*, 91(2):161–169, 1997. doi: 10.1016/S0092-8674(00)80399-2.

[104] Lav R. Varshney, Beth L. Chen, Eric Paniagua, David H. Hall, and Dmitri B. Chklovskii. Structural properties of the *Caenorhabditis elegans* neuronal network. *PLoS Computational Biology*, 7(2):e1001066, 2011. doi: 10.1371/journal.pcbi.1001066.

[105] Andrés Vidal-Gadea, Kristi Ward, Celia Beron, Navid Ghorashian, Sertan Gokce, Joshua Russell, Nicholas Truong, Adhishri Parikh, Otilia Gadea, Adela Ben-Yakar, and Jonathan Pierce-Shimomura. Magnetosensitive neurons mediate geomagnetic orientation in *Caenorhabditis elegans*. *eLife*, 4:e07493, 2015. doi: 10.7554/eLife.07493.

[106] Samuel Ward. Chemotaxis by the nematode *Caenorhabditis elegans*: identification of attractants and analysis of the response by use of mutants. *Proceedings of the National Academy of Sciences of the United States of America*, 70:817–821, 1973.

[107] Duncan J. Watts and Steven H. Strogatz. Collective dynamics of 'small-world' networks. *Nature*, 393(6684):440–442, 1998. doi: 10.1038/30918.

[108] Quan Wen, Michelle D. Po, Elizabeth Hulme, Sway Chen, Xinyu Liu, Sen W. Kwok, Marc Gershow, Andrew M. Leifer, Victoria Butler, Christopher Fang-Yen, Taizo Kawano, William R. Schafer, George Whitesides, Matthieu Wyart, Dmitri B. Chklovskii, Mei Zhen, and Aravinthan D. T. Samuel. Proprioceptive coupling within motor neurons drives *C. elegans* forward locomotion. *Neuron*, 76(4):750–761, 2016/02/24 2012. doi: 10.1016/j.neuron.2012.08.039.

[109] John G. White, Erica Southgate, J. Nicole Thomson, and Sydney Brenner. The structure of the nervous system of the nematode *C. elegans*. *Philosophical Transactions of the Royal Society London B Biological Sciences*, 314(1165):1–340, 1986.

[110] Stephen R. Wicks, Corry J. de Vries, Henri G. A. M. van Luenen, and Ronald H. A. Plasterk. Che-3, a cytosolic dynein heavy chain, is required for sensory cilia structure and function in *Caenorhabditis elegans*. *Developmental Biology*, 221(2): 295–307, 2000. doi: 10.1006/dbio.2000.9686.

[111] David R. Williamson. Modelling the locomotion nervous system in the nematode *C. elegans*: a developmental perspective. Master's thesis, School of Computing, University of Leeds, 2012.

[112] Jian-Xin Xu and Xin Deng. Biological neural network based chemotaxis behaviors modeling of *C. elegans*. In *Neural Networks (IJCNN), The 2010 International Joint Conference on*, pages 1–8, 2010. doi: 10.1109/IJCNN.2010.5596961.

[113] Jian-Xin Xu and Xin Deng. Complex chemotaxis behaviors of *C. elegans* with speed regulation achieved by dynamic neural networks. *The 2012 International Joint Conference on Neural Networks (IJCNN)*, pages 1–8, 2012. doi: 10.1109/IJCNN.2012.6252661.

[114] Meng Xu, Travis A. Jarrell, Yi Wang, Steven J. Cook, David H. Hall, and Scott W. Emmons. Computer assisted assembly of connectomes from electron micrographs: Application to *Caenorhabditis elegans*. *PLoS ONE*, 8(1):e54050, 2013. doi: 10.1371/journal.pone.0054050.

Appendices

A Jansen Lab experimental results

The results below are not my own, and are summarized here only for the convenience of the reader.

A.1 Prolonged exposure to NaCl sensitizes ASER and desensitizes ASEL

In contrast to earlier work [80, 97, 100], the Jansen Lab found that the ASER neurons did not respond to NaCl concentration decreases at low or high concentrations (Figure A.1A). Additionally, pre-exposure to NaCl sensitized ASER over a time scale of 10 minutes, explaining why prior studies did find a response to NaCl downsteps (Figure A.1B). For ASEL an opposite adaptation was found, with sensory neurons responding in naive animals but becoming fully desensitized over 10 minutes of pre-exposure (Figure A.1C), but returning back to baseline in 5 minutes (Figure A.1D). Interestingly, ASEL while desensitized to the pre-exposure concentration, continued to respond to higher concentrations (Figure A.1E). These data suggest that ASEL desensitization involves threshold modulation, while ASER sensitization appears more like gain modulation. Finally, several mutants (synaptic, serotonin, dopamine, neuropeptide) had normal ASEL and ASER adaptation, suggesting they are mostly cell-autonomous (data not shown).

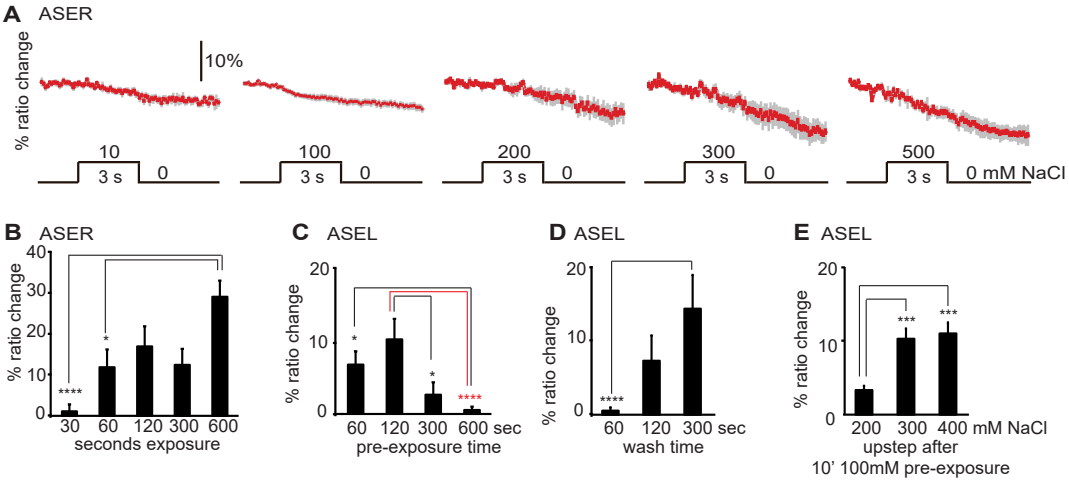

*Figure A.1: Ca^{2+} Responses of ASER (A,B) and ASEL (C,D,E) neurons. (A) No response is seen in ASER upon removal of 0.01 to 0.5M NaCl. (B,C,D,E) Average maximum ratio changes (± SEM). (B) ASER sensitizes upon pre-exposure. (C) ASEL responses were significantly reduced after pre-exposure. (D) 2 minutes or longer wash with a NaCl-free buffer restored the Ca^{2+} response of ASEL to 100 mM NaCl. (E) Animals pre-exposed to 100mM NaCl still respond to higher concentrations. Statistical significance *: p<0.05,***: p<0.005, ****: p<0.001.*

A.2 Prolonged exposure sensitizes ASH

In naive animals, ASH does not respond to a 200mM NaCl upstep (Figure A.2B), but does respond to 300mM and higher concentration (osmotic shock). However, in pre-exposed animals the Jansen lab found that animals now respond to upsteps from 100mM to 200mM (Figure A.1A,B) with an amplitude comparable to the naive response to 500mM. Pre-exposure did not affect Ca^{2+} transients in ASH neurons upon exposure to 300 or 500 mM NaCl (Figure A.2A and 2B). In contrast to ASEL and ASER, ASH recruitment is not cell-autonomous, but depends on ASE (Figure A.2 C,D and E), serotonin, dopamine and synaptic transmission (data not shown).

B Publications

The following publications, produced from the work in this thesis, are included.

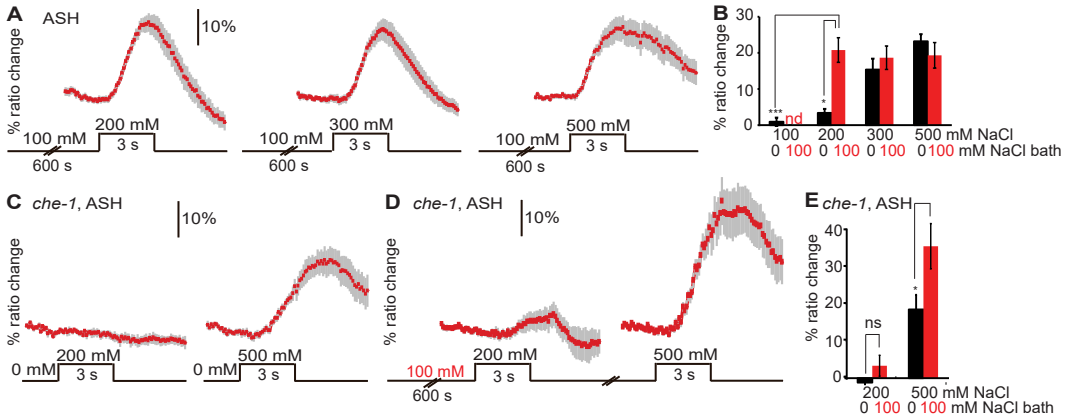

*Figure A.2: Prolonged exposure to NaCl sensitizes ASH. (A) The response of ASH to 200 mM NaCl was increased after pre-exposure to 100 mM NaCl while the responses to 300 and 500 mM NaCl were unchanged. (B) Average maximum ratio changes (± SEM) in ASH after exposure to 100, 200, 300, or 500 mM NaCl, in animals pre-exposed to 100 mM NaCl for 600 seconds, or to control condition (100 or 0 mM NaCl bath solution, respectively). (C,D and E) che-1 null mutant with defective ASE, shows a normal osmotic response, a normal response to 200mM without pre-exposure (C,E), but a significantly reduced response to 200mM after pre-exposure (D,E). Statistical significance ns: $p>0.05$, *: $p<0.05$, *** $p<0.005$.*

Cohen, N, and Sanders, T, 2014, Nematode locomotion: dissecting the neuronal-environmental loop, in *Current Opinion in Neurobiology*, 25:99-106.